Tampere University

KOSTIANTYN NECHAY

# High-Power VECSELs Operating at the 700-800 nm Wavelength Range

Tampere University Dissertations 179

Tampere University Dissertations 179

KOSTIANTYN NECHAY

# High-Power VECSELs Operating at the 700-800 nm Wavelength Range

ACADEMIC DISSERTATION
To be presented, with the permission of
the Faculty of Engineering and Natural Sciences
of Tampere University,
for public discussion in the auditorium Pieni sali 1 (FA032)
of the Festia building, Korkeakoulunkatu 8, Tampere,
on 22 November 2019, at 12 o'clock.

ACADEMIC DISSERTATION
Tampere University, Faculty of Engineering and Natural Sciences
Finland

*Responsible supervisor and Custos*
Professor
Mircea Guina
Tampere University
Finland

*Supervisor*
Academy Postdoctoral Researcher
Hermann Kahle
Tampere University
Finland

*Pre-examiners*
Professor
Udo Pohl
Technical University of Berlin
Germany

D. Sc.
John-Mark Hopkins
Fraunhofer Centre for Applied Photonics
United Kingdom

*Opponent*
Professor
Harri Lipsanen
Aalto University
Finland



Cover design: Roihu Inc.

ISBN 978-952-03-1360-9 (print)
ISBN 978-952-03-1361-6 (pdf)
ISSN 2489-9860 (print)
ISSN 2490-0028 (pdf)
http://urn.fi/URN:ISBN:978-952-03-1361-6

PunaMusta Oy – Yliopistopaino
Tampere 2019

Dedicated to my grandfather Alexander

# ACKNOWLEDGEMENTS

This work has been carried out at the Optoelectronics Research Centre, Tampere University (former Tampere University of Technology), Tampere, Finland.

I would like to express my deepest gratitude to my supervisor, professor Mircea Guina, for all the guidance, mentorship and relentless support he has provided throughout the work. I also would like to warmly thank my Master's thesis supervisor Esa Saarinen, who has introduced me into the world of lasers, and without whose help and support this doctoral work would not be initiated.

I want to thank all my colleagues at the ORC and, particularly, my co-authors: Jussi-Pekka Penttinen, Hermann Kahle, Antti Tukiainen, Sanna Ranta, Patrik Rajala. My gratitude goes to the collaborators at the École Polytechnique Fédérale de Lausanne and at the Rennes University, whose contributions to this work cannot be overestimated.

I would like to acknowledge fellow doctoral students Riku Isoaho, Marcello Piton, Eero Koivusalo for countless beer tasting sessions at the K. Apina and for their vital assistance in the exploration of the local music scene. As well, I would like to thank Andrei Fedotov for being a great roommate.

The pre-examiners professor Udo Pohl and Dr. John-Mark Hopkins are gratefully acknowledged for the valuable comments and suggestions they have kindly provided.

I am infinitely grateful for all the support, inspiration and love my family has provided me with.

# ABSTRACT

Optically pumped vertical-external-cavity surface-emitting lasers (OP-VECSELs) constitute a very flexible laser platform, delivering high-power and high-brightness emission at a vast wavelength range. However, there are certain spectral gaps where efficient VECSEL operation has remained elusive. To this end, the main objective of the thesis was to demonstrate a high-power direct-emitting VECSEL in the 700–800 nm wavelength region, which has not been addressed significantly before this work. Two different approaches were followed to fulfill the research objective.

In a first path we focused on direct emitting quantum well (QW)-based VECSELs exploiting AlGaAs/GaAs material system. Record-high output powers of 4.24 W and 3.25 W at the 755 nm and 765 nm were demonstrated, respectively. As negative points of this approach, we note the peculiarity of polarization features and the relatively short lifetime arising from defects within the structure.

A second approach of this thesis was to realize intracavity second-harmonic generation (SHG) of the infrared 1.5 μm VECSELs. Furthermore, the work on the 1.5 μm VECSELs has also followed two complementary directions, resulting in: i) development of the first 1.5 μm quantum dot (QD)-based VECSEL, and ii) development of the first flip-chip QW VECSEL at the same wavelength. QD-based gain media can offer additional advantages over conventional QW devices, such as wider gain bandwidth. Whereas, the flip-chip thermal management scheme avoids the usage of expensive intracavity heat spreaders (that can distort the laser beam profile), paving the way for large volume manufacturing of such VECSELs. The achieved results at the fundamental wavelength include 2.25 W from the QD-based VECSEL and 3.65 W from the flip-chip QW-VECSEL. Finally, SHG of 750 nm emission was realized from both QD and QW VECSELs yielding 1.2 W and 2.25 W of output power, respectively. The demonstrated SHG results constitute a more viable alternative to the direct emitting structures due to much longer lifetime.

As possible applications of the laser technology developed in the thesis, we would mention biophotonics and medicine due to high penetration depth of 750 nm light into human tissues. In addition, further development of 750 nm lasers would lead to demonstration of UV emission around 380 nm, which will be particularly useful in atomic molecular and optical physics applications.

# CONTENTS

# ABBREVIATIONS

| | |
|---|---|
| AFM | Atomic force microscopy |
| $Al_2O_3$ | Aluminium oxide |
| AlAs | Aluminium-arsenide |
| AlGaAs | Aluminium-gallium-arsenide |
| AlGaInAs | Aluminium-gallium-indium-arsenide |
| AMO | Atomic, molecular and optical (physics) |
| As | Arsenic |
| Au | Gold |
| BHF | Buffered hydrofluoric acid |
| BiBO | Bismuth borate |
| CCD | Charged-coupled device |
| Cr | Chromium |
| CTE | Coefficient of thermal expansion |
| CVD | Chemical vapor deposition |
| CW | Continuous wave |
| DPSSL | Diode-pumped solid-state laser |
| EEL | Edge-emitting laser |
| EP | Electrically pumped |
| FSR | Free spectral range |
| FWHM | Full width at half maxima |
| GaAs | Gallium-arsenide |
| GaInNAsSb | Gallium-indium-nitrogen-arsenide-antimonide |
| GaN | Gallium-nitride |
| GaSb | Gallium-antimonide |
| HCl | Hydrochloric acid |
| HeNe | Helium-neon laser |
| IC | Intracavity |
| InGaAs | Indium-gallium-arsenide |
| InP | Indium-phosphide |
| IR | Infrared |

| | |
|---|---|
| MBE | Molecular beam epitaxy |
| ML | Monolayer |
| MOCVD | Metalorganic vapour-phase epitaxy |
| Nd | Neodymium |
| OP | Optically pumped |
| PL | Photoluminescence |
| QD | Quantum dot |
| QW | Quantum well |
| RoC | Radius of curvature |
| RPG | Resonant periodic gain |
| RTA | Rapid thermal annealing |
| SDL | Semiconductor disk laser |
| SEM | Scanning electron microscopy |
| SESAM | Semiconductor saturable absorber mirror |
| SHG | Second-harmonic generation |
| SiC | Silicon carbide |
| $SiO_2$ | Silicon dioxide |
| TDR | Temperature-dependent reflectivity |
| TEM | Transverse electromagnetic mode |
| Ti | Titanium |
| TRPL | Time-resolved photoluminescence |
| UV | Ultraviolet |
| VCSEL | Vertical-cavity surface-emitting laser |
| VECSEL | Vertical-external-cavity surface-emitting-laser |
| YAG | Yttrium-aluminium garment |
| Yb | Ytterbium |

# ORIGINAL PUBLICATIONS

Publication I H. Kahle, K. Nechay, J.-P. Penttinen, A. Tukiainen, S. Ranta, and M. Guina, "AlGaAs-based vertical-external-cavity surface-emitting laser exceeding 4 W of direct emission power in the 740–790 nm spectral range," *Optics Letters,* vol. 43, no. 7, pp. 1578-1581, 2018.

Publication II K. Nechay, H. Kahle, J.-P. Penttinen, P. Rajala, A. Tukiainen, S. Ranta, and M. Guina, "AlGaAs/AlGaInP VECSELs With Direct Emission at 740–770 nm," *IEEE Photonics Technology Letters*, vol. 31, no. 15, pp. 1245-1248, 2019.

Publication III A. Mereuta, K. Nechay, A. Caliman, G. Suruceanu, A. Rudra, P. Gallo, M. Guina, and E. Kapon, "Flip-Chip Wafer-Fused OP-VECSELs Emitting 3.65 W at the 1.55-μm Waveband," *IEEE Journal of Selected Topics in Quantum Electronics*, vol. 25, no. 6, 2019.

Publication IV K. Nechay, A. Mereuta, C. Paranthoen, G. Brévalle, C. Levallois, M. Alouini, N. Chevalier, M. Perrin, G. Suruceanu, A. Caliman, M. Guina and E. Kapon, "InAs/InP quantum dot VECSEL emitting at 1.5 μm," *Applied Physics Letters*, vol. 117, no. 17, pp. 171105, 2019.

Publication V K. Nechay, A. Mereuta, C. Paranthoen, G. Brévalle, C. Levallois, M. Alouini, N. Chevalier, M. Perrin, G. Suruceanu, A. Caliman, M. Guina and E. Kapon, "High-power 750 nm VECSEL based on QD gain mirror," *IEEE Journal of Quantum Electronics*, (Submitted), 2019.

# AUTHOR'S CONTRIBUTION

Author's contribution to the publications included into this thesis is following:

I. Author has performed most of the experimental work under the guidance of H. Kahle and has taken part in writing the paper. S. Ranta fabricated the epitaxial wafers. J.-P. Penttinen has provided support for gain mirror processing and laser demonstration. A. Tukiainen designed the quantum well heterostructure. M. Guina has devised and coordinated the experiments.

II. Author has performed all experimental work concerning the VECSEL demonstration under the guidance of H. Kahle. He also had the main role in interpreting the results and writing the manuscript. S. Ranta and P. Rajala are credited for growing the sample. J.-P. Penttinen has provided support for gain mirror processing and laser demonstration. A. Tukiainen contributed to the design of the gain structures. M. Guina was involved in planning the experiments and contributed to the finalization of the manuscript.

III. Author has performed the experimental work concerning the VECSEL set-up and wrote significant part of the paper including the interpretation of the results. A. Mereuta and the team at the EPFL fabricated the gain mirror. All authors contributed to defining the experimental procedure and writing the manuscript.

IV. Author has written the first version of the paper and performed all the experimental work. C. Paranthoen, G. Brévalle, C. Levallois, M. Alouini, N. Chevalier, M. Perrin are credited for designing and manufacturing the quantum dot active region, A. Mereuta is credited for the DBR growth and the wafer-fusion procedure. M. Guina contributed to the devising of the experiments, interpretation of the results, and finalization of the manuscript.

V. Author has performed all the experimental work concerning VECSEL the frequency conversion of the VECSELs. C. Paranthoen, G. Brévalle, C. Levallois, M. Alouini, N. Chevalier, M. Perrin are credited for designing and manufacturing the quantum dot active region. A. Mereuta is credited for the DBR growth and the wafer-fusion procedure. M. Guina contributed to the design of the experiments, interpretation of the results, and finalization of the manuscript.

# 1 INTRODUCTION

"*The laser is a solution seeking for a problem*". This well-known quote was legitimately characteristic of the early days of laser development, when the laser was a laboratory-bound, unexplored, unreliable technology unable to serve as a foundation for the real-world applications. However, this quote has certainly lost its validity and it can hardly relate to modern society, where laser-based technologies are ubiquitous to the point where an ordinary person may carry several of miniaturized lasers integrated into a smartphone in his pocket. Laser light, due to its fundamental nature, can be perceived as an ultraprecise tool, which, for example, enables formation of ultrashort pulses or light-matter interactions beyond capabilities of incoherent light sources. Lasers have become a backbone of numerous fields and applications, such as telecommunications, medicine, metrology, spectroscopy, material processing and atomic manipulation. Thus, nowadays, there are plenty of *problems*, which are continuously seeking for better *laser solutions*.

Each laser application determines specific set of requirements of laser output, such as, output power, emission spectrum, beam quality, tunability, linewidth, pulse width, etc. Various laser platforms are capable of tailoring these output parameters with different levels of success, depending on fundamental aspects underlying the operation principle of each laser type. The most general and important categorization of the lasers by type can be done accordingly to the active region the laser platform is employing. *Active region* or *gain medium* is a component responsible for the light generation and amplification. Moreover, the *feedback* and the *pump* are two other vital components of a laser, which correspondently enable stimulated emission and supply energy to the system.

Traditionally, the solid-state gain medium is mentioned first, since it was the very first medium where *light amplification by stimulated emission radiation* was demonstrated by T. Maiman in 1960 [Maiman et. al., 1960]. In that particular case, the solid-state gain medium was represented by a ruby crystal comprised of Cr ions embedded into $Al_2O_3$ matrix. Generally, solid-state gain media can be characterized as crystalline or glass matrixes doped with rare earth or transition metal ions [Huber et. al., 2010]. Optical pumping is employed for exciting ions to higher energetic states in solid-

state lasers [Byer et. al., 1988]. Emission spectra of solid-state media correspond to discrete atomic transitions of the embedded ions. This aspect can be considered as both an advantage and disadvantage of this type of gain media. Atomic transitions provide very narrow gain bandwidth, which is favourable for lasing in a single-frequency regime; while on the other hand, these atomic transitions are spectrally limited, with the exception of vibronic lasers [Budgor et. al., 1984]. The same spectral limitations are inherent to gas lasers: HeNe, xenon and argon-ion lasers. Gas lasers have pioneered the early days of laser technology, succeeding solid-state lasers [Bennett et. al., 1965; Javan et. al., 1961]. Although many milestones have been achieved in the early days of laser development, such as single-frequency operation, Q-switching [McClung et. al., 1962], mode-locking [Ippen et. al., 1972], and second-harmonic generation [Franken et. al., 1961] etc., spectral coverage of the lasers available by that time was still scarce.

The path for the semiconductor lasers, which will become the most spectrally versatile lasers, was paved in 1962 by R. Hall [Hall et. al., 1962]. It took seven more years to realize the first double heterostructure laser, demonstrated by Zh. Alferov [Alferov et. al., 1969], the concept which afterwards developed into a basic framework of semiconductor lasers. Subsequent demonstration of a quantum well laser, nine years later by N. Holonyak [Holonyak Jr et. al., 1978], made possible low-threshold laser emission at the wavelength range spanning from visible to mid-infrared. The possibility of tailoring emission wavelength by means of bandgap engineering paired with a mass volume production revolutionized many fields with this affordable laser platform. For instance, the Internet, whose impact on human progress cannot be overestimated, would not be possible in the form we know today [Winzer et. al., 2018] without a combination of advances in the semiconductor laser technology. However, semiconductor lasers suffer from several drawbacks, namely, low brightness, complex multi-stage processing and a monolithic resonator.

The laser type covered in this doctoral dissertation is named vertical-external-cavity surface-emitting laser (VECSEL) [Sandusky et. al., 1996; Kuznetsov et. al., 1997], which originates from the semiconductor laser family. This particular laser type couples features of solid-state lasers, such as a functional external resonator and optical pumping, with intrinsic gain versatility of semiconductor gain media. Such a successful combination made possible the creation of a remarkably flexible, multipurpose laser platform, capable of precise tailoring of output parameters in accordance even to the most strict applications, for instance in atomic, molecular, and optical physics (AMO) [Burd et. al., 2016; Burd et. al., 2015].

Particularly, VECSELs with emission wavelength at the 700–800 nm wavelength interval can benefit a multitude of applications. For instance, due to the large penetration depth at the wavelengths around 750 nm [Jacques et. al., 2013], such a VECSEL can be applied in medicine, dermatology and biophotonics. VECSEL-based cavity-enhanced detection of molecular oxygen (the absorption peak lies at 763 nm) can enrich the field of spectroscopy [Gianfrani et. al., 1999]. Furthermore, direct emitting VECSEL at this wavelength range constitute a particular interest, since they open an avenue for efficient second-harmonic generation (easily attainable with VECSELs) to the UV wavelength range. In spite of the high demand of UV lasers, the UV waveband coverage with high-brightness, high-power lasers remains very poor. One of the most prospective fields where UV lasers find a great need is AMO physics. AMO physics involves atom manipulations by means of addressing certain atomic transitions with photons. Notably, a large number of atomic transition lines are located in the UV wavelength range, where a precisely tuned narrow-linewidth laser can wield them. UV VECSELs have already proved themselves as a very practical and viable laser platform for AMO physics, when applied in the quantum computation field with a purpose of ion cooling and ion trapping [Burd et. al., 2015]. Another noteworthy application of UV VECSELs in the AMO field is the medical radioisotope separation technique called MAGIS, where VECSELs were proposed to be used as optical pumps [Mazur et. al., 2014]. The MAGIS technique allows separation of the stable isotopes, which later are used for manufacturing of the radioactive medical isotopes. For instance, $Tc^{99m}$ is the most demanded medical radioisotope in the world [Ponsard et. al., 2012], which contributes the most to nuclear medicine diagnostics [Charlton et. al., 2015]. Manufacturing of this particular isotope requires a narrow-linewidth laser with emission at 380 nm, the wavelength range that is outside the scope of convenient and efficient laser platforms, but which can be covered by the frequency-doubled 760 nm VECSEL.

## 1.1 What VECSELs can offer in comparison to other lasers

As mentioned above, VECSELs belong to a semiconductor laser family. However, compared to traditional semiconductor lasers, there are several major differences in the laser architecture and pumping scheme utilized in this laser type. Contrary to the ubiquitous electrically pumped (EP) laser diodes, VECSELs are typically optically pumped (OP). At the first glance, this fact may be considered as a drawback of VECSELs, especially when compared to the relatively easy electrical pumping of

p-n junctions employed in diode lasers. Indeed, optical pumping applied to a common diode laser structure alone would not be a viable modification, yet in a VECSELs, optical pumping is advantageously exploited in an external cavity created between an external mirror(s) and the so-called 'gain mirror' structure. This configuration is depicted in Fig.1. The design and geometry of the external resonator dictates the mode size diameter on the VECSEL surface. In turn, mode spot is overlapping with the pump beam of a slightly bigger diameter, ensuring stable operation with circular beam geometry and high power. Such combination of excellent beam quality and high power is one of the major advantages of VECSELs, effectively classifying them as high-brightness lasers.

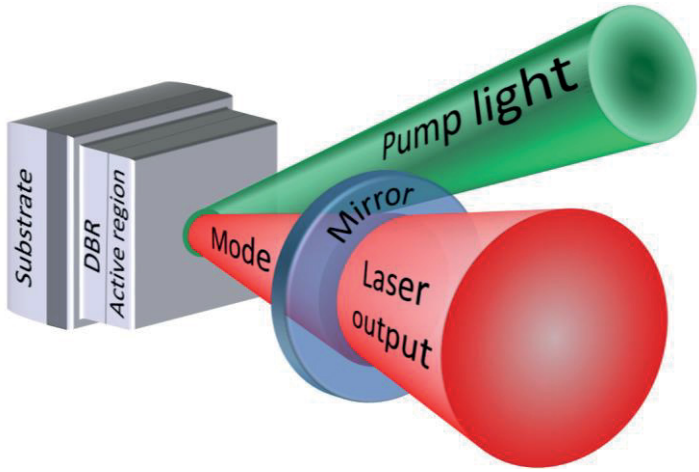


**Figure 1.** Schematic illustration of an optically pumped vertical-external-cavity surface-emitting laser. Resonator is created between a DBR and a curved highly reflective mirror (with typical reflectivity of ~97-99%), which couples out laser output.

Surface emission is another notable aspect of VECSEL architecture, which allows power-scaling with multi-Watt output. Scaling the pump spot diameter translates into scaling of the power by increasing the effective gain volume, contrary to the laser diodes where gain region volume is rather small and fixed.

Despite the larger gain volume compared with vertical cavity laser diodes, for successful laser operation, the combined resonator losses (which include laser output) should not exceed several percent; therefore, the amount of power concentrated inside the cavity exceeds the output power values by a factor of tens to hundreds. In turn, the high level of intracavity field intensity enables efficient nonlinear conversions expanding even more the operation regimes of VECSELs.

| Laser type | Wavelength versatility | Power levels | Ultra-short pulse operation | Beam quality | Footprint | Cost |
|---|---|---|---|---|---|---|
| **Solid-state** | ★☆☆☆ | ★★★★ | ★★★★ | ★★★☆ | ★★☆☆ | ★★☆☆ |
| **Fiber lasers** | ★★☆☆ | ★★★★ | ★★★★ | ★★★★ | ★★☆☆ | ★★★☆ |
| **Dye laser** | ★★★☆ | ★★★★ | ★★★★ | ★★★☆ | ★☆☆☆ | ★☆☆☆ |
| **Gas lasers** | ★☆☆☆ | ★★★★ | ★★☆☆ | ★★★☆ | ★★☆☆ | ★★★☆ |
| **EEL diodes** | ★★★★ | ★★★☆ | ★★☆☆ | ★☆☆☆ | ★★★★ | ★★★★ |
| **VCSELs** | ★★★☆ | ★☆☆☆ | ★★☆☆ | ★★★★ | ★★★★ | ★★★★ |
| **VECSELs** | ★★★☆ | ★★★☆ | ★★★★ | ★★★★ | ★★★☆ | ★★★☆ |

**Table 1.** Main laser types with ratings corresponding to their performance: ★☆☆☆- poor, ★★☆☆ – fair, ★★★☆ – good, ★★★★- excellent

Moreover, an open resonator allows insertion of various intracavity optical elements in order to modify the emission properties of the laser or initiate ultrafast short-pulse operation.

This notable combination of features distinguishes VECSELs among other laser concepts and makes it a very application-targeted laser platform. Table 1 indicates general properties of the most common laser types, including VECSELs.

## 1.2 VECSEL spectral coverage

Bandgap engineering and mature semiconductor growth technology allow emission from semiconductor gain media at a very broad wavelength range, spanning from UV to mid-IR [Guina et. al., 2017]. However, there are a few notable exceptions of spectral regions where direct emission from semiconductor gain media cannot be efficiently achieved. These spectral regions, where laser emission is very challenging to achieve or where emission cannot be achieved at all, are commonly referred to as *spectral gaps*. For semiconductor lasers, there are notable *green* and *orange* spectral gaps, where direct emission is currently unavailable or the lifetime of the lasers is very short, making them impractical. Commonly, the spectral gaps originate from the lack of semiconductor compounds with adequate bandgap, crystalline, and injection properties corresponding to the given spectral regions. VECSEL technology therefore faces the same problems, typical to the whole semiconductor laser family. In fact, the spectral versatility of VECSELs is subject to these limitations even in higher degree when compared to the standard edge-emitting technologies. These additional limitations for the spectral versatility of VECSELs arise because the semiconductor gain mirror elements are composed of two parts: one being the light-emitting active region (which requires bandgap engineering and quantum well/barrier lattice-matching compounds) and the other the DBR (which demands two additional semiconductor compounds, both being closely matched to the substrate). Thus, the presence of the DBR adds an additional factor that must be taken into account during VECSEL design, implicating that the DBR should be lattice-matched to both an active region and a substrate. This fact significantly complicates VECSEL design and even prevents lasing at several spectral regions in addition to the general spectral gaps intrinsic to all semiconductor lasers. Figure 2 illustrates the spectral coverage of GaAs- and InP-based VECSELs, including direct and frequency converted emissions. The data does not reflect all results, but rather focuses on the highest achieved output powers in the CW regime (pulsed VECSELs are outside the scope of this thesis and are excluded from the discussion). As can be seen from the Fig. 2 the output power values achieved in the different wavebands vary significantly, and in some cases over orders of magnitude. The record output powers were achieved at the wavelength region slightly longer than 1 μm. This fact can be attributed to the high-gain and thermal robustness of InGaAs quantum wells, which are used to achieve emission at this wavelength region. Mature fabrication technology in combination with careful optimization allowed the achievement of over 100 W of output power in CW regime [Heinen et. al., 2012], which is, to date,

the highest output power value demonstrated with VECELs. Nevertheless, there are multiple regions where the development of a high-power VECSEL was not as dynamic and successful as at the 1 μm range. Thus, the development of high-power VECSELs at challenging and less addressed spectral regions is the main scope of this doctoral dissertation.

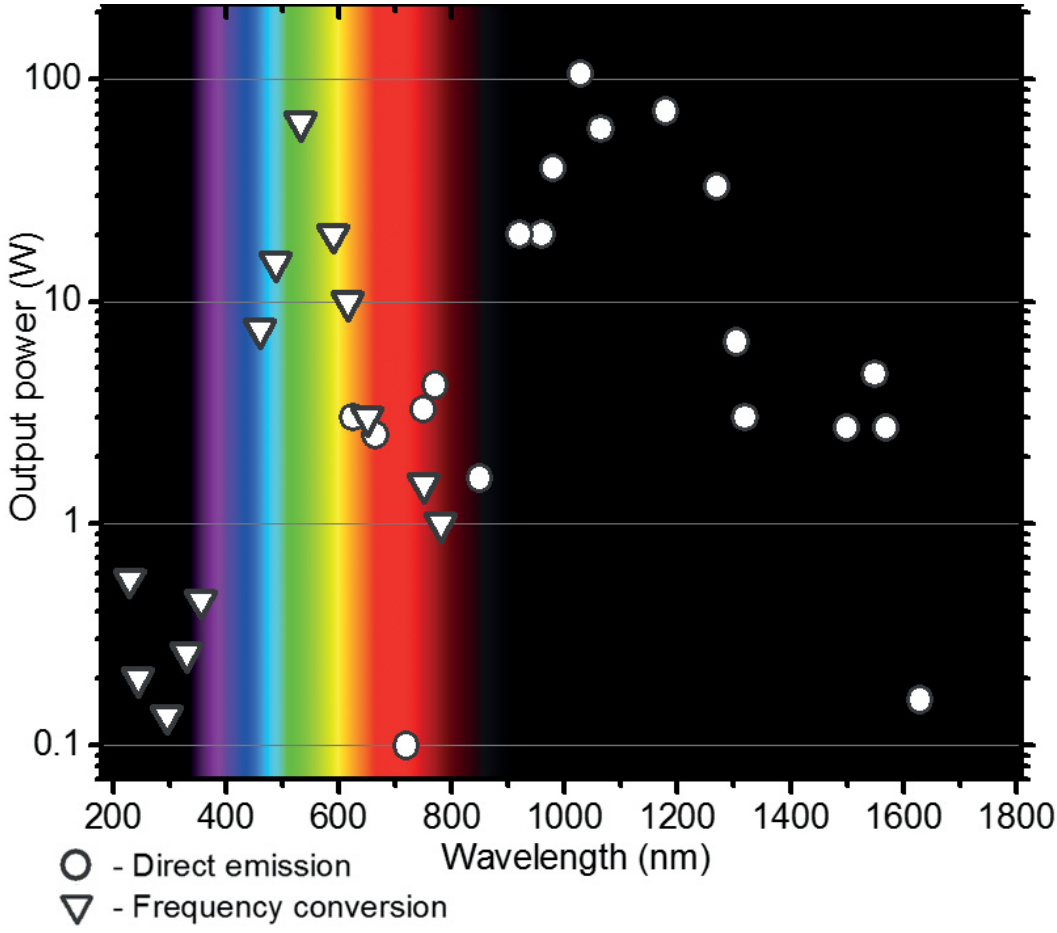


**Figure 2.** Emission wavelength map composed of the results demonstrated with the GaAs and InP-based VECSELs in CW mode. Figure summarizes only the leading results of the CW output powers [Guina et. al., 2017] and references therein.

## 1.3 Research objectives

The generic objective of the thesis was to expand high-power operation of VECSELs to spectral regions that so far have not been properly addressed. In particular, the main goal was to develop VECSELs targeting the wavelength region around 750 nm. The research strategy followed a complementary path addressing direct emitting and frequency doubled VECSELs with fundamental operation at 1.5 μm and is illustrated in Fig.3.

The main tasks and corresponding alternative approaches were:

- Demonstrating direct emitting VECSEL at 750 nm wavelength
- Developing flip-chip VECSEL at 1500-1550 nm range
- Demonstrating quantum dot-based 1500 nm VECSEL (alternative to previously demonstrated quantum well-based VECSELs)
- Achieve frequency doubling from 15XX nm down to 7XX nm region from quantum dot-based VECSEL
- Make comparison of these two approaches of achieving 7XX emission from VECSELs

The challenges of achieving 700–800 nm emission from VECSELs arise from the scarce availability of lattice-matched, direct bandgap semiconductor compounds that can offer both emission and sufficient carrier confinement for operation at elevated temperatures, especially when moving towards the shorter wavelengths in this range. This thesis includes the very first demonstration of direct emitting VECSELs in this wavelength range and discusses two different designs of active regions employed for the VECSEL gain mirrors with emission at slightly different wavelengths. The first design of the active region was composed solely from AlGaAs and was developed for operation at the longer wavelength end of the 700–800 nm range. The second design was targeted to the shorter wavelength end, therefore, materials with larger bandgaps were used, both for the quantum wells and for the claddings.

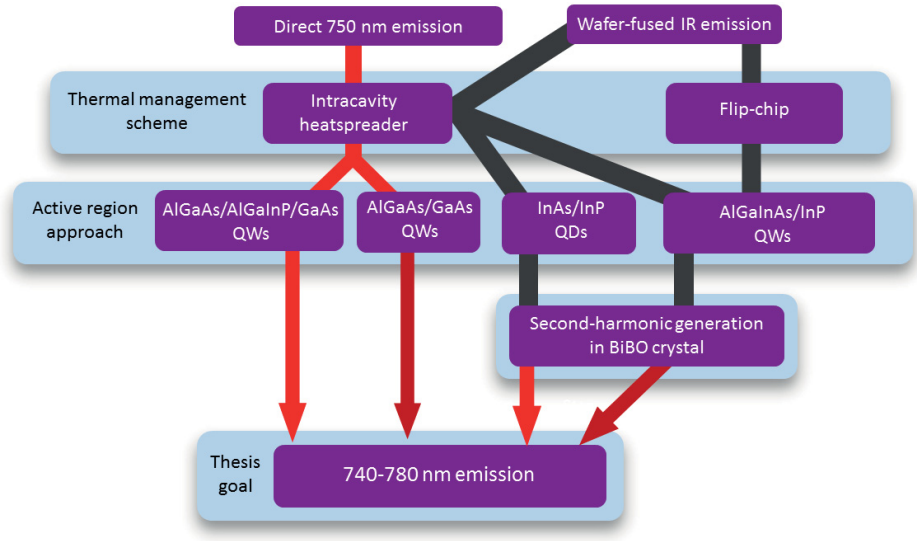


**Figure 3.** Step-scheme illustrating the research directions following different approaches with the aim of achieving visible and IR VECSEL emission in the challenging wavelength 700–800 nm regions.

On the other hand, the approach exploiting frequency doubling of 1.5 μm VECSEL suffers from the lack of availability of lattice-matched compounds for the DBR and the gain region. Hence, achieving VECSEL emission at this wavelength range resorts to the wafer-fusion approach, which allows the combining of separately grown GaAs-based DBRs and InP-based active regions. The novel aspects we tackled in relation to 1.5 μm VECSELs are: i) development of QW-based gain mirrors in flip-chip configuration, and ii) demonstration of QD-dots based gain mirrors. These novel approaches provide benefits in terms of manufacturing and functionality, and in particular, in terms of wavelength tuning capability.

## 1.4 Thesis outline

This thesis is structured as follows. Chapter 2 focuses on the theoretical and practical aspects of VECSELs. Chapter 3 shows the experimental results obtained with 750 nm direct-emitting VECSELs, which correspond to P1 and P2. Chapter 4 shows the experimental results achieved with the wafer-fused IR VECSELs with fundamental emission that correspond to publications P3 and P4, as well as results of frequency conversion, which correspond to P5. Chapter 5 summarizes the main results and makes a comparison between the approaches followed.

# 2 VECSEL BASICS

Optically-pumped (OP)-VECSELs may be understood as wavelength and brightness converters, since they absorb low-brightness broad spectrum light from inexpensive, widely available laser diodes, and efficiently transform it into high-brightness laser emission, with parameters that may be precisely engineered.

## 2.1 VECSEL architecture

The distinctive features of VECSEL architecture can easily be illustrated and emphasized by schematically comparing it to the architecture of other semiconductor laser types, such as the edge-emitting laser (EEL) diode, the extended cavity diode laser, and the vertical cavity surface emitting laser diode (VCSEL). Although several other architecture variations are possible, such as an electrically-pumped VECSEL or optically-pumped VCSEL, the four types shown schematically in Fig. 4 are the most typical semiconductor laser designs. The electrically-pumped EEL diode, depicted in Fig.4(a), is the most common semiconductor laser type. Its laser emission is generated in a planar active region with a thickness of tens to hundreds of nanometers and a width in the range of a few micrometers to tens of micrometers. This asymmetric configuration of the active waveguide creates high astigmatism and results in poor quality beam profiles. Fig.4(b) schematically illustrates an external cavity laser diode [Liu et. al., 1981], where the resonator is created between one cleaved facet and an external mirror. The external cavity configuration opens possibilities for wavelength tuning or single-frequency operation by means of implementing a passive feedback element, yet the complexity is increased and power levels remain modest being limited by the rather small gain volume of the waveguide. Then the planar active region of a VCSEL, shown in Fig. 4(c), is situated between two DBRs creating a high-finesse resonator, which results in narrow-linewidth emission with circular, low-divergence output beams of much higher beam quality than the EEL equivalent.

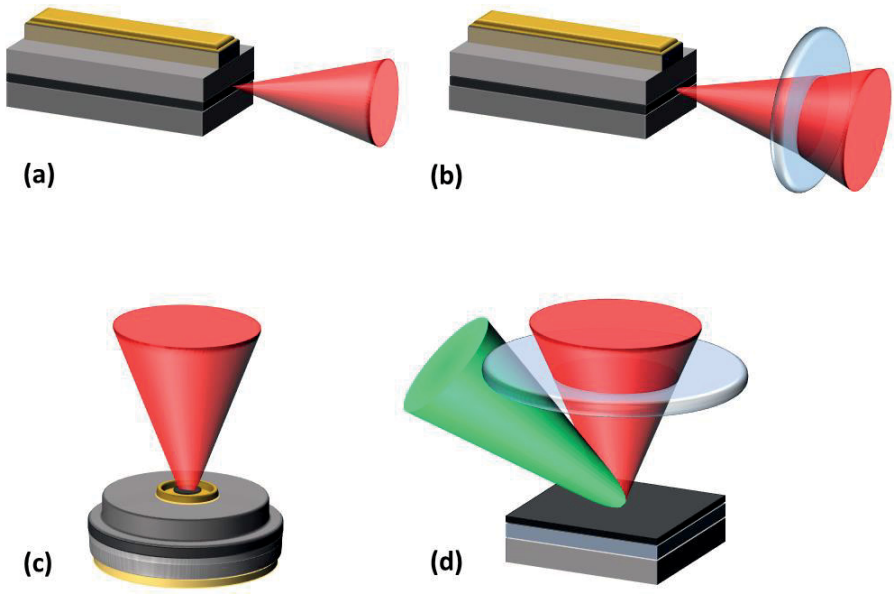


**Figure 4.** Main semiconductor laser types: a) edge-emitting laser diode. b) external cavity laser diode c) VCSEL d) OP-VECSEL. Yellow colored regions correspond to the electrical contacts of structures; when black colored regions correspond to active regions of lasers.

Pumping of VCSELs is implemented through ring contacts, where guiding of current occurs through a tunnel junction aperture. The aperture size therefore defines the mode volume and, consequently, the optical power of a VCSEL. An increase in aperture size eventually leads to an uneven current distribution across the active region and, thus, compromises the beam quality of the VCSEL as well. In practice, the output power of a single-mode VCSEL is limited to several mW. As it can be seen from Fig. 4(d), the VCSEL is the most closely related laser type to the VECSEL, in both name and in architecture. VECSEL technology evolved from VCSEL technology in 1996 [Sandusky et. al., 1996], and the first high-power room-temperature optically-pumped VECSEL was demonstrated by Kuznetsov in 1997 [Kuznetsov et. al., 1997]. Just for general information, we want to note that the first theoretical design of a VECSEL-like architecture was proposed by Basov et. al. already in 1966 [Basov et. al., 1966]. Switching to optical pumping allowed uniform carrier injection into the active region. Furthermore, optical pumping excluded the need for complicated processing steps required for electrical injection, typical for VCSELs and most importantly allowed simplification of the semiconductor material growth, no longer demanding p- and n-doping of semiconductor material. Another major improvement implemented in VECSELs targeted the thermal management of

the devices, which will be discussed further in detail. In this way, the replacement of the VCSEL's top-DBR with an external mirror and switching to optical pumping led to the demonstration of the new laser concept with much higher versatility.

## 2.2 Gain mirror fabrication

The semiconductor part of the VECSEL is generally referred to as a gain mirror, since it is composed of a highly-reflective DBR with an optical gain section placed on top of it. Such gain mirrors are grown by means of molecular beam epitaxy (MBE) or metal-organic chemical vapor deposition (MOCVD) on a variety of substrates, most common of which are GaAs, InP and GaSb. The active region and the DBR are grown in a sequence, which is determined by the thermal management of choice. Lattice constants of all semiconductor materials involved should be matched to each other, although certain lattice mismatch (i.e. strain) is allowed. Strain can be either tensile or compressive depending on the sign of the lattice coefficients difference between the grown material and the substrate. Strained layers can be grown if their thicknesses do not exceed the critical layer thickness value. In fact, certain amount of compressive strain in a QW can be beneficial by lifting the heavy hole/light hole degeneracy in the valence band and, thus, reducing density of states in the ground state of the QW, which decreases lasing threshold. [Zory et. al., 1993]. Layers with lattice constants opposite in sign to the accumulated strain may be introduced into a structure in order to compensate the strain [Nishi et. al., 1986]. This technique is called strain compensation, which has been routinely used for VECSEL fabrication at the wavelength range longer than 1.1 μm [Fan et. al., 2007; Ranta et. al., 2011; Ranta et al., 2012].

### 2.2.1 Gain section

Conventionally, VECSELs employ QW- or QD-based active media [Okhotnikov 2010]. QW is a particular case of heterostructure, where a thin film (several nanometers) of semiconductor compound, with an engineered bandgap, is sandwiched between two thicker layers (barriers) of semiconductors with higher bandgaps. QWs provide one-dimensional carrier confinement, whereas QDs exhibit three-dimensional confinement of carriers on the nanoscale. Such QW (or QD) layers are usually combined into groups, which are separated by cladding layers. This

cladding has a larger bandgap energy than the barriers and correspondingly higher than the QWs. The cladding constitutes a larger volume of a gain section. Thus, most of the pump light gets absorbed in the cladding layers, exciting carriers (electron and holes) to higher energy states. Furthermore, these carriers subsequently relax and diffuse from the higher bandgap cladding to lower bandgap barriers, and finally are trapped into QWs, where carriers radiatively recombine via stimulated emission. Barriers with higher bandgap values prevent an escape of carriers from QWs, thus, making population inversion possible, which is required for lasing. The difference in the bandgap energies between QWs/QDs and barriers can be referred as a carrier confinement value. An energy value of carrier confinement needs to be several times higher than the thermal energy of the carriers at an operating temperature in order to prevent a thermal escape that leads to a decreased gain. Furthermore, a window layer at the air/semiconductor interface is engineered to have one of the highest bandgap energies in the structure in order to prevent carrier diffusion to the surface and their subsequent non-radiative surface recombination — another source of carrier recombination, gain reduction and even damage.

The spatial arrangement of QW grouping inside an active region follows the so-called resonant periodic gain (RPG) design [Corzine et. al., 1989; Raja et. al. 1989], exemplary depicted in Fig. 5. Such an arrangement allows placing QW or QD groups at the antinodes of a standing wave formed inside the *microresonator* or *microcavity*. An overlap of the electric field antinodes with the QWs provide higher effective gain at the particular lasing wavelength. In this way, it is possible to obtain higher gain. The amplitude of the field enhancement inside the microcavity depends on the detuning between the laser wavelength and the wavelength corresponding to the micro cavity resonance, which can be engineered by the microcavity thickness and the top coatings. Thus, the gain mirror designs are typically categorized as *resonant* and *antiresonant* structures. Resonant designs are advantageous in terms of threshold minimization and operation with higher output coupling ratios for higher output powers. Antiresonant designs are commonly employed in widely tunable VECSELs or mode-locked VECSELs, where wide gain bandwidth is preferable for the creation of ultrashort pulses [Keller et. al., 2006].

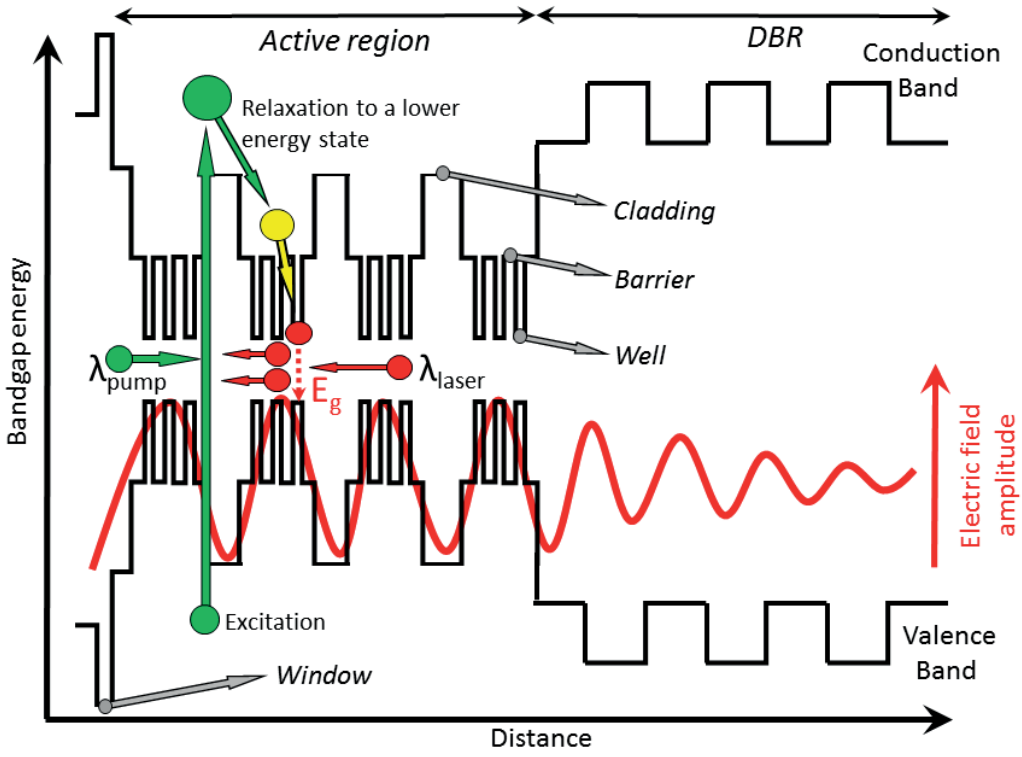


**Figure 5.** Schematics of resonant periodic gain structure usually employed in VECSELs

Another aspect in RPG design is the number of QWs per group, which can be decreased towards the bottom of the gain mirror to follow the pump absorption distribution and keep all QWs pumped at somewhat similar carrier densities.

The temperature of an active region rises accordingly with the amount of absorbed pump light. This temperature increase leads to bandgap reduction in QWs, a typical effect for semiconductor materials. While the bandgap decreases with temperature, the refractive indices of the semiconductor materials increase. Therefore, upon increasing the pumping, the PL, the gain peak, the reflectivity stop-band of the DBR, and microcavity resonance wavelength undergo a red-shift, but at a different rate. Thus, in order to accurately match the desired emission wavelength at certain output powers and temperatures, it is necessary to define an unpumped *detuning* of a particular structure. This detuning can be understood as the spectral difference between room-temperature PL and PL at elevated temperatures caused by pumping. A properly designed detuning allows achievement of efficient high-power operation, because the red shifted lasing wavelength will spatially overlap with QWs inside the VECSEL and will spectrally overlap with microcavity resonance

under the desired pumping values and heatsink temperature [Schulz et. al., 2007]. Thus, for this particular structure it is important to know the rate of the spectral shift of the QW PL and gain peak in correspondence to induced pump power.

### 2.2.2 Distributed Bragg reflector

The distributed Bragg reflector is another integral part of the VECSEL. A DBR is composed of alternating thin layers of high ($n_H$) and low refractive ($n_L$) index compounds. Thicknesses of these layers correspond to a quarter of the central wavelength of the waveband that the particular DBR is designed to reflect. The basic operation principle of a DBR is based upon constructively interfering reflections from each inner boundary of a DBR. Thus, the number of layer pairs defines the reflectivity of the DBR. Figure 6 demonstrates simulation of a GaAs/AlAs DBR consisting from the different number of pairs, where $n_H$=3.5 and $n_L$=2.9.

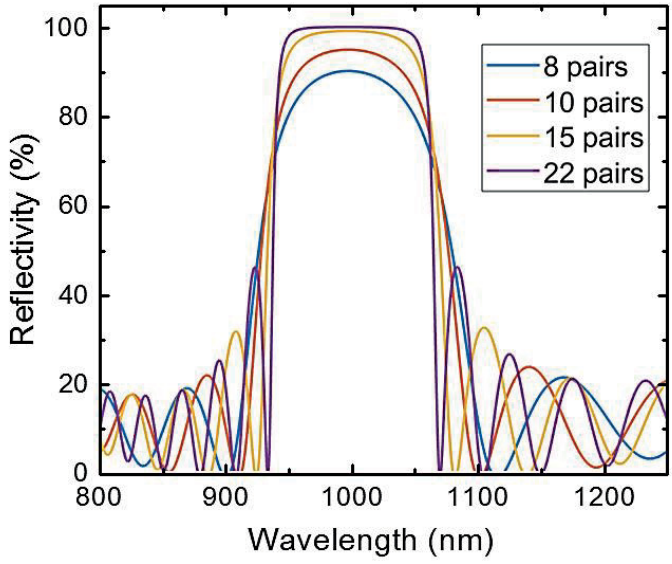


**Figure 6.** DBR reflectivity simulated for different number of pairs in the GaAs/AlAs DBR, where $n_H$=3.5 $n_L$=2.9 .

On the other hand, increasing a refractive index contrast between pairs allows for a reduction of the number of pairs needed for achieving a certain reflectivity value. Absolute refractive indices of semiconductor compounds, number of pairs, and the

contrast between the pairs, are therefore important design aspects of a VECSEL. Furthermore, a VECSEL DBR must be transparent at the signal laser wavelengths in order to avoid absorption losses detrimental to lasing operation and, preferably, at the same time be transparent for residual unabsorbed pump light as well, in order to avoid heat generation in a DBR. Thus, DBR parameters have to be specifically tailored for a particular wavelength range while accounting for the active region composition, its thickness, wavelength of the pump laser, and the chosen thermal management configuration.

The ideal choice of DBR material for GaAs-based VECSEL gain mirrors is GaAs/AlAs: this material combination provides the largest refractive index contrast, allowing the manufacture of thin DBRs with high thermal conductivity, and is lattice matched to GaAs. Since GaAs absorbs light below 880 nm, when developing 750 nm VECSEL the DBR materials are slightly changed to AlGaAs/AlAs to avoid absorption of the laser light.

## 2.3 VECSEL characterization

Characterization procedures for VECSELs can be categorized into two areas: the first area is characterization of a VECSEL gain mirror, while the second phase is characterization of VECSEL laser properties.

### 2.3.1 VECSEL gain mirror characterization

Upon growth, a VECSEL wafer undergoes material characterization in order to obtain information, such as wavelength and the intensity distribution of photoluminescence (PL) across a wafer, wafer reflectivity, surface roughness, crystal quality, etc. PL measurement is one of the most basic and useful procedures of evaluation of optical quality. PL wavelength is also measured during intermediate calibrations of growth parameters in order to optimize the operation wavelength in terms of detuning from the cavity resonance. Intensity of PL signal can be used for a post-growth material quality assessment, since PL intensity is usually proportional to semiconductor crystal quality. Generally speaking, assessment of PL signals can be made by collection from the front surface (PL measured in a growth direction) or from the edge of the semiconductor wafer (measured from a cleaved facet). The front PL is easier to measure using routine equipment but it is filtered by the DBR

and cavity resonance [Tropper et. al., 2006]. Therefore, edge PL is typically employed for a precise PL peak wavelength analysis of a VECSEL. Fig. 7 demonstrates comparison between front and edge PL measured from the same VECSEL gain mirror structure.

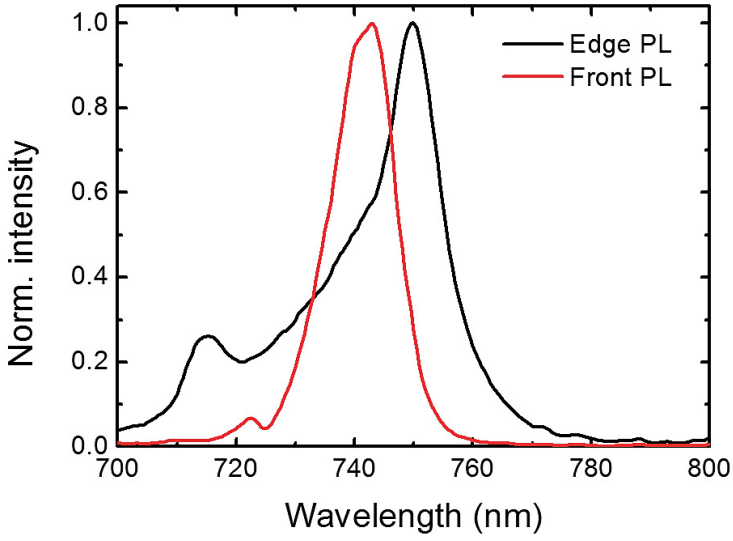


**Figure 7.** Normalized front PL and edge PL signals measured from the same VECSEL structure, described in [P2]. Due to presence of a microcavity resonator (created between DBR and air/semiconductor surface) the spectrum of front PL is narrower and shifted in comparison to the edge PL.

Another method of assessing structure on a presence of defects is PL signal imaging via mapping [Hein et. al., 2012]. Fig 8 demonstrates such PL mapping taken through an intracavity heat spreader bonded to a gain mirror surface. The excitation was done with a 532 nm collimated laser beam, which was filtered out from the photograph by means of a long-pass filter. Such a method renders possible surface quality investigation and inspection of the structure for the presence of dark lines and dark spots, which may originate due to strain or misfit dislocations.

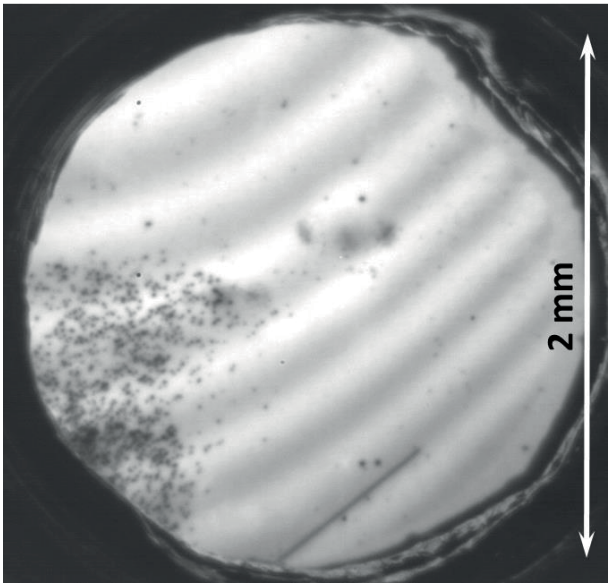


**Figure 8.** A stitched CCD photograph of large area PL of a VECSEL surface taken through an aperture of copper mount. The VECSEL was excited with 532 nm unfocused beam, which was filtered out by means of a long-pass filter (600 nm), transmitting only PL. Dark spots/non-radiative recombination centers (left) can be seen as well as a dark line (bottom). Diagonal black and white fringes originate from interference inside a diamond heat spreader bonded to VECSEL surface.

Time-resolved PL (TRPL) is instrumental in carrier lifetime measurement, indirectly evidencing crystal quality of a structure [Cooley et. al., 1998]. Moreover, temperature-dependent reflectivity (TDR) is employed for determining an exact value of the micro cavity resonance. TDR is measuring the reflectivity of a structure as a function of temperature. This information of the exact location and spectral shift rate of the cavity resonance is essential for laser operation optimization under specific pumping and, therefore, temperatures. Fig. 9 demonstrates the TDR measurement of a structure, where the microcavity resonance was determined to be at 747 nm, and the lowest dip in the reflectivity curve was measured at a temperature of 75°C. In this particular case (AlGaAs QW VECSEL described in chapter 3), the TDR indicated that the detuning of the structure is negative, meaning that the microcavity resonance is located at the shorter wavelength in regards to the gain peak at the operating temperature, which brings additional losses to the laser operation.

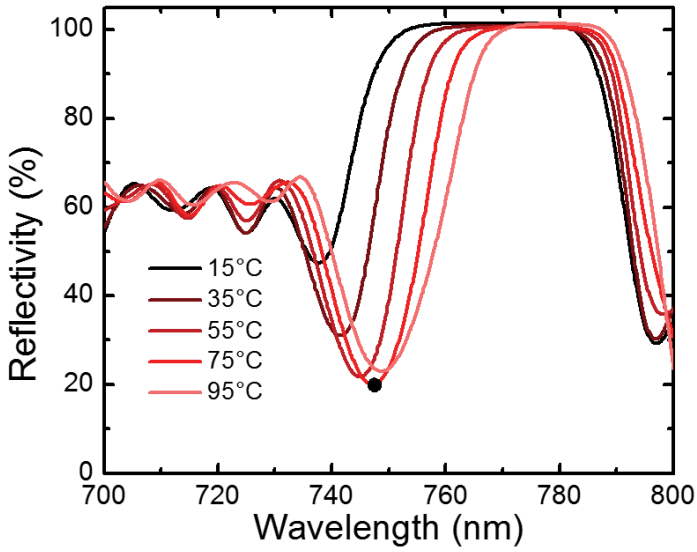


**Figure 9.** Temperature dependent reflectivity measurement of a VECSEL structure (described in chapter 3). In this particular case, micro cavity resonance was measured at ~747 nm (marked with a dot).

Additional techniques used routinely in semiconductor fabrication include: scanning electron microscopy (SEM) imaging of a cross-section of a VECSEL for assessing the layer sharpness and precise measurement of the layers thicknesses (see Fig. 23), atomic force microscopy (AFM) for imaging the surface morphology and for measuring wafer roughness (see Fig. 36), and X-ray diffraction (XRD) for examining the crystal quality and estimation of the accumulated strain [Ranta et. al., 2011].

### 2.3.2 Characterization of VECSEL laser operation

Lasing parameters of VECSELs can be categorized into two subclasses: i) tailorable parameters and ii) the intrinsic features of the gain mirror. Output power and tuning can be referred to as the tailorable features, since various design techniques can be applied in order to adjust these parameters. For example, output power can be increased via increasing the pumping spot area. In that case, thermal roll-over will be the limiting factor for further output power increase, which is dictated by the heat transfer dynamics inside the active region and the heat spreader. Thus, the thermal roll-over can be thought of as an intrinsic parameter of the gain mirror (although this is also affected by the heat spreader technology). Furthermore, an optimal

output coupling ratio plays an important role in achieving the highest output power values. Thus, several output coupling ratios are typically tested in order to find out an optimal value for a particular structure and parameters. Combined intrinsic optical losses of a VECSEL can be estimated by means of the Findlay-Clay analysis [Findlay et. al., 1966] or the Caird plot [Hartke 2008]. In addition, active loss mechanisms can be detected, for instance, parasitic or lateral lasing that can occur under high pumping powers in a lateral in-growth-plane resonator, which substantially decreases lasing efficiency due to carrier depletion [Chernikov et. al., 2010]. Lateral parasitic lasing can be detected either by means of a CCD camera, or by optical spectrum measurements. Lateral lasing usually occurs at longer wavelengths, for which an un-pumped gain region is transparent. Lateral lasing is detectable by macrophotography during operation.

Laser spectra can be seen both a tailorable and intrinsic feature since free-running spectrum is defined by the intrinsic parameters (e.g. bandgap), but at the same time is susceptible to changes in a temperature and pump power or to a presence of intracavity elements, such as, etalons or birefringent filters.

Another example of tailorable VECSEL parameter with high relevance for application is the laser beam divergence or beam quality, described by the $M^2$ factor. Since the lowest order transverse laser mode possess the lowest divergence ($TEM_{00}$), measured $M^2$ factor can be used for the characterization of the transverse mode content of the laser output. As a rule of thumb, laser beams with $M^2$ factor lower than 1.5 are composed from a single transverse mode, or fundamental mode. Due to an uncomplicated mode adjustment of a VECSEL, laser operation can be easily changed from fundamental mode to multimode operation, thus increasing the $M^2$ factor.

## 2.4 Thermal management

Thermal management of any laser is a crucial design aspect drastically affecting the high-power operation capability. In a VECSEL, the origin of the heating can be summarised as consequences of the quantum defect and the non-radiative carrier recombination [Bedfort et. al., 2005]. Quantum defect can be understood as the energy difference between the absorbed higher energy pump photons and the emitted lower energy laser photons. This energy difference is dissipated as heat via lattice vibrations as the carriers relax into the barrier and the QW regions as described previously. Excessive heat can be efficiently extracted from an active

region using one of the three conventional thermal management schemes, shown schematically in Fig. 10.

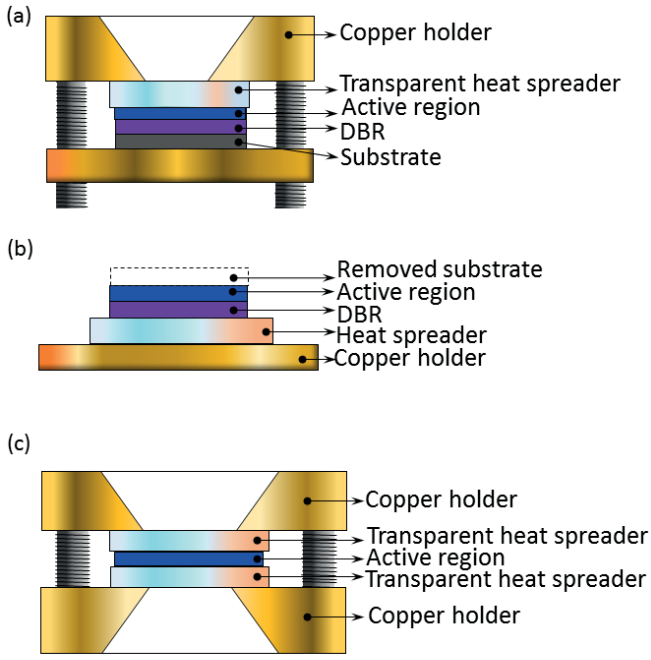


**Figure 10.** VECSEL thermal management approaches: (a) the intracavity heat spreader approach (b) the flip-chip approach (c) DBR-free, double heat spreader approach

### 2.4.1 Intracavity heat spreader approach

Fig. 10 (a) illustrates the intracavity (IC) heat spreader approach [Alford 2002], which can be considered as the most simple thermal management method. This approach exploits a CVD-grown transparent heat spreader of high-thermal conductivity (usually single-crystal diamond or SiC) which is capillary bonded to the VECSEL surface (Fig. 11). Thus, heat from an active region is extracted through a transparent heat spreader and subsequently conducted to the cooled copper mount. In this case, there is no processing of semiconductor material involved (except wafer dicing into chips) and it can be easily and quickly implemented.

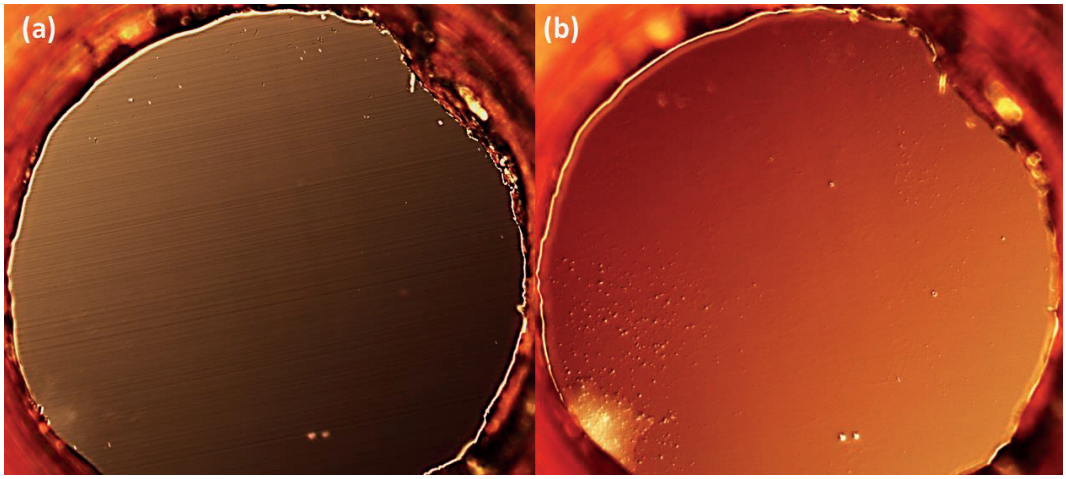


**Figure 11.** Microscope photographs of a VECSEL gain mirror (the same presented at Fig.8) bonded to an IC diamond. Image (a) is focused on the top diamond surface, where surface polishing grooves can be seen. Image (b) is focused onto the semiconductor/diamond interface, where semiconductor surface imperfections and a region of the weak bonding (white spot at the left bottom part) can be seen. Uniform coloring and absence of interference fringes are the criteria of a good capillary bonding. The aperture diameter is approximately 2 mm.

On the other hand, this approach possesses a number of disadvantages. The first disadvantage arises from the fact that the IC heat spreader is situated inside the resonator (hence the name *intracavity*), and, therefore, this brings a set of critical requirements in terms of optical quality of the heat spreader: low-absorbance, low-scattering and low-birefringence. Hence, only single-crystalline and smoothly polished heat spreaders must be used, which significantly adds to their cost. Even a small amount of birefringence (originating from internal stresses during crystal growth) can compromise laser operation, causing polarization losses which lead to distorted laser beam profile and multimode operation [van Loon et. al., 2006]. Fig. 12 shows a photograph of a birefringent IC heat spreader. The photograph was taken by means of a microscope equipped with a Nomarsky prism. Investigations done with a Nomarsky prism or in cross-polarization can give only qualitative understanding about the amount of intrinsic birefringence inside a heat spreader.

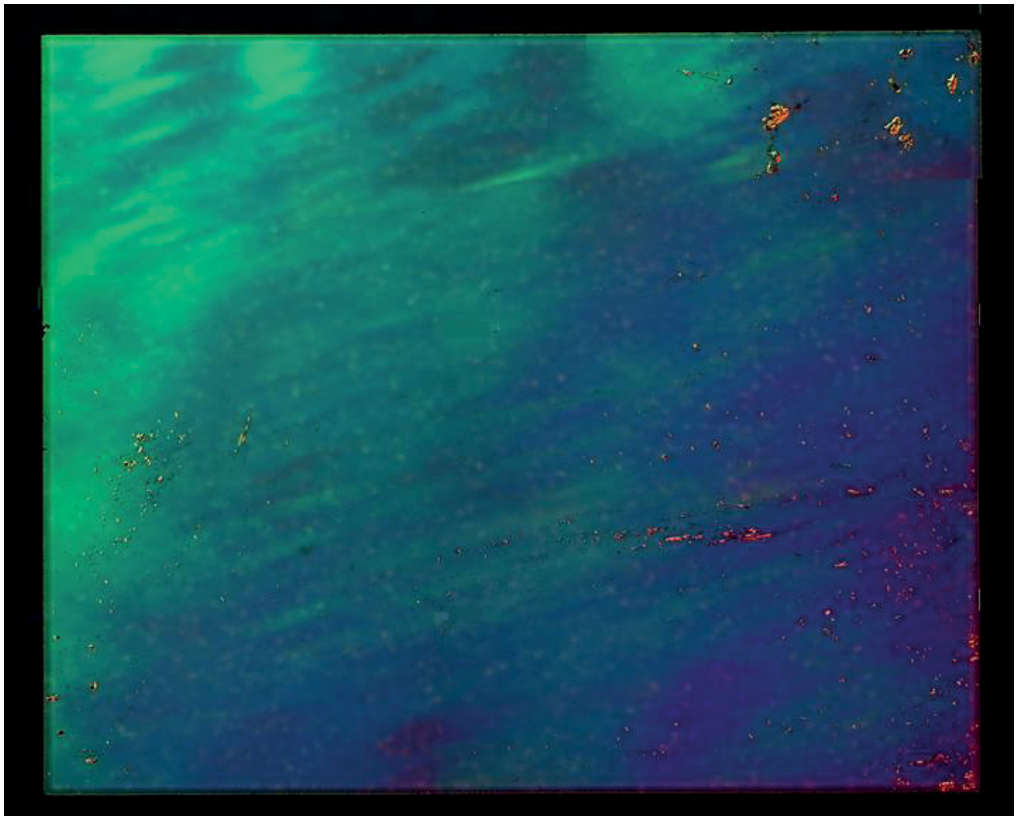

**Figure 12.** A single-crystalline intracavity heat spreader (3x3 $mm^2$) demonstrating high birefringence (colored pattern). The stitched photograph was taken by means of a microscope equipped with the Nomarsky prism.

Another disadvantage of the IC approach is related to the parasitic Fabry-Perot etalon inside a resonator that alters the output spectrum of a laser. To illustrate this, Fig. 13 shows lasing spectra comparison of a VECSEL using the IC heat spreader and the flip-chip configurations. In this case, an IC diamond with a refractive index of 2.4 (at 1.2 μm) and with a thickness of ~335 μm creates the Fabry-Perot etalon with a free spectral range (FSR) of 1 nm. Modulation of the output spectrum can be considered as a major drawback in applicaions where continuous tuning and flat spectral intensity is desired, for instance, in spectroscopy applications. Although deposition of an anti-reflective coating onto a heat spreader can somewhat mitigate spectrum fringes by decreasing the etalon finesse, often spectrum modulation cannot be avoided completely. Another way to reduce spectrum modulation caused by the IC heat spreader is to use a wedged heat spreader [Maclean et. al., 2008].

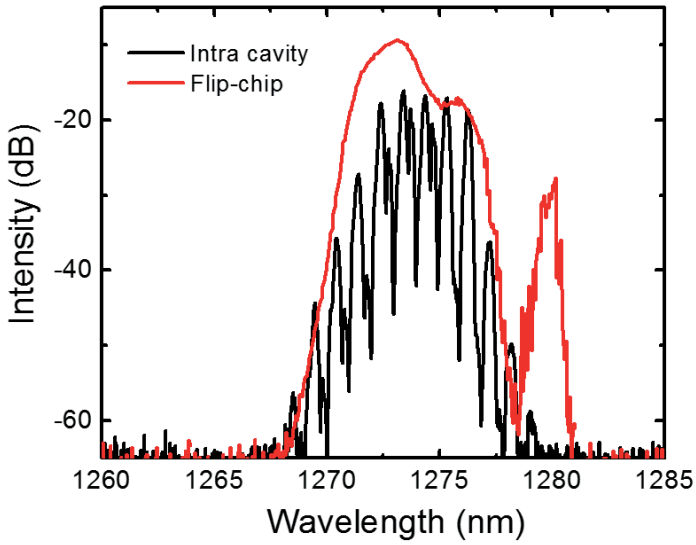


**Figure 13.** Output spectra of VECSELs with different thermal management methods. The black curve shows modulated output spectrum due to the Fabry-Perot etalon introduced by the IC heat spreader. The active regions used for these measurements, namely, InP-based wafer-fused VECSELs, are similar to the ones reported in [Rantamäki et. al., 2015].

One more drawback of an IC heat spreader approach is related to the limitations of power- and production volume scalability of such VECSELs. A heat spreader's efficiency in extracting heat is directly proportional to its thickness and inversely proportional to the diameter of the pump spot (i.e. heated area). Since power scaling in VECSELs is implemented through pump spot size increase, IC heat spreader thickness ultimately hinders the VECSEL power scalability [Kemp et. al., 2005; Rantamäki et. al., 2015]

### 2.4.2 Flip-chip approach

The flip-chip approach utilizes heat extraction through the bottom of a chip, thus conveying heat from the active region via DBR to the bottom heat spreader and eventually to a copper plate [Kuznetsov et. al., 1997]. Fig. 14 illustrates the stages of gain mirror processing implemented in the flip-chip configuration. First, semiconductor growth of an active region and a DBR is performed onto a substrate (in reverse order), with an active region grown first (Fig. 14(a)), which is followed by metallization of the DBR with Ti and Au. The purpose of metallization is two-fold: i) to compensate for the low reflectivity of a thin DBR by adding highly-reflective

metal layers (with a thickness in the range of hundreds of nanometers), ii) to allow metal-to-metal bonding of the semiconductor to a metallized diamond (or SiC) heat spreader (Fig. 14(b)) [Perez et. al., 2010; Rantamäki et. al., 2013]. Furthermore, the bonded assembly undergoes etching in a solution specifically targeting the substrate material, thus exposing the active region to air (Fig. 14(c)). The last step of flip-chip processing (Fig. 14(d)) is soldering the semiconductor/diamond assembly to a temperature-stabilized copper block.

Contrary to the IC heat spreader approach, the flip-chip method allows manufacturing of VECSELs at the wafer scale, and it also avoids the usage of the expensive optical grade diamond. However, despite the many advantages the flip-chip approach can offer, it requires additional design and processing aspects to be taken into account. One of the main considerations for a flip-chip design is related to the thickness and thermal conductivity of an available DBR for the particular wavelength region. AlAs/GaAs DBRs are considered to be advantageous, since AlAs and GaAs offer the highest refractive index contrast available ($n_H$=3.5 $n_L$=2.9), maintaining perfect lattice matching to a GaAs substrate. Large refractive index contrast permits reduction of the number of pairs needed for achieving 99.9% reflectivity and, thus, reduces DBR thickness, which leads to lower thermal impedance of a DBR, vital for an efficient flip-chip. One potential disadvantage is that the DBR, however thin, still remains an additional barrier between the active region and the cooling manifold representing a thermal impedance. In practice, the advantage of cost/processing and power scalability of flip-chip approach, outweigh the volume-limited cooling of the IC approach.

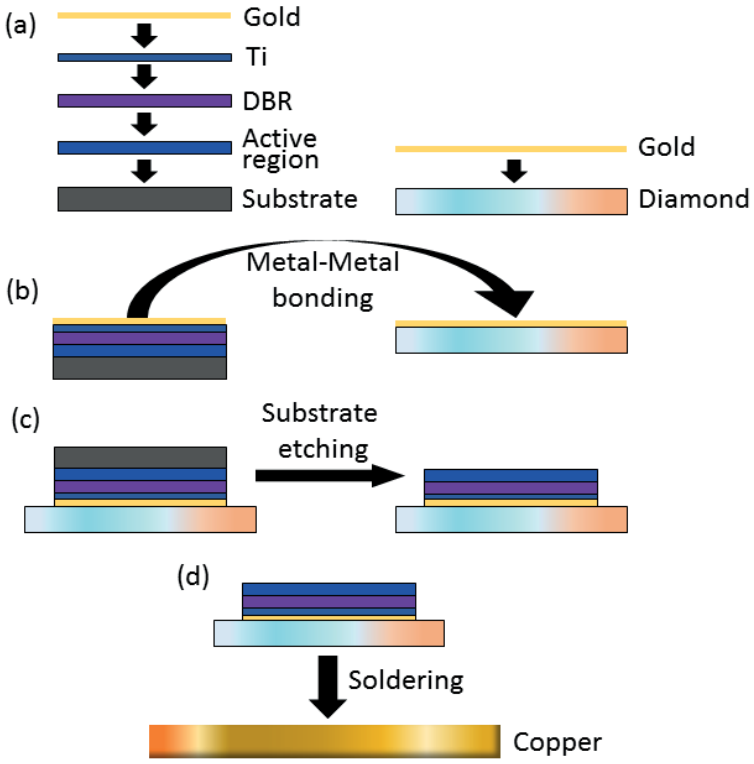


**Figure 14.** Schematics of the flip-chip manufacturing. Where: (a) MBE/MOVPE deposition of an active region and a DBR onto a substrate, with the subsequent metallization by Ti (optional) and gold (left), and diamond metallization by gold (right); (b) metal-to-metal bonding of a VECSEL chip to a diamond with an intermediate gold layer; (c) substrate etching of the bonded assembly; (d) metal soldering of the VECSEL/diamond assembly to a water-cooled copper block.

In such a way, the AlAs/GaAs DBRs are practical and easy to integrate into GaAs-based VECSELs with emission spanning from 880 nm up to 1.3 μm (which is a limit for long wavelength emission of GaAs-based VECSELs). Meanwhile, VECSELs with emission shorter than 880 nm resort to AlAs/AlGaAs DBRs, which possess smaller refractive index contrast as a penalty for higher bandgap AlGaAs layers. Hence, when moving towards emission with shorter wavelengths, DBRs exhibit increased thickness and thermal resistivity (due to AlGaAs compounds having inferior thermal conductivity when compared to both AlAs and GaAs [Harrold et. al., 1994]). In that case, thermal conductivity of such DBRs can be increased by reducing the number of pairs and compensating the lacking reflectivity with highly reflective metal layers, such as, Al, Ag, Au [Rantamaki et. al., 2015]. Such metal layers

also serve as pump light reflectors, recycling part of unabsorbed pump light back into the active region.

Another practical aspect of flip-chip design and fabrication is to match the coefficients of thermal expansion (CTE) between the DBR, the intermediate metal/dielectric layer, and the heat spreader [Moutanabbir et. al., 2010]. Since the gain mirror bonding to a heat spreader is performed under elevated temperatures, CTE mismatch can introduce strain into an assembly upon cooling of unevenly shrunken volumes. Rapid thermal dynamics of a pumped spot can lead to strain relaxation resulting in gain mirror de-bonding from a heat spreader with subsequent thermal damage, and by this leaving a burnt spot compromising operation in that chip area. Fig. 15 demonstrates such an occurrence, where Fig. 15 (a) shows photograph of a flip-chip before operation and Fig. 15 (b) shows photograph of the flip-chip after operation, where the burnt spot can be clearly visible.

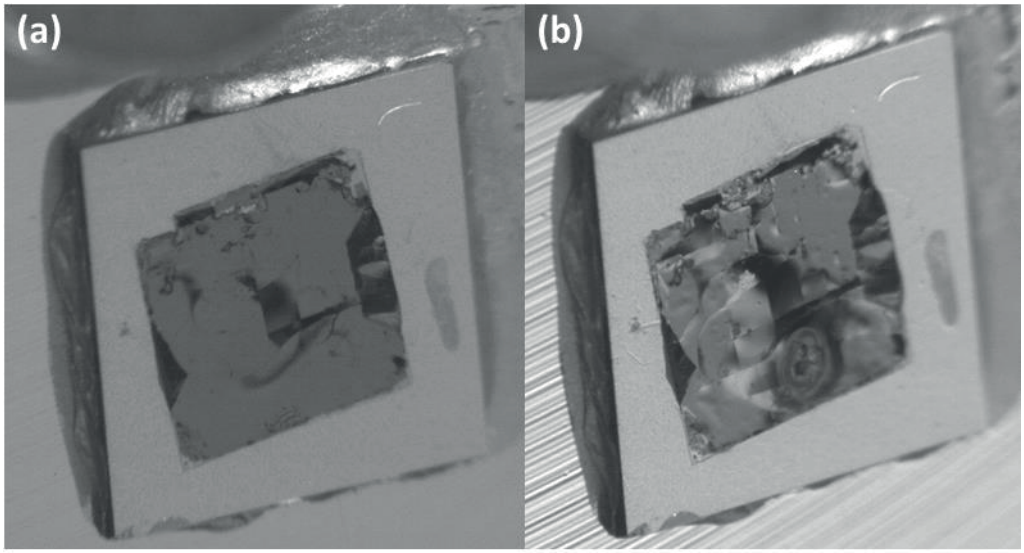


**Figure 15.** Flip-chip before (a) and after operation (b) demonstrating gain mirror de-bonding and subsequent developing of the burnt mark at the pumping spot at the bottom of a chip.

## 2.5 Wafer-fusion

As it has been mentioned before, GaAs/AlAs DBRs are considered to be superior due to large refractive index contrast between pairs, which allows achieving the highest reflectivity by employing lower number of mirror pairs. However, the fact of

GaAs/AlAs lattice matching to a GaAs substrate limits its use for VECSELs with emission longer 1.3 μm, where usually InP-based AlGaInAs QWs with much larger lattice constant are employed [Karim et. al., 2000]. Typically, materials lattice-matched to InP suffer from poor refractive index contrast, which results in thick DBRs with inferior thermal conductivity [Lindberg et. al., 2005]. Thus, conventionally, for VECSELs with emission wavelength greater than 1.3 μm, separate growth of a GaAs-based DBR and an InP-based active region sections is practiced, which is followed by the subsequent bonding of these two wafers [Sirbu et. al., 2011] using so-called wafer-bonding techniques. In this thesis, the wafer-fusion, which can be classified as a direct bonding method, was applied for combining GaAs and InP wafers. Wafers prior to the fusion are carefully cleaned and treated by acids in order to remove oxide layers. The fusion process is performed at the temperatures exceeding 500 °C and under the pressures in the range of 3 kPa-3 MPa. Such wafer-fusion technique, first applied to the long-wavelength VCSELs, enabled record emission at the challenging wavelength range of 1.2-1.6 μm [Lyytikäinen et. al., 2009; Rautiainen et. al., 2008].

## 2.6 Optical pumping

As it has been mentioned in the introductory section, optical pumping offers numerous advantages, namely, precise mode control and power scaling capabilities, as well as avoiding the necessity of material doping and electrical contacts processing. Pumping of a VECSEL is implemented in either two ways: barrier-pumping or in-well pumping, illustrated in Fig. 16. Conventional barrier pumping (Fig. 16(a)) is implemented by means of a pump laser with photon energies that are higher than bandgap energies of the barriers, thus making the active region structure heavily absorbing within the whole volume. In the case of barrier-pumping, the absorbed photons of higher energy create electron-hole pairs along pump beam path, which subsequently diffuse into lower energy states, until they finally get trapped into QWs, where they radiatively recombine. A RPG section must be carefully designed with regard to a pump laser of choice. Thus, the number of QW groups (and number of QWs per group), as well as the thickness of cladding layers should be engineered in a fashion to keep all QWs pumped equally. At the same time, pump light has to be sufficiently absorbed within the active region in order to refrain its leakage into the DBR (especially if the DBR absorbs pump wavelengths).

On the other hand, the in-well pumping (Fig. 16(b)) involves a pump laser with photon energies lower than the barrier bandgap and higher than the QWs bandgap. Thus, the absorption of the pump light occurs solely in the QWs with little heat generation due to the negligent quantum defect compared to the barrier pumping. However, the very small volume of QWs results in a weak one-pass absorption of pump light. Hence, multi-pass pumping configuration are often employed for the in-well pumping, by means of recycling the pump beam multiple times within an active region [Beyertt et. al., 2007]. For this, the DBR stop-band must extend to the pump wavelengths to permit multiple passes for the pump light. By means of the in-well pumping, record output powers were demonstrated, owing to reduced internal heating [Mateo et. al., 2016].

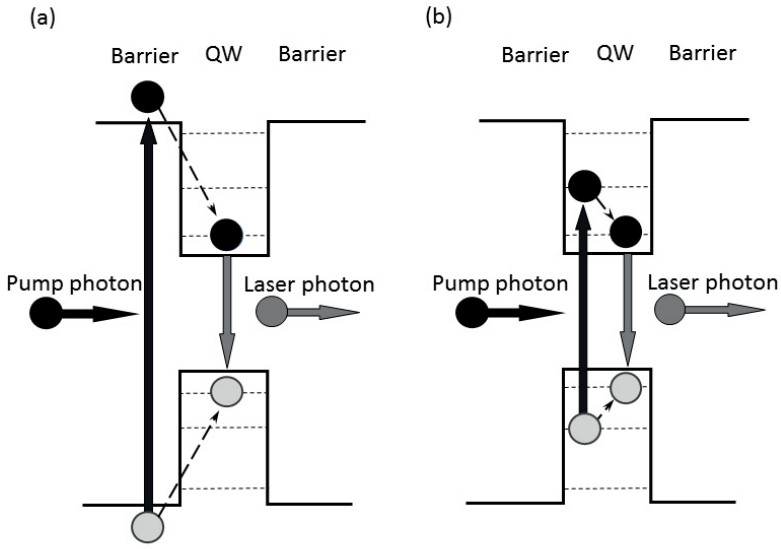


**Figure 16.** Optical pumping schemes of VECSELs: (a) the barrier pumping and (b) the in-well pumping. The pump photon energy in (a) exceeds that in (b).

Generally, the design parameters of an active region of a VECSEL relies on the available pump lasers, since the active region design offers more flexibility than the emission wavelength of a pump laser. Pump lasers constitute the biggest part of a VECSEL overall cost, even though inexpensive commercially available multimode lasers are usually employed for VECSEL pumping. For instance, mid-IR and IR VECSELs are usually pumped with either 808 nm or 980 nm pumps. Advanced development of these lasers over the years has been motivated by the need for

efficient laser pumps for solid-state lasers (for pumping Nd and Yb ions) [Hughes et. al., 1992] and fiber lasers and amplifiers [Laming et. al., 1989]. Due to this, VECSELs heavily benefit from widely available inexpensive laser diode pumps with long lifetime at these wavelengths. Overall, VECSELs have relatively relaxed requirements for the pump light source parameters, contrary to solid-state lasers, where efficient absorption concentrated over narrow wavebands or happens at a certain polarization of pump light (Ti:Sapphire, Nd:YAG, Alexandrite) [Fan et. al., 1988]. Furthermore, due to the thin-disk geometry of VECSELs (with thicknesses in the range of microns), there is no need for sophisticated pump optics in order to maintain an even longitudinal pump light profile inside the active region, unlike with solid-state lasers, where active media rods have dimensions in the range of millimeters to centimeters [Koechner et. al., 2006].

On the other hand, the optical pumping of VECSELs emitting in the visible range is becoming more restrictive due to the scarce availability and the high-cost of pump sources. Frequency-doubled diode-pumped solid-state lasers (DPSSL) emitting at 532 nm have been a typical pump source for many systems, including visible direct-emitting VECSELs [Hastie et. al., 2005] and Ti:Sapphire lasers [Ell et. al., 2001]. Ironically, the commercial frequency-doubled IR VECSELs have become viable and lower-cost alternative for the DPPS lasers at the same wavelength ["Verdi G-Series | Coherent", 2019]. Recently, substantial progress in the development of high-power red laser diodes with emission around 640 nm has been achieved ["Coherent | DILAS: High-power diode lasers", 2019] and, by this, the pumping options for near-IR direct-emitting VECSELs are expanding.

## 2.7 VECSEL cavity

The external cavity significantly adds to the VECSEL functionality. Besides offering a possibility for mode control enabling high brightness, it offers a possibility of inserting IC elements for numerous purposes. The external cavity allows easy and effective reconfiguration depending on the requirements. Fig. 17 illustrates the most common VECSEL cavity configurations.

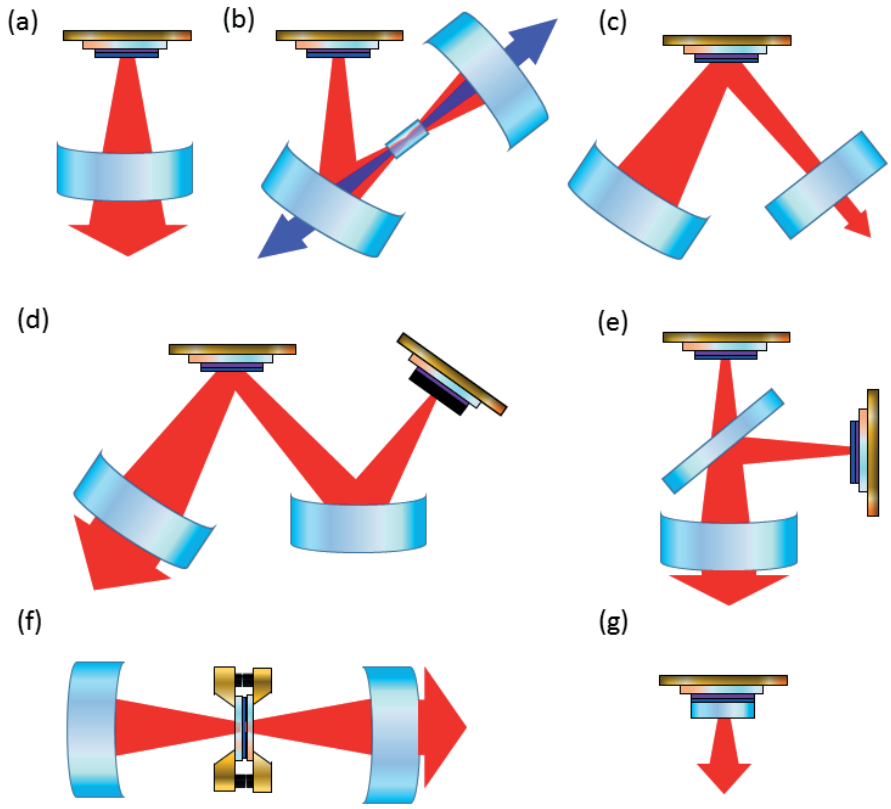


**Figure 17.** Conventional cavity geometries of VECSELs, where: (a) a linear cavity; (b) a V-cavity; (c) a V-cavity with a gain mirror as a folding mirror; (d) a Z-cavity with a SESAM; (e) a T-cavity; (f) a linear cavity with DBR-free VECSEL in transmission; (g) a microchip cavity. The pump optics and pump light was not depicted here for the sake of schematic clarity.

Fig. 17(a) schematically illustrates a generic linear cavity or I-cavity, which comprises a curved output coupler mirror and a VECSEL gain mirror. The laser mode geometry and cavity mode size at the gain mirror surface is defined by a radius of curvature (RoC) of the output coupler and a distance between the gain mirror and this mirror. Translational movement of an output coupler perpendicularly to the gain mirror surface plane is used to adjust the resonator mode size. The V-cavity depicted at Fig. 17(a, b) allows usage of one curved and one flat mirror or two curved external mirrors. The possibility to use a flat output coupler is considered beneficial due to the wider selection and availability of flat couplers rather than curved ones. A V-cavity with two curved mirrors allows forming the mode waist inside the cavity,

which creates very high intensities of electric field, favourable for non-linear effects (frequency conversion, etc.). Fig. 17 (c) is a V-cavity with a gain mirror serving as a folding mirror. Positioning of a gain mirror at an angle, changes the optical thicknesses of an active region and a DBR. Therefore, such configuration allows manual shifting of the DBR stop band and adjustment of the micro cavity resonance as a function of the folding angle [Zhang et. al., 2017]. A Z-cavity (Fig. 17(d)) can be considered as the most flexible geometry, with five adjustable parameters (two RoC and three distances). The Z-cavity is instrumental for mode-locking, where it is crucial to create adjustable mode waists onto the both flat components (gain mirror and SESAM located at the right end of the cavity). Fig. 17(e) represents, a so called T-cavity, or a multi-chip interferometric cavity, where two interferometer arms creating Michelson interferometer can be considered as the linear cavities, which are coupled via a beam splitter [Nechay 2017]. Multichip cavities allow bypassing the thermal roll-over limitations set for one chip and, thus, increases the power scalability of VECSELs [Chilla et. al., 2007]. Fig. 17(f) shows a DBR-free [Yang et. al., 2016] or membrane external cavity surface emitting laser (MECSEL) [Kahle et. al., 2016], which does not employ the on-chip mirror, but instead it, operates in transmission. Such scheme permits superior thermal management in addition to the possibility of double-sided pumping [Kahle et. al., 2019]. A microchip VECSEL is shown at Fig. 17(g). In this particular case, the VECSEL cavity is composed of a DBR and, typically, a dielectric coating deposited onto the outer surface of an IC heat spreader. A microchip VECSEL allows quite limited mode control, since there are no adjustable parts. Mode control in such case is mainly implemented through thermal lensing [Kemp et. al., 2006]. On the other hand, single-frequency operation is more easily achievable in a microchip VECSEL due to the short resonator and therefore, the large FSR.

# 3 RESULTS FOR THE 750 NM DIRECT-EMITTING VECSELS

The very first demonstration of a direct-emitting VECSEL at the 7XX nm wavelength range was done with InP QDs, although quite modest output powers (in the range of tens of miliWatts) were achieved [Schlosser et. al., 2009]. First Watt-level output powers were demonstrated by means of the SHG from 1500-1580 nm VECSELs [Rantamäki et. al., 2012; Saarinen et. al., 2015]. Although, such an approach allowed achieving two orders of magnitude power increase, it is not efficient for frequency conversion to the UV, since forth-harmonic generation is substantially less efficient when compared to second-harmonic generation. Thus, this combination of factors has motivated the development of the direct-emitting VECSELs at this range.

Several semiconductor heterostructure architectures have been proposed for 750 nm VECSEL realization depicted at Fig. 18. Fig. 18 (a, b) shows QW design solely involving AlGaAs compounds, with different Al content for barrier and well layers, which influence carrier confinement. Obviously, the design depicted in Fig. 18 (b) is advantageous over (a) since it provides a higher level of confinement, which is beneficial for operation at elevated temperatures. Another approach, involving the same QW composition, but AlGaInP barriers, (Fig. 18(d)) possesses better confinement, especially for holes. Thus, these two designs involving AlGaAs/AlGaAs and AlGaAs/AlGaInP QWs were selected for implementation.

AlGaInAs QWs (Fig. 18 (c, e)) were not grown due to increased complexity in epitaxy

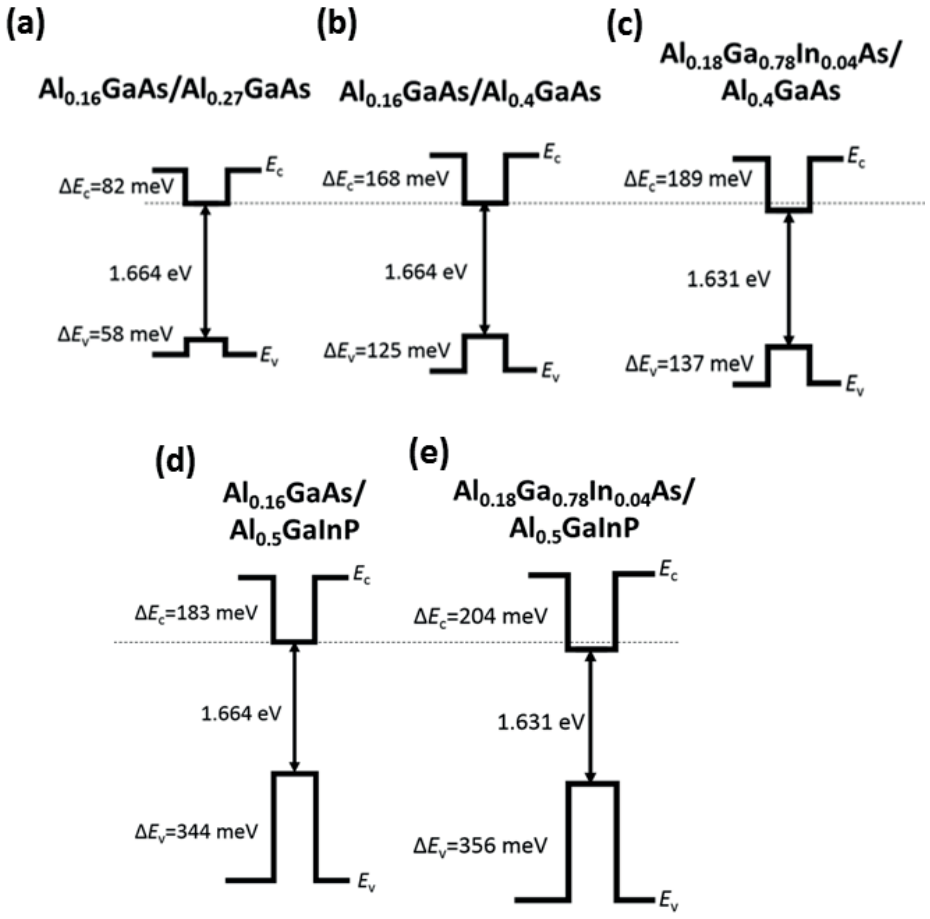


**Figure 18.** Different proposed QW/barrier heterostructures designed for emission at 750 nm with increasing electron and hole confinement from *a* to *e*.

The initial growth implementation of all-AlGaAs structures, performed by means of MBE with different microcavity resonances, did not yield operating VECSELs. Extensive characterization and post processing procedures were applied to the grown VECSEL structures. For instance, a sequence of rapid thermal annealing (RTA) treatments was performed to the structures in order to improve the gain structure's crystal quality and thus to improve radiative properties. The RTA treatment recipe for the temperature and the treatment time have been experimentally developed. Fig. 19 shows a chart of PL intensity before and after

RTA treatment of different durations and temperatures. Before treatment, all VECSEL chips (3x3 mm$^2$) were coated with a 200 nm $SiO_2$ protective cap layer in order to prevent As diffusion from the structure surface, which was etched after treatment by buffered HF acid (BHF).

As it can be seen from Fig. 19, the RTA treatment at 550 °C for a duration of 3 minutes has been found to be the optimum, yielding the highest increase in PL intensity. Several chips underwent the same RTA treatment in order to obtain statistically averaged data.

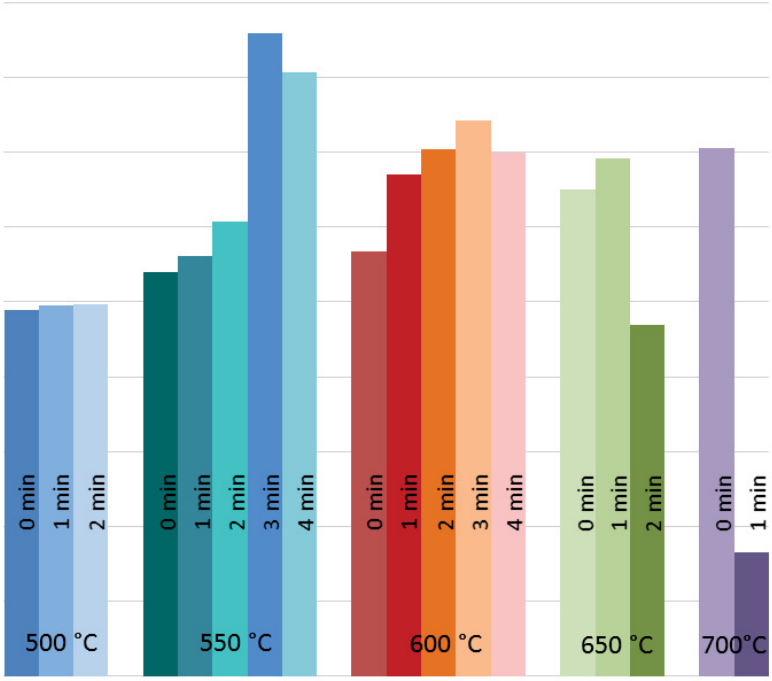


**Figure 19.** PL intensity recorded after RTA treatments of different duration and temperature. The initial intensities of chips differ due to varying pumping conditions provided by the PL mapper. The correspondent altered intensities of the chips after the RTA treatment were normalized to the initial intensity of the particular chip, thus revealing the change of intensity as a result of a chosen treatment.

In spite of the PL intensity increase after RTA treatment, lasing with the treated chips was still not achieved. Time resolved PL (TRPL) characterization was performed with the aim of measuring the carrier lifetime of the VECSEL structures. Fig. 20 shows the results of the VECSEL structures in comparison with a lasing reference sample at 1180 nm. As seen from Fig. 20, the 750 nm VECSEL

demonstrated substantially lower carrier lifetime in comparison to a strain-compensated 1178 nm lasing sample. Not achieving lasing with these structures can be assessed as a consequence of short carrier lifetime.

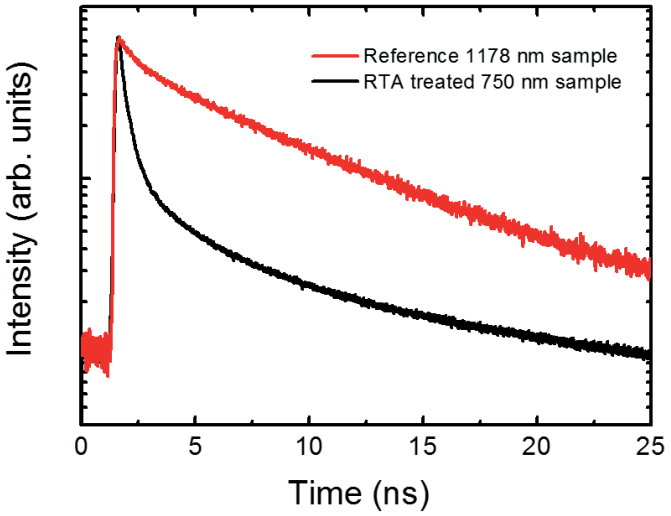


**Figure 20.** Time resolved PL of an RTA treated 750 nm VECSEL in comparison with lasing reference sample @1178 nm, showing substantially lower carrier lifetime of the 750 nm VECSEL.

After the first unsuccessful growth sequence of VECSELs, improved designs of VECSEL gain mirror were proposed. In particular, additional outer cladding layers with higher bandgap energies were integrated into the structure for better charge carrier confinement in the QW groups. Fig. 21 illustrates the bandgap profile of the two gain mirror designs: the first one involving an all-AlGaAs structure (a) [P1]; and the second structure with AlGaAs QWs and barriers, and AlGaInP cladding layers (b)[P2]. The both structures were realized, although with slight modifications, namely: the all-AlGaAs structure targeted longer wavelength emission (approximately at ~770 nm), whereas the AlGaAs/AlGaInP structure was meant to cover shorter wavelength side (with targeted emission at ~755 nm).

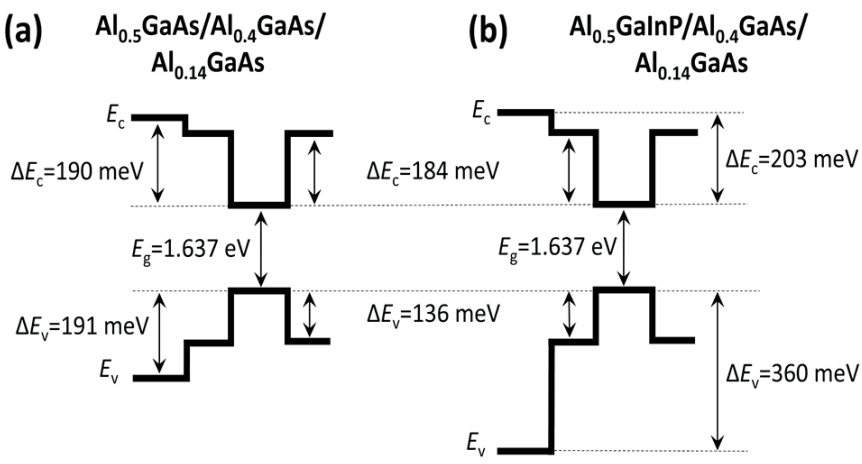


**Figure 21.** Bandgap profile of the next generation active region design of the 750 nm VECSELs [P2], illustrating comparison of electron and hole confinement when utilizing different cladding layers, namely AlGaAs (a), and AlGaInP (b).

This new generation of 750 nm VECSELs successfully lased and demonstrated multi-Watt laser emission [P1, P2]. Fig. 22 shows a long-exposure photograph of VECSEL operation in a linear cavity (pump light is filtered out from the photograph).

Fig. 23 shows an exemplary cross-section SEM photograph of the AlGaAs/AlGaInP structure. Fig. 24 shows the output power characteristics of the all-AlGaAs (a) and the AlGaAs/AlGaInP (b) VECSEL. The both wafers were cleaved into chips with size of 2.7×2.7 $mm^2$. The chips were, in turn, capillary bonded to the IC uncoated flat diamond with the lowest birefringence among the available diamonds. The dimensions of the IC diamond were 3×3×0.35 $mm^3$. The bonded chip-diamond assembly was then pressed against a copper heatsink mount with an aperture (with a diameter of ~2 mm). Indium foil was placed, in between the diamond-chip assembly and the copper heatsink plate to reduce thermal resistivity of the heat path. Subsequently, the chip-diamond assembly was clamped down to ensure the bonding (Fig. 10(a)). The heatsink temperature was kept at 14 °C during all experiments. The linear cavity was created with a curved output coupler with RoC of -100 mm (Fig. 22). The output coupler mirror was placed at a distance of 99.8 mm to create a pump-spot-matching mode size on the gain mirror surface. The highest output powers were achieved by utilizing a 3% output coupler, while the optimal pumping spot diameter for both structures was found to be around 62 μm.

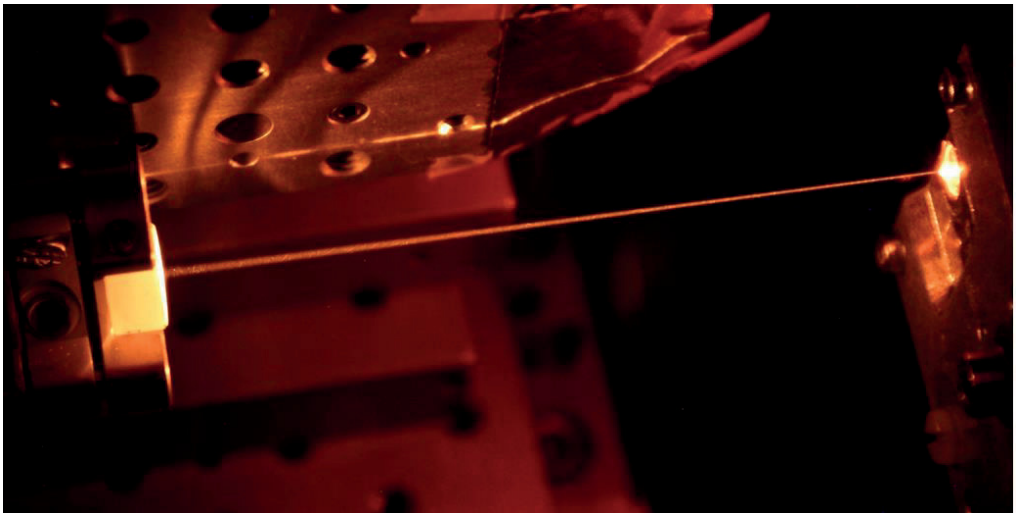

**Figure 22.** Long-exposure photograph of 760 nm VECSEL operating in a linear optical cavity composed from VECSEL gain mirror assembly (right) and output coupling mirror (left) [P1]. Green pumping light was filtered out by means of a long-pass filter.

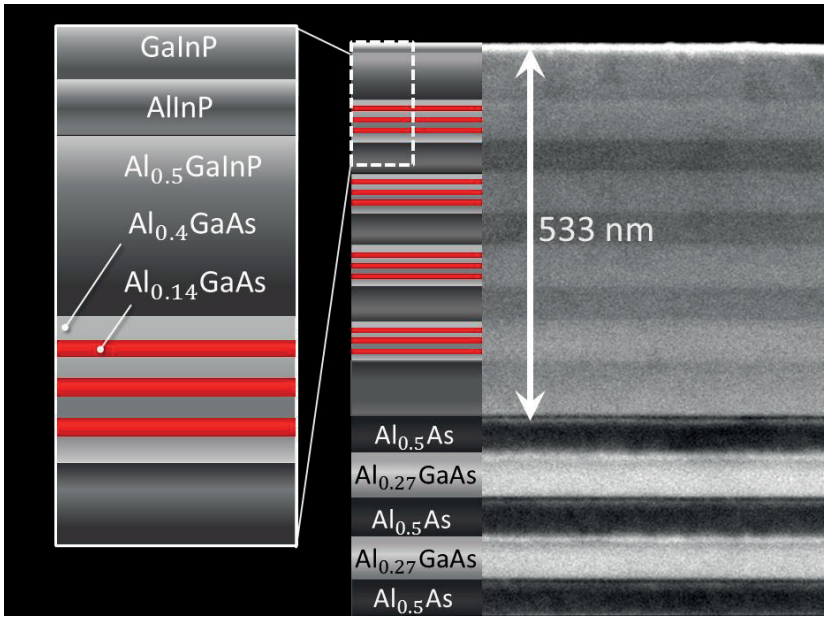


**Figure 23.** SEM cross-section of the AlGaAs/AlGaInP VECSEL active region (top) and part of the DBR (bottom).

Fig. 25 shows the tuning measurements that were performed in the V-cavity by means of inserting a birefringent filter with a thickness of 0.5 mm, where Fig. 25 (a) corresponds to the all-AlGaAs structure and Fig. 25 (b) to the AlGaAs/AlGaInP structure. Output spectra and power were measured as a function of birefringent filter rotation. Furthermore, the spectra were normalized and subsequently multiplied by the correspondent optical power values, thus resulting in a graph where the height of each spectral plot is linked to the output power values.

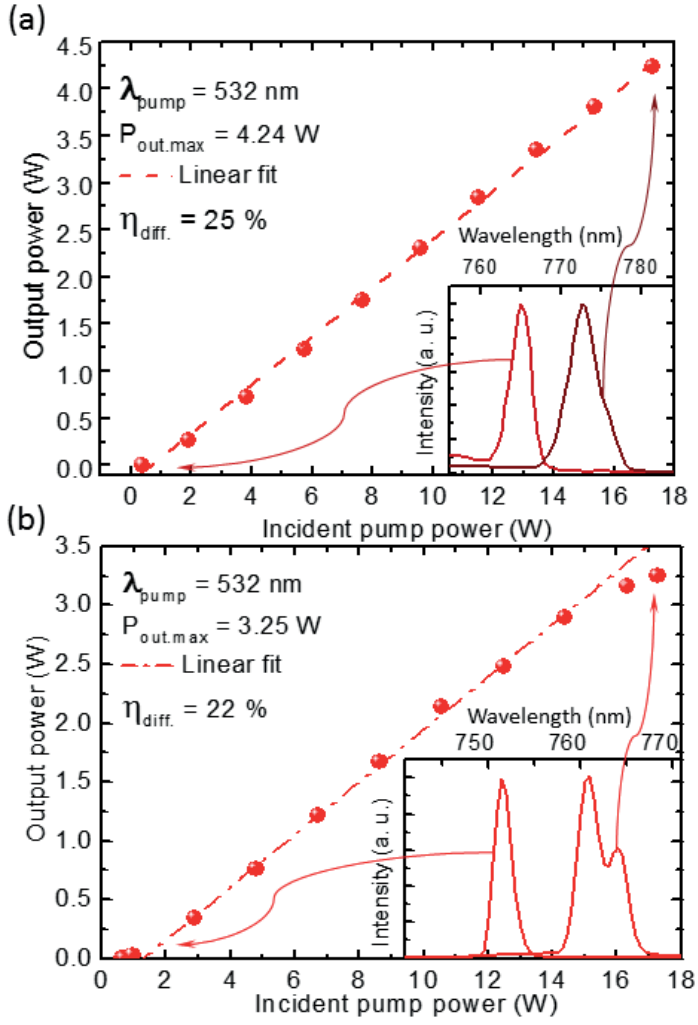


**Figure 24.** Power characteristics of the all-AlGaAs (a) and the AlGaAs/AlGaInP VECSELs (b) [P1, P2]. Insets of (a) and (b) show spectra near threshold and thermal-roll over in order to illustrate the spectral shift.

Thus, the AlGaAs QW direct-emitting structures have surpassed the previous results of the direct-emitting VECSELs at the same wavelength range by a factor of ~100 [Schlosser et. al., 2009], yielding a maximum output power of 4.24 W (with the central wavelength around 770 nm) [P1] and 3.25 W (with the central wavelength around 755 nm) [P2].

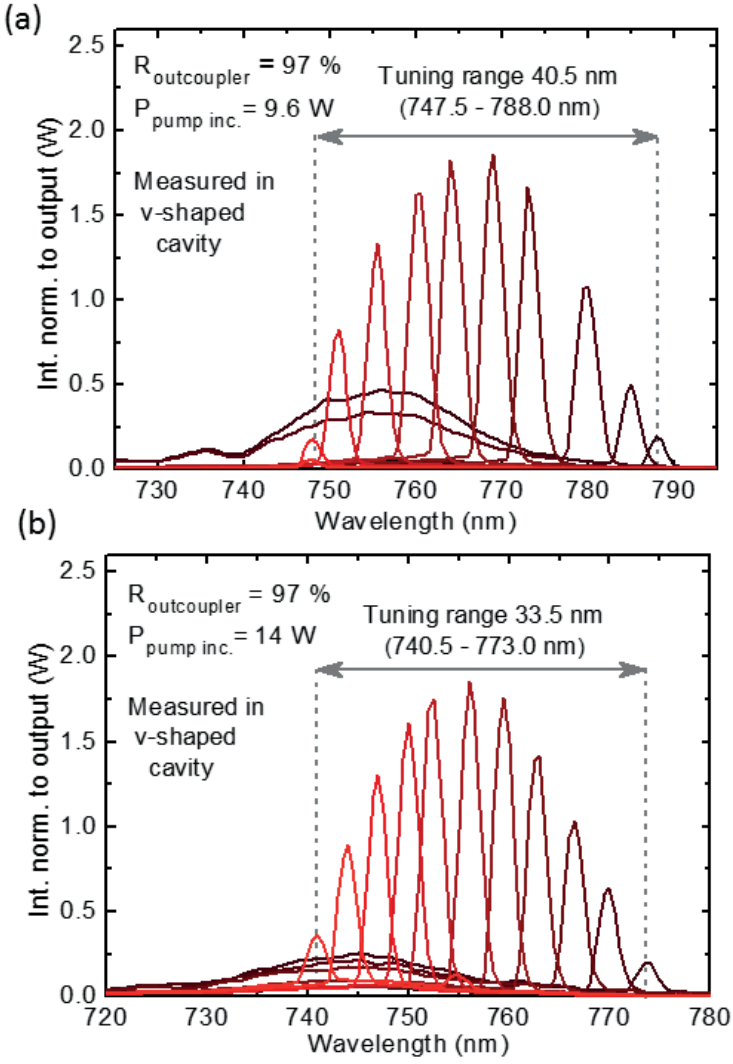


**Figure 25.** Tuning characteristics of the all-AlGaAs (a) and the AlGaAs/AlGaInP VECSEL (b) [P1, P2].

The reflectivity profile of the OC mirror was quite flat within the whole tuning range and even wider (stopband of ~100 nm @760 nm), therefore, we assume the gain profile was a limiting factor for the tuning range, especially when the laser was tuned to the shorter wavelength side (Fig. 9 shows the DBR stopband). The usage of an HR mirror would probably increase the tuning range, especially for the operation at the longer wavelength side, by decreasing intracavity losses and thus increasing the band for net gain.

Despite such notable output power increase, the direct-emitting structures with AlGaAs QWs exhibited certain drawbacks. One of the major drawbacks was short laser lifetime. Upon exposure to pump light, the maximum output power of the laser started to decline at a steady rate. Fig. 26 shows the measured output power as a function of time. The linear fit curve showed a degradation of 11% of initial output power per hour. The substantial power drop that occurred after around 7 minutes of operation can be attributed to a switch from single mode operation to multimode operation due to laser mode form redistribution. Such mode redistribution can be considered as a more detrimental factor compared to the steady linear power degradation, since the former destroys high-brightness operation of the VECSEL.

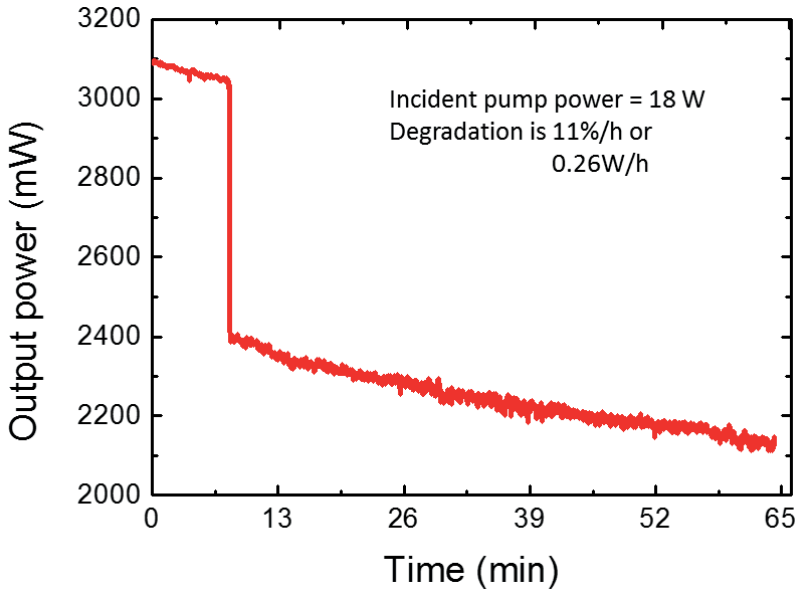


**Figure 26.** Output power of the AlGaAs/AlGaInP VECSEL as a function of time. The recorded curve illustrates laser structure degradation and steady output power decrease as a result after initial single-spatial mode collapse.

Degradation of the VECSEL structures could also be observed by means of the previously discussed large area PL imaging. Fig. 27 shows large PL photographs of the structure before (a) and after the laser operation (b).

Furthermore, the AlGaAs/AlGaInP VECSEL structure exhibited peculiar polarization behavior [P2]. The polarization as well as the beam profile of the laser took different orientation and form when measured across the chip. Laser beam profiles recorded at the different chip location are demonstrated in Fig. 28, showing high-order spatial mode structures visible, as well as photographs of output beam peculiarities — in the form of spurious light emission. The beam profiles were taken behind the OC mirror with an OPHIR Beamstar-FX-66-NT beam profile camera.

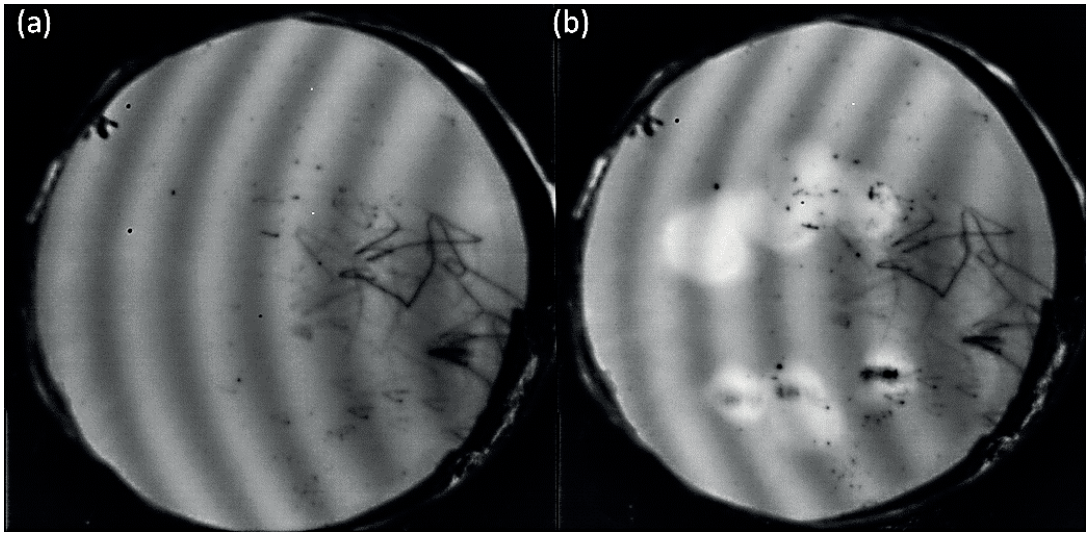


**Figure 27.** Large area PL macrophotograph of the 755 nm VECSEL before (a) and after (b) operation, demonstrating degraded areas, which correspond to pumping spots. Dark lines at the right side of the photograph correspond to surface scratches resulted from a bonding process.

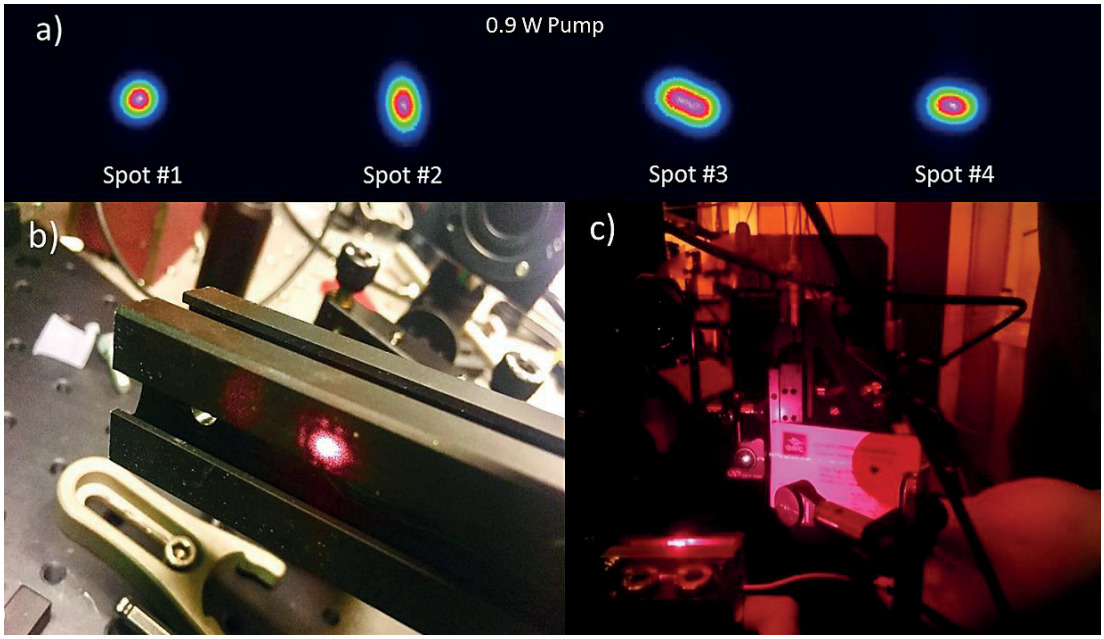


**Figure 28.** VECSEL beam profile variation across a chip recorded under the incident pump power of 0.9 W (a) [P2]. Photograph of the output beam with visible halo around it (b) and photograph of the cavity showing signal light scattering off the gain mirror in horizontal plane (photograph done by means of long-pass filter, filtering green pump laser) (c).

Thus, further experimental investigation of the polarization behavior of the structure (experimental setup shown at Fig. 29) was carried out due to the manifestation of these beam profile polarization and structural instabilities. Here, a polarizer was fixed at a certain position (Orientation I in Fig. 29(a)) corresponding to laser polarization immediately after the laser threshold was reached. After that the pump power was gradually increased, while the output power transmitted through the polarizer was simultaneously recorded, as well as the VECSEL beam profile. Furthermore, the polarizer was set to the orthogonal orientation (orientation II in Fig 29 (b)) and the experiment was repeated.

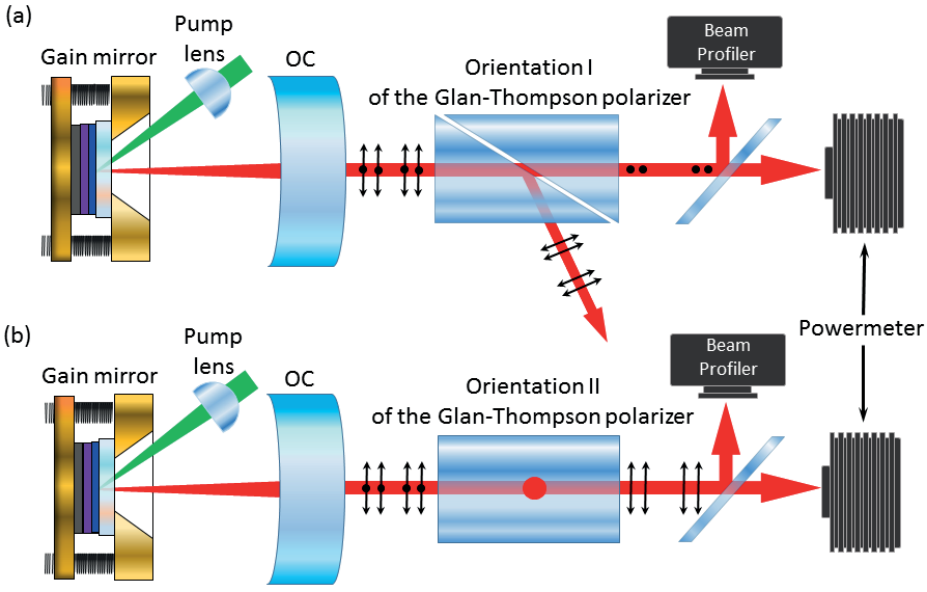


**Figure 29.** Schematics of the experimental setup used for the investigation of the VECSEL polarization behavior under the increasing pumping. The output of the VECSEL was polarized by a Glan-Thompson polarizer with extinction ratio of 100000:1.

The resultant output power curves were plotted in Fig. 30. As it can seen from the figure, there is an inverse feedback between the output power at orthogonal polarizations and pump power. Two conclusions can be drawn from the experiment: the first is that the polarization of the laser is not stable and it changes under the increase of pump power, and the second is that mode competition between orthogonal polarization modes is occurring. The beam profiles recorded at the same pump power but at the different polarizer orientations suggest non-overlapping intensity distribution of orthogonal polarization modes within the pump spot.

Intracavity elements have the strongest impact on the polarization orientation of the VECSEL output. Intracavity heat spreader (if utilized) can contribute to the polarization selectivity, due to its residual birefringence or wedge. Thus, in the absence of polarization selective elements inside the cavity, polarization orientation of VECSEL is typically defined by the QW/QD gain anisotropy, as a consequence of the strain (if any). In this case, polarization orientation is aligned to the crystal axis, which are parallel to the growth plane. However, the polarization orientation switching under the increase of pump power is not a typical behavior of VECSELs.

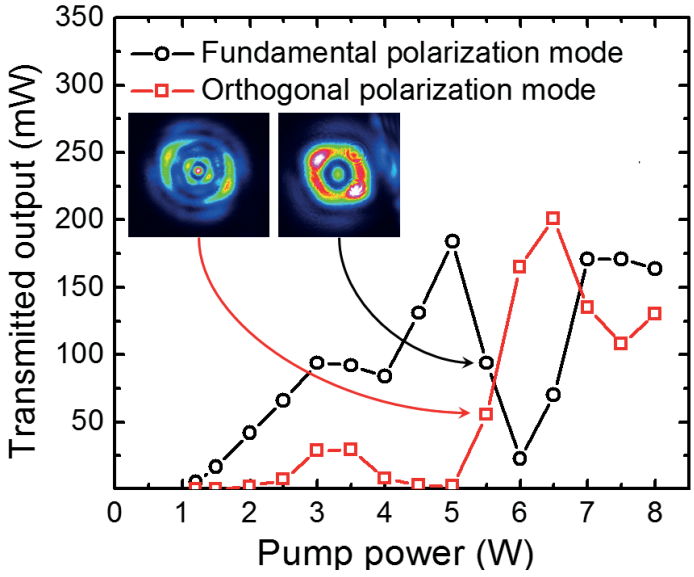


**Figure 30.** Output of the VECSEL measured as a function of pump power through a polarizer set in two orthogonal orientations. The laser mode with polarization orientation established at the laser threshold is called fundamental polarization mode [P2]. Insets reveal beam profiles at orthogonal polarizations under the same incident pump power.

Fig. 31 shows the beam profile sequence of the transmitted output, recorded as a function of increasing pump power. In this case, the output was transmitted through the polarizer, which was set to transmit the fundamental polarization mode (mode with polarization orientation established at the laser threshold). Therefore, the beam profile sequence corresponds to the red curve from the previous figure, Fig. 30.

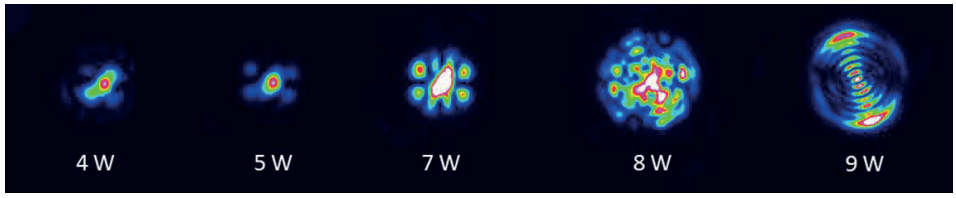


**Figure 31.** The beam profile evolution of the orthogonal polarization mode transmitted through the polarizer under increasing pump power [P2].

The polarization instabilities of AlGaAs/AlGaInP VECSEL can be attributed to the ordering effects of the AlGaInP claddings [Moritz et. al., 1995; Gomyo et. al., 1988.]. Ordering of AlGaInP and GaInP material is a studied phenomena occurring in these

particular material systems and leads to bandgap shrinkage and ordering-induced birefringence due to the breaking of crystal cubic symmetry [Wirth et. al., 1998.]. Although the AlGaInP layers play a passive role serving as pump-absorbing layers, they constitute the majority of active region volume of a VECSEL and thus greatly influence the laser operation.

In conclusion, the 750 nm direct-emitting VECSELs exploiting AlGaAs QWs permitted achieved multi-Watt level output powers, which are two orders of magnitude higher compared to that of the previously demonstrated QD-based VECSEL. However, low laser lifetime, mode redistribution due to material degradation, and polarization instabilities render the state-of-the-art direct-emitting VECSELs impractical. This is especially true, as one of the key prospects of the 750 nm direct-emitting VECSEL is the possibility for frequency conversion down to the UV waveband, which in this case cannot be efficiently implemented with these structures, due to aforementioned drawbacks.

# 4 1.5 μM WAFER-FUSED VECSELS

Semiconductor lasers emitting at 1.5 μm are traditionally associated with optical fiber-based telecommunication technologies. The wavelength-dependent loss mechanism of the silica fiber, with minima centered at 1.55 μm, has driven the rapid world-wide development of transceivers and amplifiers. The development timing of low-loss fibers [Miya et. al., 1979] coincided with a breakthrough in semiconductor lasers. Thus, the optical communication systems have employed InP-based diode lasers with emission at 1.5 μm as transmitters, stimulating great advances in this type of semiconductor laser. In the context of this thesis InP-based 1.5 μm VECSELs were developed and studied as a viable alternative for achieving 750 nm emission via frequency doubling.

Typically, 1.5 μm emission can be generated by means of AlGaInAs QWs grown on an InP substrate. However, as it has been noted before, there is a notable lack of high index contrast materials that can be lattice-matched to InP. This fact results in DBRs of substantial thicknesses, which leads to poor thermal conductivity, rendering them impractical for implementation in a flip-chip configuration. Thus, in order to implement InP-based active regions with thin DBRs suitable for flip-chip configuration, wafer bonding of GaAs-based DBRs is applied. Worth mentioning here is that a VECSEL with a monolithically grown active region structure involving dilute nitride quinternary QWs (GaInNAsSb) and a GaAs DBR has been demonstrated [Korpijärvi et. al., 2015], although output powers achieved with that approach were very modest, in the order of hundreds of miliWatts.

The work here focused on 1.5 μm VECSELs has taken three main directions: the first one is the demonstration of a 1.5 μm flip-chip VECSEL which paves the way for inexpensive, mass-produced VECSELs at this wavelength range; the second one is the demonstration of a novel QD-based active medium, which has certain benefits in comparison to QWs; the third is the realization of frequency conversion from 1.5 μm to 750 nm.

## 4.1 Flip-chip wafer-fused VECSEL emitting at 1.5 μm

A flip-chip thermal management scheme can be considered superior over intracavity heat spreaders, as has been noted previously. However, realization of flip-chip VECSELs largely depends on the material system of the VECSEL. Thus, the main aspects that can impede obtaining flip-chip VECSELs are: a thick DBR with low thermal conductivity, and the availability of etchant/etch-stop combinations for precise layer processing and surface finish. The 1.5 μm VECSELs demonstrated in this thesis are composed from an InP-based active region and a GaAs-based DBR, which were combined by means of the wafer-fusion technique described in [Sirbu et al, 2011]. Thus, first separately grown wafers were brought together by applying force of 7000 N for 30 min under the temperature of 600 °C. After that, the resulting fused wafer underwent selective etching of the GaAs substrate to expose the DBR. Subsequently, the DBR was metallized first with 5 nm thick Ti layer and then with 150 nm thick Au layer. The same metallization was applied for the polycrystalline diamond submount. Afterwards, the fused structure was diced into chips, typically, with dimensions of 3x3 $mm^2$. Further metal-to-metal bonding of the chip to the diamond submount was executed. Finally, the bonded chip-diamond assembly underwent etching of the top InP substrate in HCl, by this exposing the top surface of the chip. After that, the assembly was ready for laser operation and was further mounted onto a cooled copper heatsink surface by means of silver paste. The resultant structure therefore had two wafer/fusion interfaces between thin films of semiconductors. Fig. 32 shows the flip-chip gain mirror structure [P3].

The presence of multiple fusion/bonding interfaces somewhat limits the potential manipulation and operational margins of the structure. Different CTEs of layers that are to be combined may lead to accumulation of strain upon cooling. Thus, if materials with closely matching CTE are not available, temperature of the fusion/bonding has to be decreased in order to mitigate any introduced strain levels. On the other hand, the CTE of the heat spreader can be tailored accordingly to the values of the semiconductor material, by means of using composite materials, for instance, a copper diamond composite [Yoshida et. al., 2004]. As discussed in chapter 2.4.2, unmatched CTE coefficients between the layers and the heat spreader, when combined at high temperatures, may lead to strain relaxation, followed by layer debonding, which result in thermal damage under intensive pumping. Such behavior was observed with the demonstrated 1.5 μm flip-chip VECSELs.

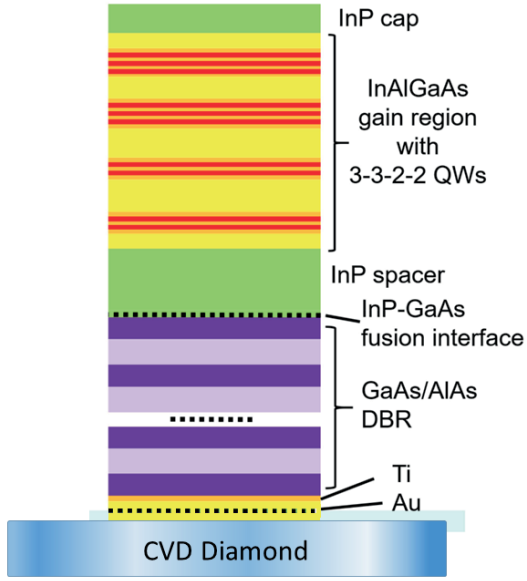


**Figure 32.** Schematic cross-section of the flip-chip gain mirror structure [P3]. The fusion and bonding interfaces are marked with doted long lines.

Fig. 33 shows a large area PL photograph of the flip-chip before operation (a), right after operation (b), next day after operation (c) and one week after operation (d). As it seen from the figure, the structure before operation already had already contained numerous of dark lines, presumably due to processing manipulations and handling. It is clearly visible that pumping resulted in optical damage of the structure, likely due to strain relaxation. Fig. 33 (b) shows four dark damaged areas with no photoluminescence that correspond to the four pumping spots (marked with dashed circles). Worth noting is that the structure continued developing new dark lines (marked with dotted-dashed circles in Fig. 33(c, d)), adjacent to the damaged areas, within the next week, even though flip-chip was not in operation since the second photograph (Fig. 33 (b)) was taken.

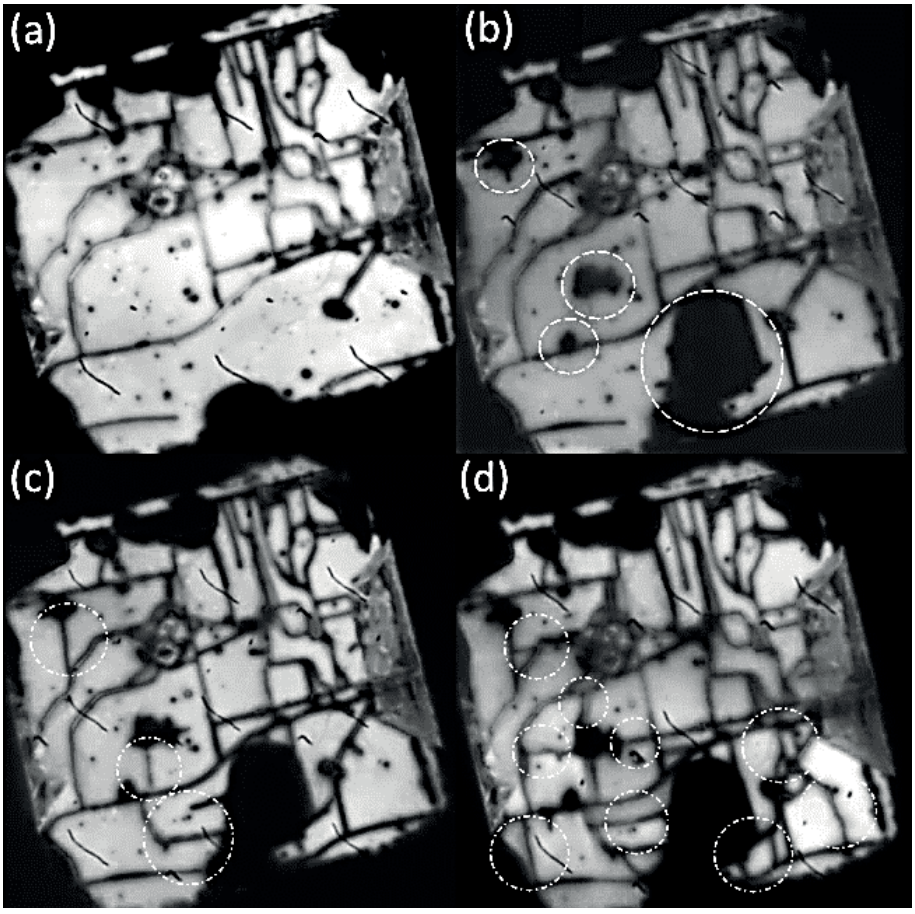


**Figure 33.** PL photograph of the flip chip: before operation (a); right after operation (b); one day after operation; (d) one week after operation. Dashed circles in (b) highlight damaged areas due to the pumping, whereas dotted-dashed circles in (c, d) highlight cracks, developed later.

Optimization of the semiconductor-to-heat-spreader bonding allowed better quality flip-chips to be achieved (Fig. 34 upper inset), which demonstrated 3.65 W of output power under 32 W of incident pump power [P3] (Fig. 34). However, the obtained values have not exceeded the record values achieved with the IC wafer-fused VECSELs with the similar active regions at the same wavelength range, reported in [Rantamäki et. al., 2012]. Although, in this work, when comparing to the IC chips, a substantial increase of the pumping spot size was possible, namely: 470 μm for the flip-chip, versus 220 μm for the IC chip. Thus, the bigger pump spot will enable further power scaling and eventually the results achieved with the IC VECSELs to be surpassed. A diamond heat spreader submount with larger dimensions can considerably increase heat extraction capabilities, delaying thermal

roll-over and allowing achievement of higher output powers, lying beyond the capabilities of the IC thermal management approach.

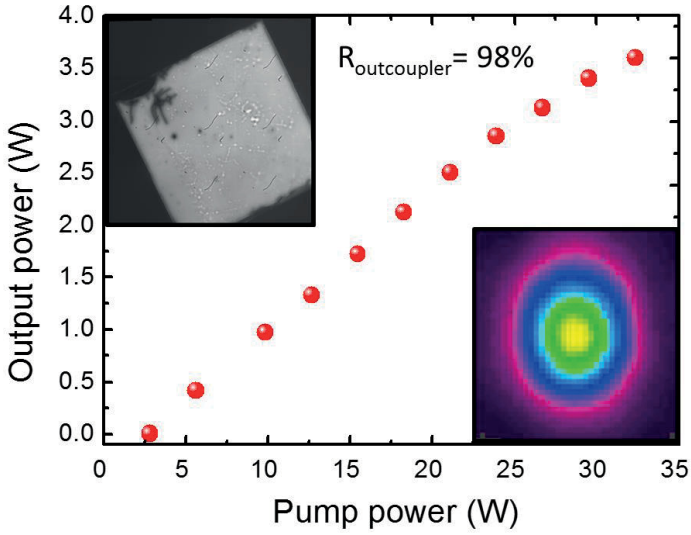


**Figure 34.** Output power of 1.5 μm flip-chip VECSEL as a function of nominal incident pump power. Upper inset shows the PL photograph of the good quality chip, while lower inset demonstrates recorded beam profile at 30 W of incident pump power. Results were published in [P3]

However, the structure has shown low tolerance for losses (the maximum output coupling ratio that could be used was ~3.5 %), which negatively affected the width of the tuning bandwidth (measured to be around 30 nm). The gain peak during tuning measurement, performed by means of inserting a birefringent filter, was tightly locked to 1537 nm, where supposedly the microcavity resonance of the structure was located. Interestingly, when the laser spectrum was forced to operate away from this resonance wavelength, a sudden spectral change was observed, shown in Fig. 35. As it seen from the figure, the spectrum possesses clear equidistant spacing, with the FSR of 1.68 nm, which coincides with the FSR that the backside diamond heat spreader would create. This fact suggests that some portion of the signal light is leaking through the DBR and creating feedback with the backside diamond heat spreader working as an etalon.

These facts are evidence that the DBR reflectivity is not optimized, since it transmits substantial amount of light through. Therefore, this constitutes one of the loss mechanism that should be mitigated in order to enhance the flip-chip performance. Utilizing Findlay-Clay analysis, the total intracavity losses (excluding

output coupler mirror transmission) are estimated to be more than 3%, which is a somewhat high number, explaining the quite low achieved power and narrow tuning curve.

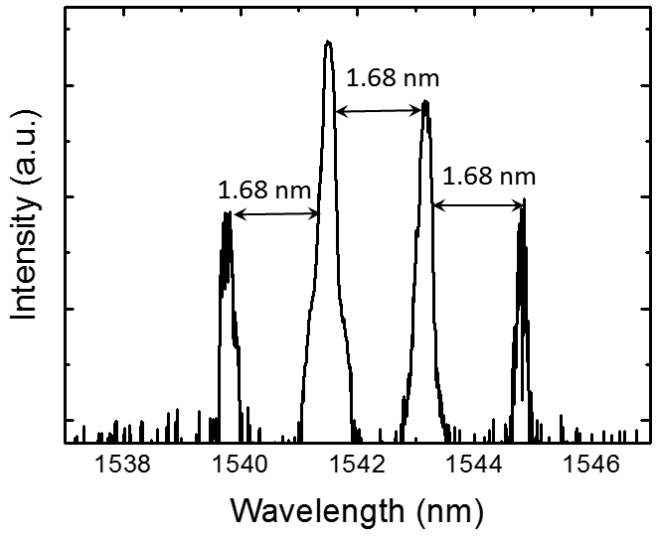


**Figure 35.** Single spectrum of the flip-chip, when the laser spectrum was tuned away from the microcavity resonance wavelength (at 1537 nm) by means of the birefringent filter. Presence of spectral fringes can be an indicator of the signal light leakage through the DBR into the backside diamond heat spreader.

In conclusion, the first 1.5 μm flip-chip VECSEL has been demonstrated in [P3]. The development of flip-chip VECSELs paves the way for inexpensive, mass produced VECSELs, which manufacturing can be done on a wafer scale, unlike IC VECSELs. In addition, omitting an expensive intracavity diamond heat spreader allows obtaining undistorted beam profiles (not influenced by the birefringence of heatspreaders [Friel et. al., 2009]), lower intra cavity losses (again, due to the absence of additional birefringence [Kim et. al., 2007]) and eventually higher output powers.

## 4.2 1.5 μm Quantum Dot VECSEL

Although QWs are conventionally employed in the active regions of the most VECSELs, QD-based VECSELs can offer advantageous lasing features such as: increased temperature stability [Germann et. al., 2008], lower threshold values, broader gain bandwidth, and correspondently broader tuning capabilities [Butkus et.

al., 2011]. On the other hand, when compared to QWs, QDs suffer from lower modal gain, due to smaller gain volume and wider gain distribution inherent to QD size dispersion [Bimberg et. al., 1997; Skolnick et. al., 2004]. Thus, most QD-based devices typically demonstrate output powers one order of magnitude lower than that of QW-based devices, which is particularly true for the 1 μm wavelength region (Fig. 36, which was adopted from [Al Nakdali et. al., 2015; Guina et. al., 2017]). When moving away from the 1 μm region, the situation shifts in the favor of QDs, where they allow generation of emission at wavelengths beyond the scope of QWs [Butkus et. al., 2010.]. In this thesis, the very first InP-based QD VECSEL with fundamental emission at 1.5 μm has been demonstrated [P4]. The output powers exceeded 2.2 W with wavelength tuning of 60 nm. This result lies within the same order of magnitude of the demonstrated 1.5 μm QW VECSELs, which makes the former an attractive light source alternative at this wavelength range!

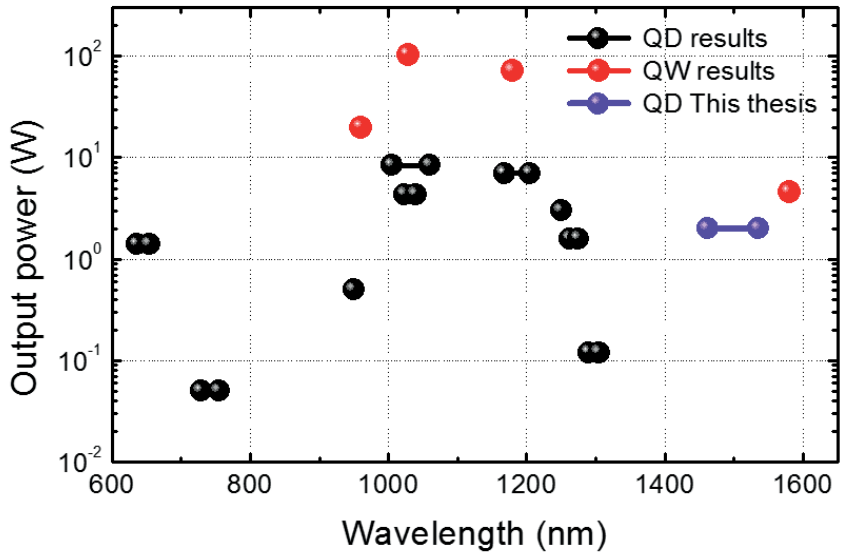


**Figure 36.** Wavelength mission map of QW and QD VECSELs plotted in terms of their output powers. Adapted from [Guina et. al., 2017; Al Nakdali et. al.,2015]

The QD VECSEL structure was comprised of an InP-based active region and an GaAs-based DBR section. The active region consisted of Stranski-Krastanov grown InAs QDs that were deposited utilizing double cap procedure (QD layers that were encapsulated by $Ga_{0.2}In_{0.8}As_{0.435}P_{0.565}$ alloy with a typical bandgap of 1.18 μm). This allowed independent control of QD density and emission wavelength [Paranthoen et. al., 2001]. Fig. 37 shows the QD density measured by means of AFM on a single

uncapped QD layer as a function InAs monolayer (ML) thickness. By increasing the thickness of the InAs ML from 1 to 2.5, the QD density was increased from $5x10^{10}$ $cm^{-2}$ up to the value of $11x10^{10}$ $cm^{-2}$. High-density QD layers were organized into five groups with four layers per group and placed at the antinodes of a simulated electric field within the microcavity. The resonant design of the structure allowed round trip gain enhancement (which in case of the QDs is typically quite small), but at the same time it increased the temperature sensitivity of the structure. The structure employed the IC heat spreader thermal management.

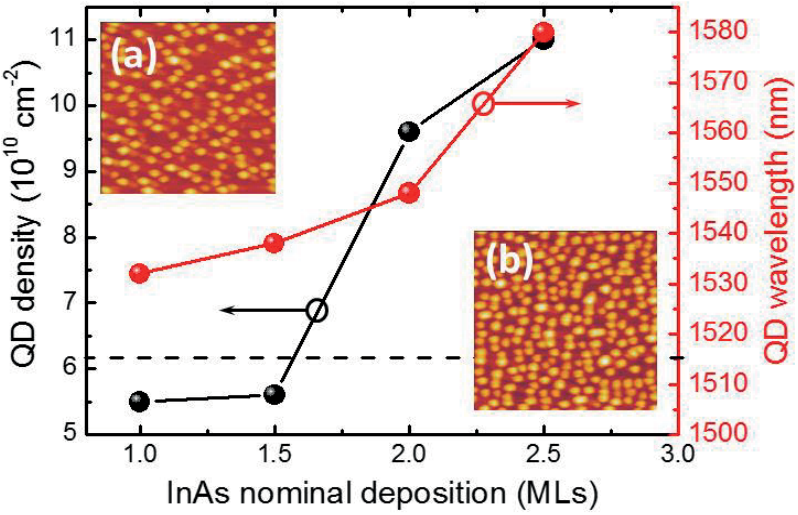


**Figure 37.** QD density (black) and wavelength (red) variation as function of the InAs monolayers (MLs). Insets (a) and (b) are AFM scans (0.5x0.5 μm²) of the uncovered QD for InAs with a thickness of 1 and 2.5 MLs respectively [P4].

The obtained results with 1.5 μm QD VECSELs are summarized in Fig. 38 and Fig. 39. The maximum output power was obtained with a pump spot/mode size ratio of 220/180 μm, and the optimum transmission of the output coupler was found to be <1%. The grown structure exhibited variation in the active region thickness across the wafer, which led to the fluctuation of the microcavity resonance as a function of the wafer location. Thus, it was possible to experimentally determine the optimal value of the detuning factor (difference between the room temperature PL and the microcavity resonance wavelength). The chip #2 demonstrated the highest output power of 2.25 W. The detuning of that chip can be estimated to be around 5 nm (much lower value in comparison to the typical detuning of QW VECSELs), which can be explained by much broader QD peak gain and its slower temperature-induced red shifting.

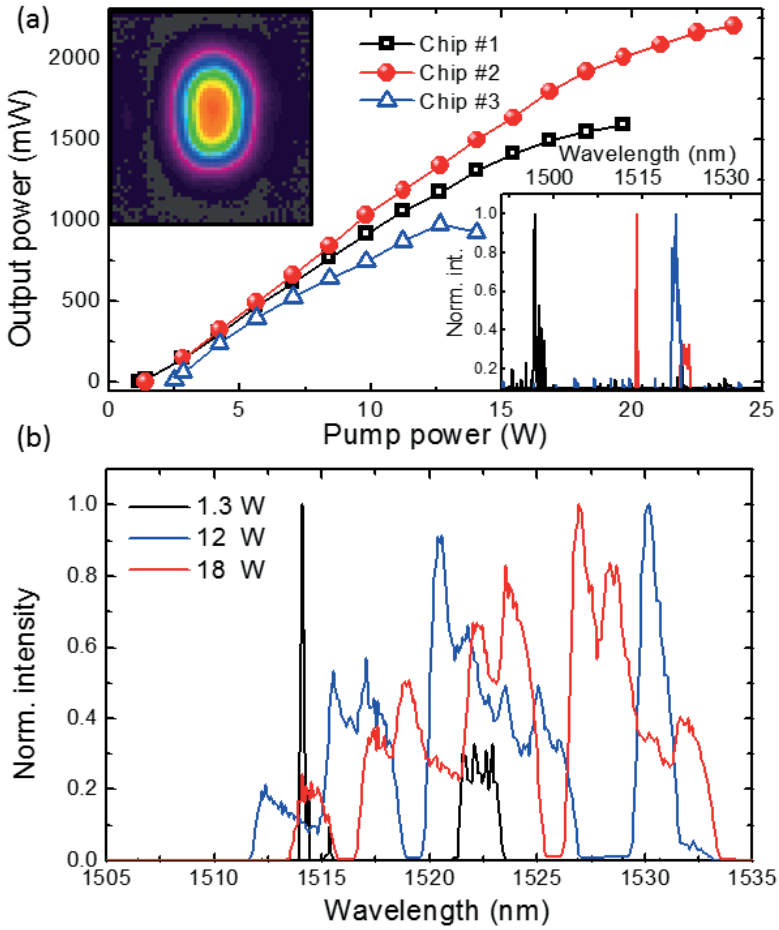


**Figure 38.** (a) Output power characteristics of three chips taken from different wafer locations. Lower inset shows threshold spectra of corresponding chips. Upper inset shows exemplary beam profile at 22 W of incident pump power [P4]. (b) Spectra of chip #2 recorded as a function of the incident pump power.

Fig. 39(a) presents a tuning curve that was measured by means of intracavity birefringent filter rotation (0.5 mm thickness) under constant incident pump power of 12 W. Fig. 39(b) presents the polarization behavior of the structure. In order to conduct this experiment, a 2 mm thick fused silica plate was subsequently inserted inside the cavity at two orthogonal orientations to enforce laser operation at the P- and S-polarization. The fused silica plate, unlike a birefringent filter, did not influence spectra besides introducing an additional etalon with a very narrow FSR. Thus, it

was possible to measure the differences in laser efficiencies when operating at the different polarizations, as well as slightly different spectra.

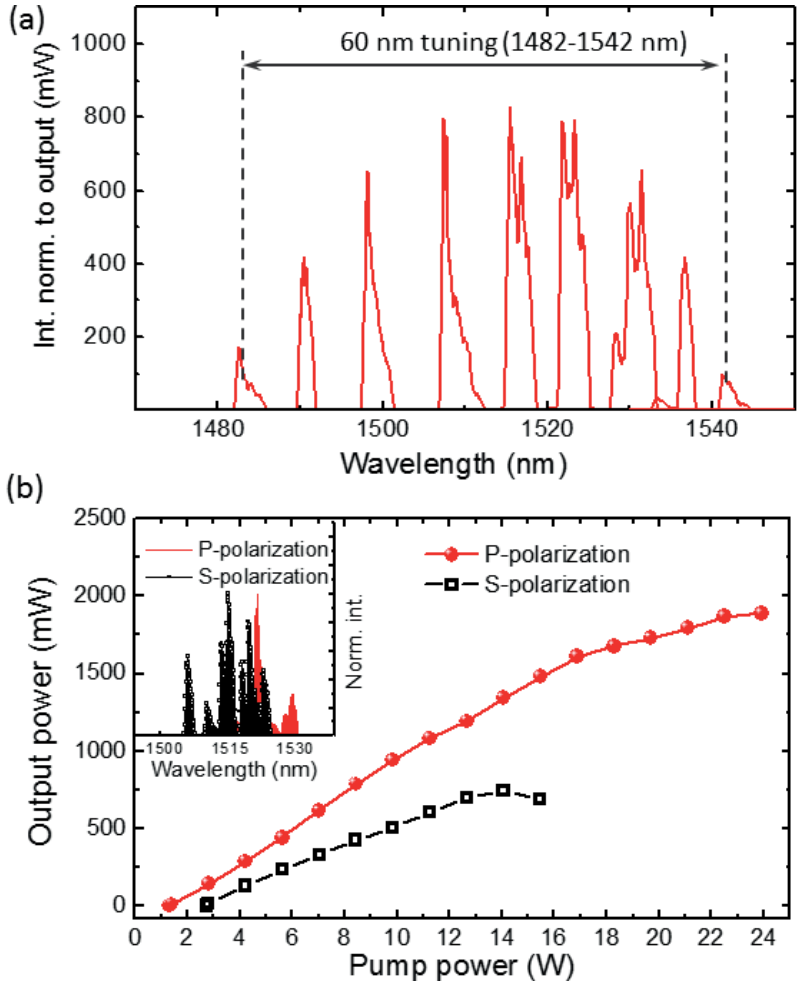


**Figure 39.** (a) Tuning characteristic of the QD VECSEL under 12 W of incident pump power, recorded as a function of the birefringent filter rotation [P4] (b) Output power curves as a function of incident pump power, at two predetermined polarization orientations of the laser [P5].

In conclusion, the first realization of the InP-based QD VECSEL with the emission at 1.5 μm allowed the achievement of excellent results, both power- and tuning-wise. The power characteristics of the QD VECSEL at theses wavelengths are on par to the QW VECSEL, which in this context can be considered outstanding given the different stages of development maturity of the two gain media types.

## 4.3 Frequency conversion of the 1.5 µm VECSELs down to 750 nm

This chapter summarizes the results concerning the second-harmonic generation to 750 nm, utilizing the 1.5 µm VECSELs. Two structures have been employed for this frequency conversion. The first one is the QD-based structure that was described in the previous chapter, whereas the other one was a QW VECSEL with 12 AlGaInAs QWs and an active region very similar to the one reported in [P3]. The fused DBR section was identical for these two structures, consisting of 29 pairs of AlAs/GaAs (with pairs thicknesses of 134 nm and 114 nm correspondently) for the reflection of the signal wavelength, and 11 pairs of AlAs/GaAs (with thicknesses of 83 nm and 70 nm correspondently) for the reflection of the 980 nm unabsorbed pump wavelength. The IC heat spreader approach was applied for both of the structures.

A BiBO nonlinear crystal with length of 5 mm was utilized for the SHG experiment. The BiBO crystal was not temperature controlled and was used for the critical phase matching. Fig. 40 shows a composite photograph of the experimental setup (at dark and at illuminated conditions).

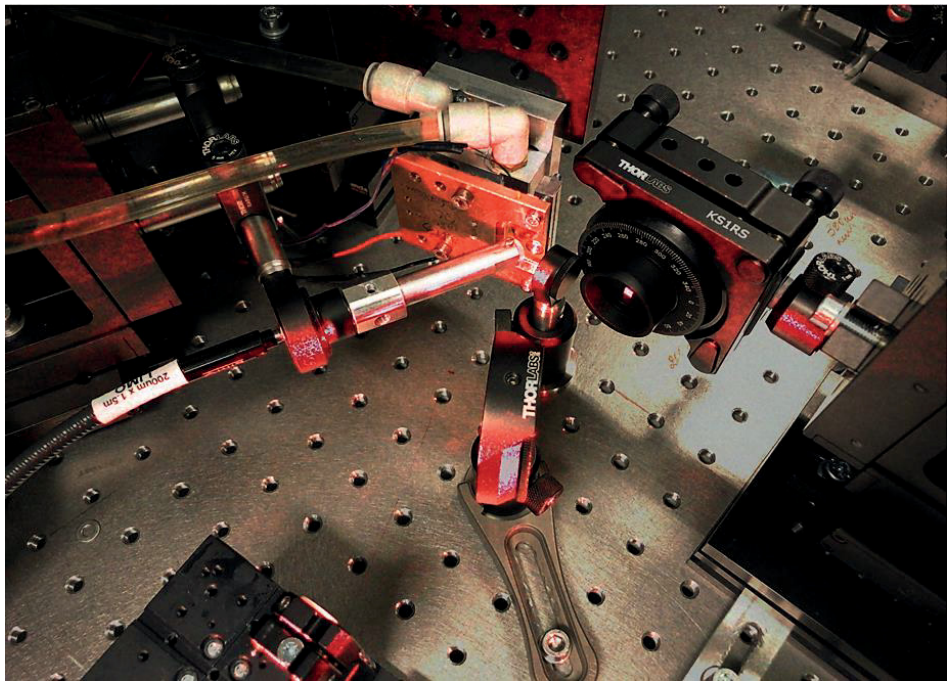


**Figure 40.** Composite photograph of the V-cavity with a BiBO crystal (in the round rotational mount) and the birefringent filter inside the resonator generating visible 750 nm emission.

Fig. 41 illustrates the schematics of the laser resonator designed for the SHG. The resonator geometry remained identical for the SHG experiment for both the QD and the QW VECSELs. Both curved mirrors were highly reflective for the fundamental wavelength (>99.8%) and highly transmitting for the SHG wavelength (>95%).

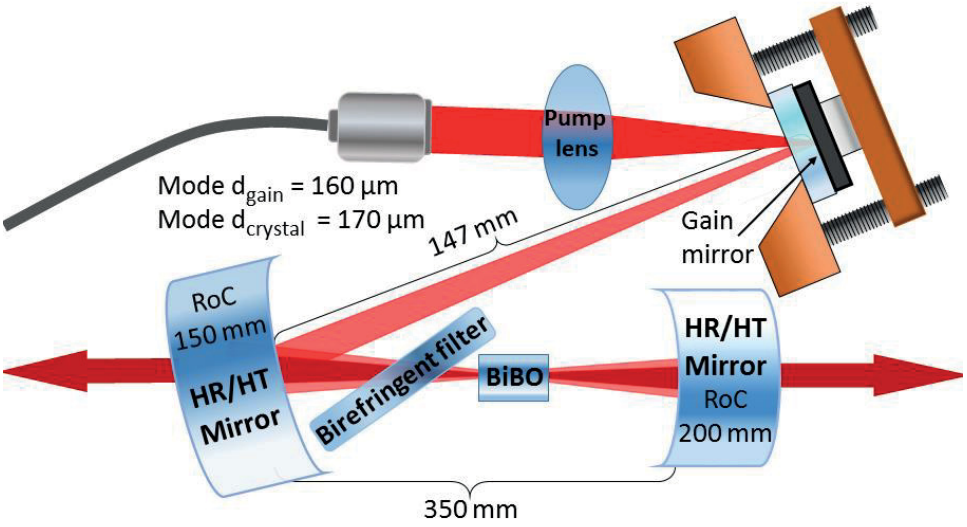


**Figure 41.** Schematically depicted resonator design for the SHG experiments [P5].

Fig. 42 shows power characteristics of the SHG from the QD (a) [P5] and the QW VECSELs (b). The highest output power for the QD VECSEL was achieved with the birefringent filter inside the cavity, whereas maximum output power for QW VECSEL was achieved without one. The SHG light was measured behind one of the mirrors and multiplied by a factor of two, whereas fundamental emission was simultaneously measured from the other output with appropriate filters. Notably, intracavity powers are approximately equal in the case of the two VECSELs under the same amount of incident pump powers. Beam profiles are shown as insets in Fig. 42. The ellipticity of the beam profiles is a result of a spatial walk-off within the BiBO crystal.

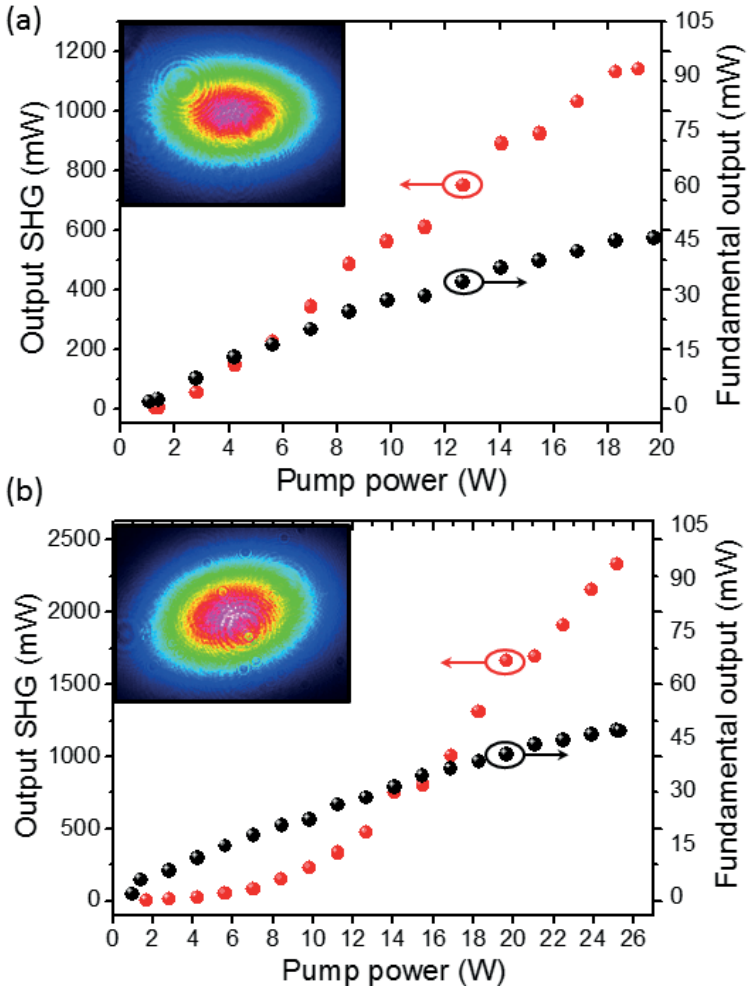


**Figure 42.** Output powers curves (left axis) of SHG emission of the QD (a) [P5] and the QW VECSELs (b) as a function of the incident pump power. Right axis shows transmitted power at the fundamental wavelength as a function of the incident pump power.

Fig. 43 shows the output spectra of the SHG from the QD and the QW VECSELs as a function of the pump power [P5]. The SHG spectrum obtained with the QD VECSEL (besides red shifting at much slower rate) is narrower when compared to the QW VECSEL because of the use of the birefringent filter. Since the FWHM of the QD VECSEL at the fundamental wavelength is intrinsically wider, the use of the birefringent filter is instrumental for the efficient frequency conversion, due to the BiBO crystal's acceptance bandwidth of 7 nm.

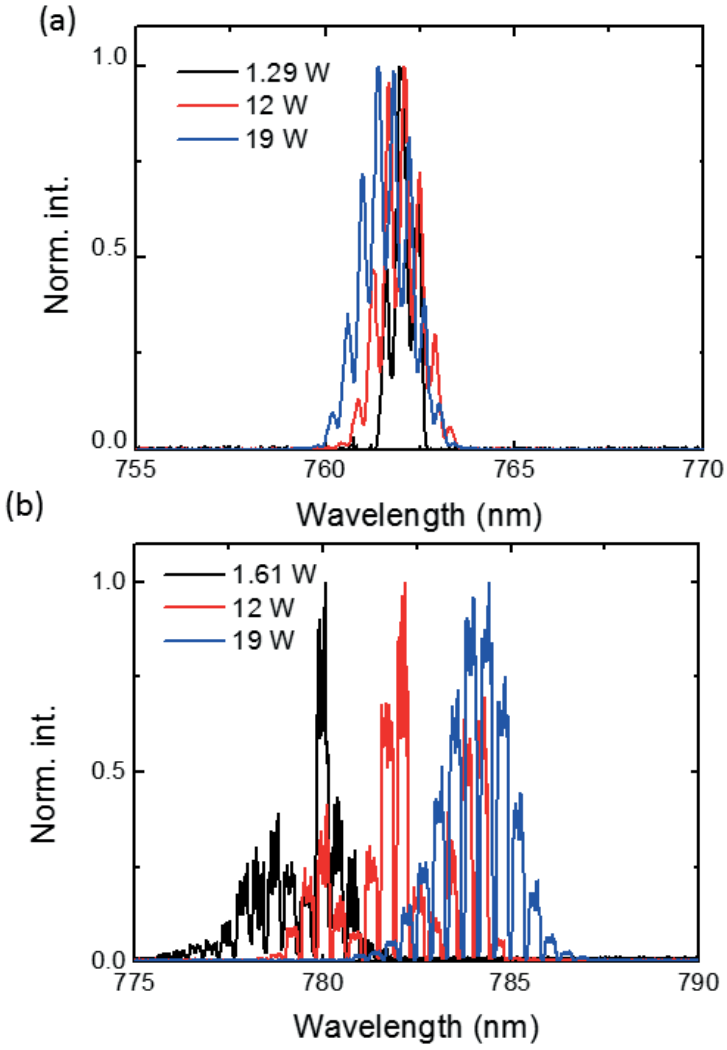


**Figure 43.** Output spectra of QD (a) [P5] and QW VECSELs (b) as a function of incident pump power.

The results of tuning experiments are shown in Fig. 44, where tuning of the QD VECSEL was done under 12 W of incident pump power [P5], and for QW VECSEL at 11 W of incident pump power. The tuning was performed by means of intracavity birefringent filter rotation.

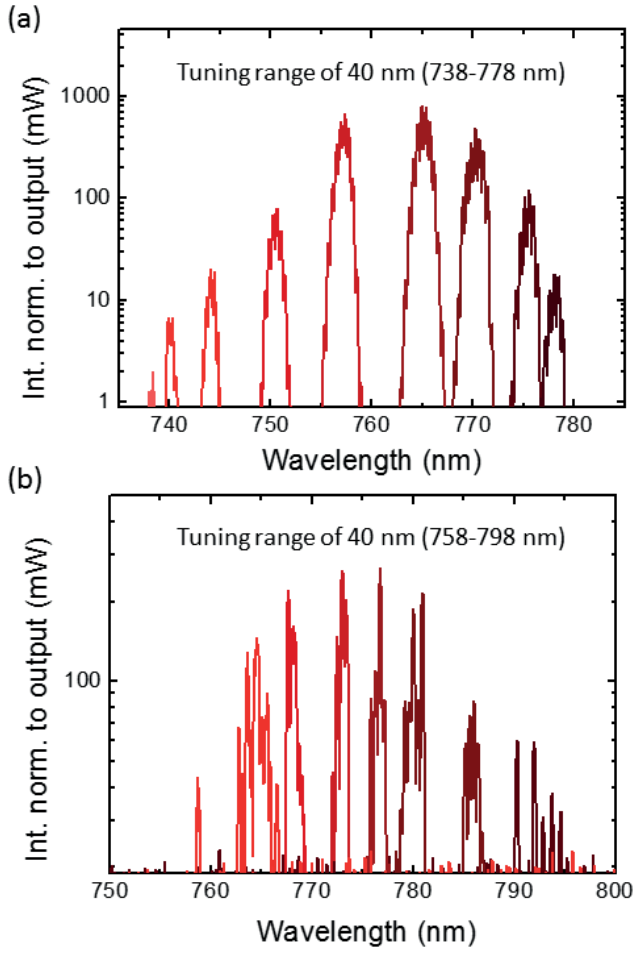


**Figure 44.** Tuning curves of the QD (a) [P5] and the QW VECSEL (b) under 12 and 10 W of incident pump power respectively.

In conclusion, the frequency conversions from the QD and the QW VECSELs have yielded 1.2 W (with central wavelength at 763 nm) [P5] and 2.3 W (with central wavelength at 784 nm), respectively. Wavelength tuning was realized from 737 nm to 779 nm for the QD VECSEL and from 758 nm to 794 nm for QW VECSELs. Although QD VECSELs have resulted in lower output power values, they have demonstrated much smaller spectra shift as a function of the pump power and wider tunability curve when targeting a shorter wavelength range. On the other hand, SHG QW VECSELs have demonstrated output powers that have surpassed previously reported values and have approached closer to the output power values of direct-emitting devices.

# 5 CONCLUSIONS

This thesis has taken different approaches of generating emission at the 750nm wavelength region by utilizing VECSEL technology. The first VECSELs, employing AlGaAs QWs, with direct multi-Watt emission at 740-780 nm wavelength range were developed. Despite the substantial increase in obtained output power, the VECSELs with AlGaAs QWs have exhibited short lifetimes rendering them currently impractical. In addition to VECSELs with AlGaInP claddings exhibited the polarization instabilities and related to this poor beam profile at the high pump powers.

At the 1.5 μm wavelength range the first wafer-fused flip-chip VECSEL was demonstrated. This thermal management scheme allowed avoid usage of the intracavity heat spreader approach, and by this, paving the way for wafer scale manufacturing. Furthermore, as an alternative to the QW active regions, a novel gain mirror based on QDs has been developed, which resulted in emission at the same power level as the 1.5 μm QW VECSELs.

As a last part of the work, frequency conversion from 1.5 μm to 750 nm region has been performed. The achieved emission can be considered as a viable alternative to the direct-emitting devices, since the 1.5 μm VECSELs do not suffer from poor lifetime and polarization issues, although with a penalty of slightly reduced output power.

Future work on direct-emitting 750 nm VECSEL could focus on development of active regions composed of alternative semiconductor compounds. In particular, one should improve the laser lifetime to the practically acceptable levels. In this particular case, compounds as GaAsP can be considered as a valuable alternative for the QWs. However, taking into account GaAsP lattice constant, the structure will accumulate strain during the growth, thus design of such active region involving GaAsP QWs must include appropriate strain compensating layers. On the other hand, fabrication of ordering-free AlGaInP claddings is another research direction that can be found beneficial, taking into account large bandgap values that AlGaInP can offer.

Thermal management of the direct-emitting VECSEL at this wavelength range further can take two main research direction: developing flip-chip VECSELs and

membrane VECSELs. DBR-free or membrane VECSEL can allow superior cooling capabilities.

Generally, the problem of heat management can be tackled from two different angle: either by increasing cooling capabilities (which is the goal of efficient thermal management) or by decreasing heat generation in an active region, which can be done by means of decreasing the quantum defect by utilizing a lower energy pump. Therefore, pursuing this development direction, the 532 nm pump can be substituted by the 640 nm red laser diode pump, which have become much more available with the reduced price per W. Thus, employment of the longer wavelength pump coupled with appropriate redesigning of active region may be an alternative solution, contrary to the limited options of thermal managements. With the same idea of reducing the heat generation, the concept of quantum well pumping can be utilized.

Therefore, combination of research in the above-mentioned directions may lead to the development of more mature direct-emitting VECSELs with a longer lifetime and absence of polarization-related issues. Such devices will then allow an efficient second-harmonic generation of high-brightness tunable UV emission at the 350-400 nm, which will benefit many applications, such as quantum technologies and AMO field in general.

On the other hand, further development of the 1.5 μm flip-chip VECSELs is another promising alternative, since flip-chip thermal management allows significant power scaling potential, which may result in tens of Watts of output power. Therefore, even when considering lower generation efficiencies of the 700–800 nm emission by means of SHG, a matured 1.5 μm flip-chip VECSEL may result in converted output power levels that will eventually be much greater than those of the direct-emitting devices. In parallel, if tens of Watts of output power would become available from 1.5 μm flip-chip VECSELs, frequency quadrupling can be considered as a good alternative to the SHG of direct-emitting VECSELs (in case of the lack of the progress on that account).

# BIBLIOGRAPHY

Al Nakdali, D., Gaafar, M., Shakfa, M., Zhang, F., Vaupel, M., & Fedorova, K. et al. (2015). High-Power Operation of Quantum-Dot Semiconductor Disk Laser at 1180 nm. *IEEE Photonics Technology Letters*, *27*(10), 1128-1131. doi: 10.1109/lpt.2015.2408619

Alferov, Z., Andreyev, V., Korol'Kov, V., & Portnoi, E. (1969). Preparation and Investigation of Epitaxial Layers of AlxGa1-xAs solid Solutions and of Heterojunctions in the AlAs-GaAs system. *Kristall Und Technik*, *4*(4), 495-503. doi: 10.1002/crat.19690040406

Alford, W., Raymond, T., & Allerman, A. (2002). High power and good beam quality at 980 nm from a vertical external-cavity surface-emitting laser. *Journal Of The Optical Society Of America B*, *19*(4), 663. doi: 10.1364/josab.19.000663

Basov, N., Bogdankevich, O., & Grasyuk, A. (1966). 9B4 - Semiconductor lasers with radiating mirrors. *IEEE Journal Of Quantum Electronics*, *2*(9), 594-597. doi: 10.1109/jqe.1966.1074111

Bedford, R., Kolesik, M., Chilla, J., Reed, M., Nelson, T., & Moloney, J. (2005). Power-limiting mechanisms in VECSELs, In *SPIE Defense and Security* 5814. Orlando: SPIE. Retrieved from https://doi.org/10.1117/12.607428

Bennett, W. R. (1965). Inversion Mechanisms in Gas Lasers. *Applied Optics* *2*(S1), 3-22. doi: 10.1364/AO.4.S1.000003

Beyertt, S., Brauch, U., Demaria, F., Dhidah, N., Giesen, A., & Kubler, T. et al. (2007). Efficient Gallium–Arsenide Disk Laser. *IEEE Journal Of Quantum Electronics*, *43*(10), 869-875. doi: 10.1109/jqe.2007.904074

Bimberg, D., Kirstaedter, N., Ledentsov, N., Alferov, Z., Kop'ev, P., & Ustinov, V. (1997). InGaAs-GaAs quantum-dot lasers. *IEEE Journal Of*

*Selected Topics In Quantum Electronics*, *3*(2), 196-205. doi: 10.1109/2944.605656

Budgor, A. (1984). Overview of Chromium Doped Tunable Vibronic Lasers. In *New Lasers for Analytical & Industrial* Chemistry 0461. Los Angeles: SPIE. Retrieved from https://doi.org/10.1117/12.941074

Burd, S., Allcock, D., Leinonen, T., Penttinen, J., Slichter, D., & Srinivas, R. et al. (2016). VECSEL systems for the generation and manipulation of trapped magnesium ions. *Optica*, *3*(12), 1294. doi: 10.1364/optica.3.001294

Burd, S., Leibfried, D., Wilson, A., & Wineland, D. (2015). Optically pumped semiconductor lasers for atomic and molecular physics. In *SPIE Lase*. San-Francisco: SPIE. Retrieved from https://doi.org/10.1117/12.2077027

Butkus, M., Rautiainen, J., Mikhrin, S., Krestnikov, I., & Rafailov, E. U. (2010). 1270 nm quantum dot based semiconductor disk lasers. In *22nd IEEE International Semiconductor Laser Conference* (pp. 71-72). Kyoto: IEEE. Retrieved from https://doi.org/10.1109/ISLC.2010.5642748

Butkus, M., Rautiainen, J., Okhotnikov, O. G., Hamilton, C. J., Malcolm, G. P. A., Mikhrin, S. S., Krestnikov, I. L., Livshits, D. A., & Rafailov, E. U. (2011). Quantum dot based semiconductor disk lasers for 1-1.3 μm. *IEEE Journal of Selected Topics in Quantum Electronics*, *17*(6), 1763-1771. doi: 10.1109/JSTQE.2011.2112638

Byer, R. (1988). Diode Laser--Pumped Solid-State Lasers. *Science*, *239*(4841), 742-747. doi: 10.1126/science.239.4841.742

Charlton, K. (2016). Medical Isotope Supply Review: $^{99}$Mo/$^{99m}$Tc Market Demand and Production Capacity Projection 2016-2021. *NEA and OECD report under The Supply of Medical Radioisotopes series*. Report number: NEA-SEN-HLGMR--2016-2

Chernikov, A., Herrmann, J., Scheller, M., Koch, M., Kunert, B., & Stolz, W. et al. (2010). Influence of the spatial pump distribution on the performance of high power vertical-external-cavity surface-emitting lasers. *Applied Physics Letters*, *97*(19), 191110. doi: 10.1063/1.3515911

Chilla, J., Shu, Q., Zhou, H., Weiss, E., Reed, M., & Spinelli, L. (2007). Recent advances in optically pumped semiconductor lasers. In *Lasers and Applications in Science and Engineering* (p. 645109). San Jose: SPIE. Retrieved from https://doi.org/10.1117/12.705907

Coherent | DILAS: High-power diode lasers. (2019). Retrieved 5 September 2019, from http://www.dilas.com/products

Cooley, W., Hengehold, R., Yeo, Y., Turner, G., & Loehr, J. (1998). Recombination dynamics in InAsSb quantum-well diode lasers measured using photoluminescence upconversion. *Applied Physics Letters*, *73*(20), 2890-2892. doi: 10.1063/1.122620

Corzine, S., Geels, R., Scott, J., Yan, R., & Coldren, L. (1989). Design of Fabry-Perot surface-emitting lasers with a periodic gain structure. *IEEE Journal Of Quantum Electronics*, *25*(6), 1513-1524. doi: 10.1109/3.29288

Ell, R., Morgner, U., Kärtner, F., Fujimoto, J., Ippen, E., & Scheuer, V. et al. (2001). Generation of 5-fs pulses and octave-spanning spectra directly from a Ti:sapphire laser. *Optics Letters*, *26*(6), 373. doi: 10.1364/ol.26.000373

Fan, T., & Byer, R. (1988). Diode laser-pumped solid-state lasers. *IEEE Journal Of Quantum Electronics*, *24*(6), 895-912. doi: 10.1109/3.210

Fan L., Hessenius, C., Fallahi, M., Hader, J., Li, H., Moloney, J. V., Stolz, W., Koch, S. W., Murray, J. T., & Bedford R. (2007). Highly strained InGaAs/GaAs multiwatt vertical-external-cavity surface-emitting laser emitting around 1170 nm. *Applied Physics Letters, 91*, 131114. doi: 10.1063/1.2790838

Findlay, D., & Clay, R. (1966). The measurement of internal losses in 4-level lasers. *Physics Letters*, *20*(3), 277-278. doi: 10.1016/0031-9163(66)90363-5

Franken, P. A. Hill, A. E., Peters, C. W. & Weinreich, G. (1961). Generation of Optical Harmonics. *Physical Review Letters 7*(4), 118-119. doi: 10.1103/PhysRevLett.7.118

Friel, I., Clewes, S. L., Dhilloh, H. K., Perkins, N., Twitchen, D. J., & Scarsbrook, G. A. (2009) Control of surface and bulk crystalline quality in

single crystal diamond grown by chemical vapour deposition. Diamond. Relat. Mater. 18(5), 808-815. doi: 10.1016/j.diamond.2009.01.013.

Germann, T. D., Strittmatter, A., Pohl, J., Pohl, U. W., Bimberg, D., Rautiainen, J., Guina, M., & Okhotnikov, O., G. (2008). High-power semiconductor disk laser based on InAs/GaAs submonolayer quantum dots. *Applied Physics Letters* 92, 101123. doi: 10.1063/1.2898165

Gianfrani, L., Fox, R., & Hollberg, L. (1999). Cavity-enhanced absorption spectroscopy of molecular oxygen. *Journal Of The Optical Society Of America B*, *16*(12), 2247. doi: 10.1364/josab.16.002247

Gomyo, A., Suzuki, T., & Iijima, S. (1988). Observation of Strong Ordering inGaxIn1−xPalloy semiconductors. *Physical Review Letters*, *60*(25), 2645-2648. doi: 10.1103/physrevlett.60.2645

Guina, M., Rantamäki, A., & Härkönen, A. (2017). Optically pumped VECSELs: review of technology and progress. *Journal Of Physics D: Applied Physics*, *50*(38), 383001. doi: 10.1088/1361-6463/aa7bfd

Hall, R., Fenner, G., Kingsley, J., Soltys, T., & Carlson, R. (1962). Coherent Light Emission From GaAs Junctions. *Physical Review Letters*, *9*(9), 366-368. doi: 10.1103/physrevlett.9.366

Harrold, S. (1994). Properties of aluminium gallium arsenide. *Microelectronics Journal*, *25*(3), 252. doi: 10.1016/0026-2692(94)90022-1

Hartke, R. (2008). *Intracavity frequency doubling of optically pumped semiconductor disk lasers to the green spectral range* (Ph.D.). University of Hamburg.

Hastie, J., Calvez, S., Sun, H., Dawson, M., Leinonen, T., & Pessa, M. (2005). High Power, Continuous Wave Operation of a Vertical External Cavity Surface Emitting Laser at 674nm. In *Advanced Solid-State Photonics* (p. WC2). Vienna: OSA Publishing. Retrieved from https://doi.org/10.1364/ASSP.2005.WC2

Hein, A., Menzel, S., & Unger, P. (2012). High-power high-efficiency optically pumped semiconductor disk lasers in the green spectral region with

a broad tuning range. *Applied Physics Letters*, *101*(11), 111109. doi: 10.1063/1.4751352

Heinen, B., Wang, T., Sparenberg, M., Weber, A., Kunert, B., & Hader, J. et al. (2012). 106 W continuous-wave output power from vertical-external-cavity surface-emitting laser. *Electronics Letters*, *48*(9), 516. doi: 10.1049/el.2012.0531

Holonyak, N., Kolbas, R., Dupuis, R., & Dapkus, P. (1978). Room-temperature continuous operation of photopumped MO-CVD AlxGa1−xAs-GaAs-AlxGa1−xAs quantum-well lasers. *Applied Physics Letters*, *33*(1), 73-75. doi: 10.1063/1.90150

Huber, G., Kränkel, C., & Petermann, K. (2010). Solid-state lasers: status and future [Invited]. *Journal Of The Optical Society Of America B*, *27*(11), B93. doi: 10.1364/josab.27.000b93

Hughes, D. W., & Barr, J. R. M. (1992). Laser diode pumped solid-state lasers. *Journal of Physics D: Applied Physics 25*(4), 563-586. doi: 10.1088/0022-3727/25/4/001

Ippen, E. P., Shank, C.V., & Dienes, A. (1972). Passive mode locking of the cw dye laser. *Applied Physics Letters 21*, 348-350. doi: 10.1063/1.1654406

Jacques, S. (2013). Optical properties of biological tissues: a review. *Physics In Medicine And Biology*, *58*(11), R37-R61. doi: 10.1088/0031-9155/58/11/r37

Javan, A., Bennett, W., & Herriott, D. (1961). Population Inversion and Continuous Optical Maser Oscillation in a Gas Discharge Containing a He-Ne Mixture. *Physical Review Letters*, *6*(3), 106-110. doi: 10.1103/physrevlett.6.106

Kahle, H., Mateo, C., Brauch, U., Tatar-Mathes, P., Bek, R., & Jetter, M. et al. (2016). Semiconductor membrane external-cavity surface-emitting laser (MECSEL). *Optica*, *3*(12), 1506. doi: 10.1364/optica.3.001506

Kahle, H., Penttinen, J., Phung, H., Rajala, P., Tukiainen, A., Ranta, S., & Guina, M. (2019). Comparison of single-side and double-side pumping of

membrane external-cavity surface-emitting lasers. *Optics Letters*, *44*(5), 1146. doi: 10.1364/ol.44.001146

Karim, A., Bjorlin, S., Piprek, J., & Bowers, J. (2000). Long-wavelength vertical-cavity lasers and amplifiers. *IEEE Journal Of Selected Topics In Quantum Electronics*, *6*(6), 1244-1253. doi: 10.1109/2944.902174

Keller, U., & Tropper, A. (2006). Passively modelocked surface-emitting semiconductor lasers. *Physics Reports*, *429*(2), 67-120. doi: 10.1016/j.physrep.2006.03.004

Kemp, A., Maclean, A., Hastie, J., Smith, S., Hopkins, J., & Calvez, S. (2006). Thermal lensing, thermal management and transverse mode control in microchip VECSELs. *Applied Physics B*, *83*(2), 189-194. doi: 10.1007/s00340-006-2151-z

Kemp, A., Valentine, G., Hopkins, J., Hastie, J., Smith, S., & Calvez, S. (2005). Thermal management in vertical-external-cavity surface-emitting lasers: finite-element analysis of a heatspreader approach. *IEEE Journal Of Quantum Electronics*, *41*(2), 148-155. doi: 10.1109/jqe.2004.839706

Kim, J.-Y., Yoo, J., Cho S., Kim, K.-S., Kim, G. B., Lee, J., Lee, S.-M., Kim, T., & Park, Y. (2007). Effect of the properties of an intracavity heatspreader on second harmonic generation in vertical-external-cavity surface-emitting laser. *J. Appl. Phys., 101,* 073101. doi: 10.1063/1.2714003

Koechner, W. (2006). *Solid-State Laser Engineering*. Berlin, Heidelberg: Springer Berlin / Heidelberg.

Korpijärvi, V., Kantola, E., Leinonen, T., Isoaho, R., & Guina, M. (2015). Monolithic GaInNAsSb/GaAs VECSEL Operating at 1550 nm. *IEEE Journal Of Selected Topics In Quantum Electronics*, *21*(6), 480-484. doi: 10.1109/jstqe.2015.2415200

Kuznetsov, M., Hakimi, F., Sprague, R., & Mooradian, A. (1997). High-power (>0.5-W CW) diode-pumped vertical-external-cavity surface-emitting semiconductor lasers with circular TEM/sub 00/ beams. *IEEE Photonics Technology Letters*, *9*(8), 1063-1065. doi: 10.1109/68.605500

Laming, R. I., Farries, M. C., Morkel, P. R., Reekie, L., Payne, D. N., Scrivener P. L., Fontana, F., Righetti, A. (1989). Efficient pump wavelengths of erbium-doped fibre optical amplifier. *IEEE Electronics Letters*, *25*(1), 12-14. doi: 10.1049/el:19890009

Lindberg, H., Strassner, M., Gerster, E., Bengtsson, J., & Larsson, A. (2005). Thermal management of optically pumped long-wavelength InP-based semiconductor disk lasers. *IEEE Journal Of Selected Topics In Quantum Electronics*, *11*(5), 1126-1134. doi: 10.1109/jstqe.2005.853730

Liu, K., & Littman, M. (1981). Novel geometry for single-mode scanning of tunable lasers. *Optics Letters*, *6*(3), 117. doi: 10.1364/ol.6.000117

van Loon, F., Kemp, A., Maclean, A., Calvez, S., Hopkins, J., & Hastie, J. et al. (2006). Intracavity diamond heatspreaders in lasers: the effects of birefringence. *Optics Express*, *14*(20), 9250. doi: 10.1364/oe.14.009250

Lyytikäinen, J., Rautiainen, J., Toikkanen, L., Sirbu, A., Mereuta, A., & Caliman, A. et al. (2009). 1.3-μm optically-pumped semiconductor disk laser by wafer fusion. *Optics Express*, *17*(11), 9047. doi: 10.1364/oe.17.009047

Maclean, A., Kemp, A., Calvez, S., Kim, J., Kim, T., Dawson, M., & Burns, D. (2008). Continuous tuning and efficient intracavity second-harmonic generation in a semiconductor disk laser with an intracavity diamond heatspreader. *IEEE J. J. Quantum Electron*. 44(3), 216–225. doi: 10.1109/JQE.2007.911704

Maiman, T. (1960). Stimulated Optical Radiation in Ruby. *Nature*, *187*(4736), 493-494. doi: 10.1038/187493a0

Mateo, C., Brauch, U., Kahle, H., Schwarzbäck, T., Jetter, M., & Ahmed, M. et al. (2016). 2.5 W continuous wave output at 665 nm from a multipass and quantum-well-pumped AlGaInP vertical-external-cavity surface-emitting laser. *Optics Letters*, *41*(6), 1245. doi: 10.1364/ol.41.001245

Mazur, T., Klappauf, B., & Raizen, M. (2014). Demonstration of magnetically activated and guided isotope separation. *Nature Physics*, *10*(8), 601-605. doi: 10.1038/nphys3013

McClung, F. J., & Hellwarth, R. W. (1962). Giant optical pulsations from ruby. *Journal of Applied Physics*, *33*(3), 828-829. doi: 10.1063/1.1777174

Miya, T., Terunuma, Y., Hosaka, T., & Miyashita, T. (1979). Ultimate low-loss single-mode fibre at 1.55 μm. *Electronics Letters*, *15*(4), 106. doi: 10.1049/el:19790077

Moritz, A., Wirth, R., Geng, C., Scholz, F., & Hangleiter, A. (1995). Effects of birefringence in ordered GaInP/AlGaInP lasers. *MRS Proceedings*, *417*. doi: 10.1557/proc-417-97

Moutanabbir, O., & Gösele, U. (2010). Heterogeneous Integration of Compound Semiconductors. *Annual Review Of Materials Research*, *40*(1), 469-500. doi: 10.1146/annurev-matsci-070909-104448

Nechay, K. (2016). *Interferometric multichip VECSEL* (M. Sc.). Lappeenranta University of Technology.

Nichi, K., Hirose, K., & Mizutani, T. (1986). Optical characterization of InGaAs-InAlAs strained-layer superlattices grown by molecular beam epitaxy. *Applied Physics Letters, 49*, 794-796. doi: 10.1063/1.97549

Okhotnikov, E. (2010). *Semiconductor Disk Lasers: Physics and Technology*. John Wiley & Sons.

Paranthoen, C., Bertru, N., Dehaese, O., Le Corre, A., Loualiche, S., Lambert, B., & Patriarche, G. (2001). Height dispersion control of InAs/InP quantum dots emitting at 1.55 μm. *Applied Physics Letters*, *78*(12), 1751-1753. doi: 10.1063/1.1356449

Perez, J., Laurain, A., Cerutti, L., Sagnes, I., & Garnache. A. (2010). Technologies for thermal management of mid-IR Sb-based surface emitting lasers. *Semiconductor Science and Technology 25*(4), 045021. doi: 10.1088/0268-1242/25/4/045021

Ponsard, B. (2012). Review of the $^{99}$Mo $^{99m}$Tc supply situation and new projects. *Radiotherapy And Oncology*, *102*, S169. doi: 10.1016/s0167-8140(12)70277-3

Raja, M., Brueck, S., Osinski, M., Schaus, C., McInerney, J., Brennan, T., & Hammons, B. (1989). Resonant periodic gain surface-emitting semiconductor lasers. *IEEE Journal Of Quantum Electronics*, *25*(6), 1500-1512. doi: 10.1109/3.29287

Ranta, S., Hakkarainen, T., Tavast, M., Lindfors, J., Leinonen, T., & Guina, M. (2011). Strain compensated 1120nm GaInAs/GaAs vertical external-cavity surface-emitting laser grown by molecular beam epitaxy. *Journal Of Crystal Growth*, *335*(1), 4-9. doi: 10.1016/j.jcrysgro.2011.08.044

Ranta, S., Tavast, M., Leinonen, T., Epstein, R., & Guina, M. (2012). Narrow linewidth 1118/559 nm VECSEL based on strain compensated GaInAs/GaAs quantum-wells for laser cooling of Mg-ions. *Optical Materials Express*, *2*(8), 1011. doi: 10.1364/ome.2.001011

Rantamäki, A., Lindfors, J., Silvennoinen, M., Kontio, J., Tavast, M., & Okhotnikov, O. (2013). Low Temperature Gold-to-Gold Bonded Semiconductor Disk Laser. *IEEE Photonics Technology Letters*, *25*(11), 1062-1065. doi: 10.1109/lpt.2013.2258147

Rantamäki, A., Rautiainen, J., Lyytikäinen, J., Sirbu, A., Mereuta, A., Kapon, E., & Okhotnikov, O. (2012). 1 W at 785 nm from a frequency-doubled wafer-fused semiconductor disk laser. *Optics Express*, *20*(8), 9046. doi: 10.1364/oe.20.009046

Rantamäki, A., Saarinen, E., Lyytikainen, J., Heikkinen, J., Kontio, J., & Lahtonen, K. et al. (2015). Thermal Management in Long-Wavelength Flip-Chip Semiconductor Disk Lasers. *IEEE Journal Of Selected Topics In Quantum Electronics*, *21*(6), 336-342. doi: 10.1109/jstqe.2015.2420599

Rautiainen, J., Lyytikäinen, J., Sirbu, A., Mereuta, A., Caliman, A., Kapon, E., & Okhotnikov, O. (2008). 2.6 W optically-pumped semiconductor disk laser operating at 1.57-μm using wafer fusion. *Optics Express*, *16*(26), 21881. doi: 10.1364/oe.16.021881

Saarinen, E., Lyytikäinen, J., Ranta, S., Rantamäki, A., Sirbu, A., & Iakovlev, V. et al. (2015). 750 nm 1.5 W frequency-doubled semiconductor disk laser with a 44 nm tuning range. *Optics Letters*, *40*(19), 4380. doi: 10.1364/ol.40.004380

Sandusky, J., & Brueck, S. (1996). A CW external-cavity surface-emitting laser. *IEEE Photonics Technology Letters*, *8*(3), 313-315. doi: 10.1109/68.481101

Schlosser, P., Hastie, J., Calvez, S., Krysa, A., & Dawson, M. (2009). InP/AlGaInP quantum dot semiconductor disk lasers for CW TEM_00 emission at 716 – 755 nm. *Optics Express*, *17*(24), 21782. doi: 10.1364/oe.17.021782

Schulz, N., Rattunde, M., Ritzenthaler, C., Rosener, B., Manz, C., Kohler, K., & Wagner, J. (2007). Effect of the cavity resonance-gain offset on the output power characteristics of GaSb-based VECSELs. *IEEE Photonics Technology Letters, 19*(21), 1741–1743. doi: 10.1109/LPT.2007.906054

Sirbu A., Volet N., Mereuta A., Lyytikäinen J., Rautiainen J., Okhotnikov O., Walczak J., Wasiak M., Czyszanowski T., Caliman A., Zhu Q., Iakovlev V., & Kapon E., (2004). Wafer-Fused Optically Pumped VECSELs Emitting in the 1310-nm and 1550-nm Wavebands. *Advances in Optical Technologies*, 1-8. doi:10.1155/2011/209093

Skolnick, M., & Mowbray, D. (2004). Self-assembled semiconductor quantum dots: Fundamental Physics and Device Applications. *Annual Review Of Materials Research*, *34*(1), 181-218. doi: 10.1146/annurev.matsci.34.082103.133534

Tropper, A., & Hoogland, S. (2006). Extended cavity surface-emitting semiconductor lasers. *Progress In Quantum Electronics*, *30*(1), 1-43. doi: 10.1016/j.pquantelec.2005.10.002

Verdi G-Series | Coherent. (2019). Retrieved 5 September 2019, from https://www.coherent.com/lasers/laser/verdi-g-series

Winzer, P., Neilson, D., & Chraplyvy, A. (2018). Fiber-optic transmission and networking: the previous 20 and the next 20 years [Invited]. *Optics Express*, *26*(18), 24190. doi: 10.1364/oe.26.024190

Wirth, R., Geng, C., Scholz, F., & Hangleiter, A. (1998). Determination of ordering induced birefringence in (Al)GaInP. *Journal Of Electronic Materials*, *27*(3), 122-126. doi: 10.1007/s11664-998-0201-5

Yang, Z., Albrecht, A., Cederberg, J., & Sheik-Bahae, M. (2016). 80 nm tunable DBR-free semiconductor disk laser. *Applied Physics Letters*, *109*(2), 022101. doi: 10.1063/1.4958164

Yoshida, K., & Morigami, H. (2004). Thermal properties of diamond/copper composite material. *Microelectronics Reliability*, *44*(2), 303-308. doi: 10.1016/s0026-2714(03)00215-4

Zhang, F., Möller, C., Koch, M., Koch, S., Rahimi-Iman, A., & Stolz, W. (2017). Impact of detuning on the performance of semiconductor disk lasers. *Applied Physics B*, *123*(12). doi: 10.1007/s00340-017-6860-2

Zory, P. S. Jr., Liao, P. F., Kelley, P. (1993). *Quantum well lasers*. Academic Press.

# PUBLICATIONS

Publication I H. Kahle, K. Nechay, J.-P. Penttinen, A. Tukiainen, S. Ranta, and M. Guina, "AlGaAs-based vertical-external-cavity surface-emitting laser exceeding 4 W of direct emission power in the 740–790 nm spectral range," *Optics Letters,* vol. 43, no. 7, pp. 1578-1581, 2018.

Publication II K. Nechay, H. Kahle, J.-P. Penttinen, P. Rajala, A. Tukiainen, S. Ranta, and M. Guina, "AlGaAs/AlGaInP VECSELs With Direct Emission at 740–770 nm," *IEEE Photonics Technology Letters*, vol. 31, no. 15, pp. 1245-1248, 2019.

Publication III A. Mereuta, K. Nechay, A. Caliman, G. Suruceanu, A. Rudra, P. Gallo, M. Guina, and E. Kapon, "Flip-Chip Wafer-Fused OP-VECSELs Emitting 3.65 W at the 1.55-μm Waveband," *IEEE Journal of Selected Topics in Quantum Electronics*, vol. 25, no. 6, 2019.

Publication IV K. Nechay, A. Mereuta, C. Paranthoen, G. Brévalle, C. Levallois, M. Alouini, N. Chevalier, M. Perrin, G. Suruceanu, A. Caliman, M. Guina and E. Kapon, "InAs/InP quantum dot VECSEL emitting at 1.5 μm," *Applied Physics Letters*, , vol. 117, no. 17, pp. 171105, 2019.

Publication V K. Nechay, A. Mereuta, C. Paranthoen, G. Brévalle, C. Levallois, M. Alouini, N. Chevalier, M. Perrin, G. Suruceanu, A. Caliman, M. Guina and E. Kapon, "High-power 750 nm VECSEL based on QD gain mirror," *IEEE Journal of Quantum Electronics*, (Submitted).

# PUBLICATION I

**AlGaAs-based vertical-external-cavity surface-emitting laser exceeding 4 W of direct emission power in the 740–790 nm spectral range**

Hermann Kahle, Kostiantyn Nechay, Jussi-Pekka Penttinen, Antti Tukiainen, Sanna Ranta and Mircea Guina

Optics Letters, vol. 43, no. 7, pp. 1578-1581, 2018. Available: 10.1364/OL.43.001578

Optics Letters

# AlGaAs-based vertical-external-cavity surface-emitting laser exceeding 4 W of direct emission power in the 740–790 nm spectral range

Hermann Kahle,* Kostiantyn Nechay, Jussi-Pekka Penttinen, Antti Tukiainen, Sanna Ranta, and Mircea Guina

*Optoelectronics Research Centre (ORC), Laboratory of Photonics, Tampere University of Technology, Korkeakoulunkatu 3, 33720 Tampere, Finland*
**Corresponding author: hermann.kahle@tut.fi*

*Received 19 December 2017; revised 26 February 2018; accepted 2 March 2018; posted 5 March 2018 (Doc. ID 315637); published 29 March 2018*

**An optically pumped vertical-external-cavity surface-emitting laser (VECSEL) for direct emission in the 740–790 nm wavelength region is reported. The gain structure is based on 12 AlGaAs quantum wells. We demonstrate wavelength tuning between 747 nm and 788 nm and free-running operation with a maximum power of 4.24 W (pump power limited) for a heat sink temperature of 14°C. This laser system addresses a spectral gap not currently covered by VECSEL technology and represents the most powerful VECSEL reported within the 7XX-nm wavelength region.** 

***OCIS codes:*** (140.7270) Vertical emitting lasers; (140.3600) Lasers, tunable; (140.5960) Semiconductor lasers.

https://doi.org/10.1364/OL.43.001578



Vertical-external-cavity surface-emitting lasers (VECSELs) were realized for the first time [1] about two decades ago. These lasers have gained a lot of attention in recent years due to their wavelength flexibility and due to the open resonator [2], which enables the use of a variety of intracavity optical elements, such as spectral filters or frequency converting elements. In previous work on AlGaAs-based VECSELs, GaAs quantum wells (QWs) were used to address wavelengths around 850 nm [3–6]. The spectral range from 700 nm to 800 nm has been barely covered by optically pumped VECSELs with a gap around 765 nm. To address this wavelength range, different methods have already been applied. The use of InP quantum dots as laser active material opened first access to fundamental $TEM_{00}$ emission from 716 nm to 755 nm [7] with VECSELs. Hereby, output powers in the sub-100 mW range were achieved. With Raman conversion of a red VECSEL [8], the wavelength range from 736.6 nm to 750.4 nm could be addressed. Also, a volume holographic grating stabilized VECSEL, solely operating at 780 nm and delivering a maximum output of 30 mW, was realized [9]. Further, with wafer-fused gain structures applying intracavity second-harmonic generation (SHG), the spectral range from 720 nm to 764 nm [10] and emission at 785 nm [11] could be realized, reaching an output power of 1.5 W and 1 W, respectively. The 780-nm-range was also addressed recently with a distributed-feedback laser [12] to realize narrow linewidth operation.

The spectral range between 700 nm and 800 nm is highly interesting for a variety of medical applications in the field of dermatology [13], thanks to the optimum penetration depth into human skin [14,15]. To this day, alexandrite lasers [16,17] are used to address these wavelengths of medical interest. Also in atomic physics [18], several useful energy transitions (rubidium Rb, 780 nm and potassium K, 766 nm [19]) lie on this spectral region. Furthermore, the new and efficient magnetically activated and guided isotope separation (MAGIS, [20]) method could strongly benefit from a 770 nm laser to excite the $4s^2S_{1/2}$ energy transition in potassium [20,21].

In this Letter, we present a VECSEL structure designed for fundamental laser emission in the long 700-nm wavelength regime. The architecture of the AlGaAs-based VECSEL gain chip as well as results of characterization are presented below. The VECSEL structure was grown on an undoped 2″ GaAs (100) ± 0.5° wafer in a V80H-10 VG Semicon solid source molecular beam epitaxy (MBE) system at a growth temperature of about 575°C. A GaAs buffer layer was first grown on the substrate followed by a distributed Bragg reflector (DBR) consisting of 33.5 pairs of $\lambda/2$-thick AlAs and $Al_{0.25}Ga_{0.75}As$ layers to create a broadband reflectance of $R_{DBR} > 99.9\%$ centered at the design wavelength of 765 nm. The active region was grown directly on top of the DBR. The structure was designed to be resonant and completely symmetric. The refractive index as well as the simulated electric field intensity distribution at the design wavelength are plotted in Fig. 1. The active region consists of 12 $Al_{0.12}Ga_{0.88}As$ QWs with a thickness of about 7 nm each, arranged in four groups of three QWs each. The QWs are separated by 8 nm thick layers of $Al_{0.4}Ga_{0.6}As$ and are also embedded with 12 nm of the same

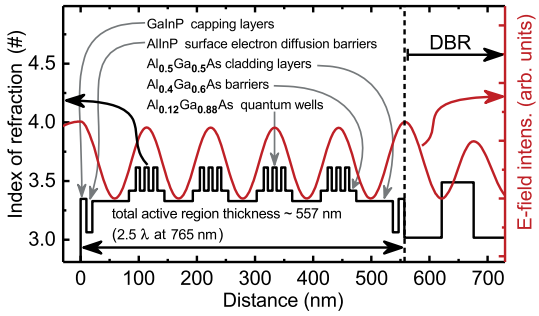


**Fig. 1.** Design of the active region of the gain chip is shown in this figure. Refractive index as well as simulated electric field distribution is plotted versus cross-section distance in the chip.

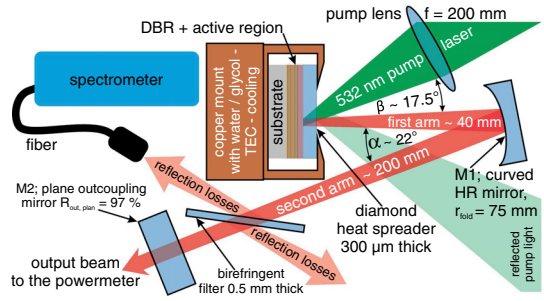


**Fig. 3.** Schematic drawing of the v-shaped cavity used for the tuning measurements (see Fig. 5). The beam profile (see Fig. 6) and the power transfer measurement at the fixed wavelength of 780 nm (see Fig. 7) were also taken in this configuration.

material. As cladding material separating the QW groups, we employ $Al_{0.5}Ga_{0.5}As$, which has an absorption edge at ~576 nm [22]. The active region was sandwiched between 10 nm thick AlInP and GaInP layers, which help in blocking the electron diffusion and act as a window layer at the semiconductor–heat spreader interface, respectively. No thinning or other processing steps were applied. The sample was cleaved into $2.7 \times 2.7$ mm$^2$ pieces, which were liquid capillary bonded [23] to an uncoated $3 \times 3$ mm$^2$ sized and 300 µm thick single crystalline intracavity diamond heat spreader. The heat spreader gain chip package is then further mounted to a thermo-electrically controlled copper heat sink, which is cooled via a water/glycol cooling system. The gain chip was incorporated in both a linear (see Fig. 2) and a v-shaped laser resonator (for details, see schematic Fig. 3), the former to allow optimized power performance, the latter to allow incorporation of a birefringent filter for spectral control. As a pump laser, we used a coherent Verdi V18 emitting at $\lambda_{pump} = 532$ nm. The collimated pump beam ($\varnothing = 2.25$ mm) was focused on the VECSEL chip with an anti-reflection coated lens ($f = 200$ mm). The angle of incidence $\beta$ of the pump beam was about 17.5° in both the linear and v-shaped resonators. This resulted in a $(18.3 \pm 0.3)$% reflection of the incident pump beam on the diamond–air interface. The pump lens distance was kept at $(197 \pm 1)$ mm, which results in a calculated pump spot diameter (short axis) of $D_{pump} = (62.5 \pm 2.8)$ µm. This pump spot diameter, and therefore the pump lens distance, was kept the same in all measurements presented in this Letter because it yielded the optimal performance. This means to adjust the laser resonator length to maximum output power while maintaining fundamental $TEM_{00}$ mode. At this condition, the pump spot diameter is equal to or slightly larger than the mode diameter but still small enough not supporting higher order transverse modes. For the linear resonator, the length was adjusted to ~99.8 mm, which results in a calculated mode diameter of ~64 µm on the VECSEL chip. In all measurements, the heat sink temperature $T_{hs}$ was kept at 14°C. The spectrometer with which all spectral measurements presented in this Letter were taken, was a StellarNet BLUE-Wave with a resolution limit of 0.8 nm. Due to the relatively low resolution of the spectrometer, Fabry–Perot resonances caused by the plane-parallel intracavity diamond heat spreader are not visible in the measured spectra. Namely, at a laser wavelength of 765 nm, the calculated free spectral range is around 0.4 nm for the 300-m thick diamond.

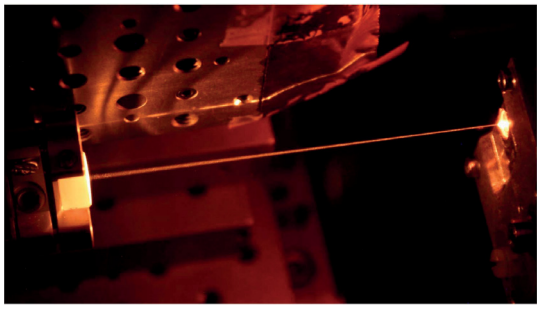

**Fig. 2.** Long-term exposure (30 s, Canon EOS 650D) photograph of the AlGaAs-VECSEL operated in the linear resonator. On the left side, one can see the HR external mirror; on the right side, the VECSEL chip (origin of the intracavity beam) is mounted.

A photograph of the operating AlGaAs-VECSEL in the linear resonator is shown in Fig. 2. The heat sink-mounted VECSEL chip is located on the right side. A highly reflective (HR) mirror with a radius of curvature of $r_{HR} = 100$ mm and diameter of 1/2″ located on the left side completes the linear resonator. The HR external mirror was used instead of an outcoupler to enhance the intracavity circulating power. The used 720 nm long-pass filter prevents over-exposure by visible wavelengths. Therefore, the pump laser beam is not visible. For optimized power performance characterization of the laser, we employed the linear cavity as shown in Fig. 2. It was operated with an outcoupler with a reflectivity of $R_{out,curve} = 97\%$ and a radius of curvature of $r_{out} = 100$ mm. Figure 4 shows the output power of the free-running VECSEL as a function of incident pump power for the linear cavity. A typical linear input–output behavior with a slope efficiency of $\eta_{diff} = 27.1\%$ can be seen. The laser threshold appears at a pump power of $P_{pump,thr.} = 0.38$ W. A maximum output power of $P_{out,max} = 4.24$ W was obtained. A thermal rollover could not be clearly identified, but it seems to appear at maximum pump power. Due to a limited amount of pump power (18 W) available in this work, a more detailed investigation was not possible. Measurements of the laser emission spectrum, plotted

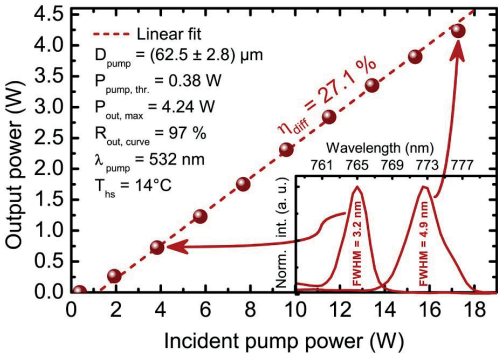


**Fig. 4.** Power transfer measurement data of the free-running VECSEL, taken in a linear resonator. Inset: two typical laser spectra taken during the input–output measurement at low and high pump powers.

in the inset of Fig. 4, show the full span of thermal shift that could be observed during the input–output measurement. The laser emission peak maximum shifts from 765 nm, obtained at very low pump powers, to 773 nm at the highest power, and consequently the full width at half maximum (FWHM) increases from 3.2 nm to 4.9 nm. Taking into account the quantum efficiency $\eta_{\text{quant}} = \lambda_{\text{pump}}/\lambda_{\text{out}}$, this is not surprising, because about 30% of the absorbed pump power is directly transferred into heat.

Wavelength tuning measurements (see Fig. 5), the beam profile measurement (see Fig. 6), and the power transfer measurement at a fixed emission wavelength of 780 nm (see Fig. 7) were performed in the v-shaped resonator (see Fig. 3). Tuning measurements were performed via rotating the intracavity birefringent filter to different angles to obtain information about the spectral distribution of the residual gain bandwidth. It is delivered by the material gain influenced by sub-cavity, heat spreader, birefringent filter, and cavity resonances, including all losses in the present VECSEL system. Several exemplary emission spectra normalized to the corresponding output power are shown in Fig. 5. The measurements were performed for the v-shaped cavity with a HR folding mirror M1 ($r_{\text{fold}}$=75mm) and a planar outcoupler M2 ($R_{\text{out,plan}}$ = 97%).

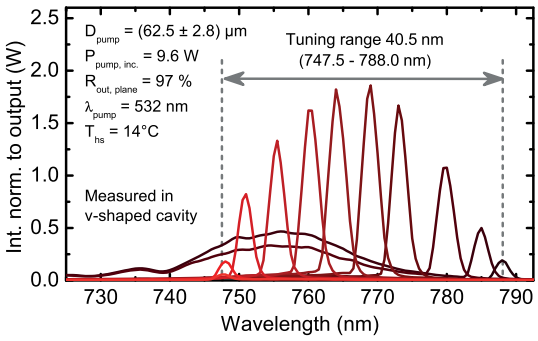


**Fig. 5.** Several exemplary emission spectra, taken for different angles of rotation of the intracavity birefringent filter, are shown normalized to the corresponding output power (v-shaped cavity; see Fig. 3).

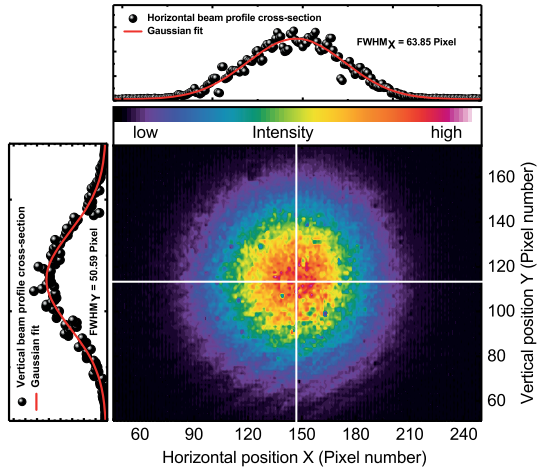


**Fig. 6.** Typical beam profile of the VECSEL, taken from the outcoupled laser beam in the v-shaped cavity. Additional vertical and horizontal cross sections including Gaussian fits are plotted.

Incident pump power during the tuning measurement was $P_{\text{pump,inc.}}$ = 9.6 W. The thickness of the used birefringent filter was 0.5 mm, resulting in a free spectral range of ~130 nm for laser wavelengths around 765 nm. A tuning range of 40.5 nm, i.e., from 747.5 nm to 788.0 nm, was attained. In Fig. 5 also, photoluminescence (PL) emission curves, centered at ~757 nm and belonging to the two long-wavelength laser emission spectra, are part of the measured data. This is the case, as the spectra were measured from one of the low-power reflections from the birefringent filter's surfaces. Due to the relatively low laser power, this reflected light contains also a more significant fraction of PL emission comparable to the laser peak intensity.

Figure 6 shows a typical beam profile taken with an OPHIR Beamstar-FX-66-NT beam profile camera at an output power of 720 mW behind the planar outcoupler in the v-shaped cavity with included birefringent filter. A perfect Gaussian intensity distribution can be seen, as it can be expected from semiconductor disk lasers. The slight ellipticity of 1.26:1 can be derived from the $\text{FWHM}_X$ and $\text{FWHM}_Y$ values given by the Gaussian fit functions applied on the intensity cross sections. Simulations of the beam propagation in the laser cavity with the open-source software "reZonator" deliver exactly the same ellipticity value. This is mainly due to the folding angle of $\alpha = 22°$ (see Fig. 3). No mode jumps or non-$\text{TEM}_{00}$ beam profiles were observed in the well-adjusted cavities during the measurements.

Regarding applications, the suitability of the VECSEL to Rb spectroscopy [24,25] was preliminarily examined by performing power transfer investigations near the D1 absorption line of Rb, which lies at the wavelength of 780 nm. The VECSEL was spectrally adjusted with the birefringent filter to this wavelength. The measurement plotted in Fig. 7 shows more than 2.8 W output power at its maximum and a slope efficiency of $\eta_{\text{diff}}$ = 21.7%. This result shows that there is sufficient laser power available, even if further losses would be induced via frequency stabilization and spectral filtering. Such stabilization

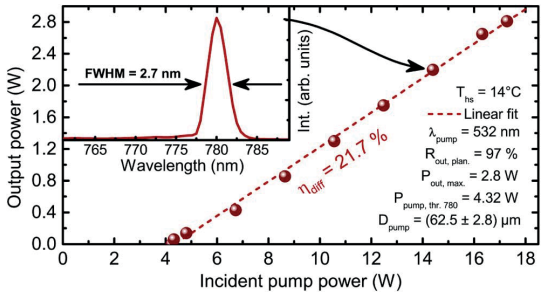


**Fig. 7.** Power transfer measurement performed in the v-shaped cavity and (inset) a typical spectrum, here taken at an incident pump power of $P_{pump} = 14.4$ W.

and spectral filtering are necessary to operate the VECSEL in the kilohertz linewidth range [26] with several hundreds of milliwatts, which are typically needed for spectroscopy applications. The laser threshold in the used v-shaped cavity occurs at a pump power of $P_{pump,thr.780} = 4.32$ W, which is a high value compared to the measurement taken in the free-running configuration. This could be expected as the 780 nm emission is located quite at the long-wavelength edge of available gain referring to the tuning measurement (see Fig. 3). The most probable explanation is that semiconductor gain typically broadens with increasing charge carrier density, which rises with increasing pump power, while its maximum shifts slightly to higher energies [27]. A thermal red shift of the gain might also play a role here, which additionally supports long-wavelength operation. The v-shaped resonator with its folding mirror M1 and the birefringent filter as intracavity element create additional losses. This further increases the laser threshold. The VECSEL's linewidth (FWHM), dictated by the transmission characteristic of the birefringent filter, was approximately at 2.7 nm during the whole measurement. A typical spectrum is plotted in the inset Fig. 7.

With this work, we demonstrated a direct emitting VECSEL that was designed to operate at wavelengths around 765 nm for the first time to our knowledge. We present fundamental characterization results of this all-AlGaAs-based double hetero-structure VECSEL. A maximum output power of 4.24 W was obtained as well as a tuning range of 40.5 nm from 747.5 nm to 788.0 nm. Fundamental transverse mode operation was always observed during VECSEL operation.

To further widen the access to the 700 nm to 800 nm range with VECSELs, slight variations in the aluminum content in the QWs would reduce emission wavelengths and enable a spectral coverage down to 700 nm [28]. In order to prevent unnecessary heating of the active region, the use of red diode lasers emitting at 640 nm or 675 nm as pump sources would be rational for future investigations. In terms of choice of material, it would also be useful to investigate, e.g., GaAsP-based gain structures and compare them with the present ones. GaAsP-based QWs have formerly been used to reach the 700-nm-regime [29–32]. Furthermore, another alternative to deliver 7XX-nm emission is represented by the AlGaInAs material system [32].

**Funding.** QUBIT, Academy of Finland (278338).

**Acknowledgment.** The authors highly appreciate the assistance in MBE growth by Patrik Rajala.

## REFERENCES

1. M. Kuznetsov, F. Hakimi, R. Sprague, and A. Mooradian, IEEE Photon. Technol. Lett. **9**, 1063 (1997).
2. M. Guina, A. Rantamäki, and A. Härkönen, J. Phys. D **50**, 383001 (2017).
3. M. A. Holm, D. Burns, P. Cusumano, A. I. Ferguson, and M. D. Dawson, Appl. Opt. **38**, 5781 (1999).
4. M. A. Holm, D. Burns, A. I. Ferguson, and M. D. Dawson, IEEE Photon. Technol. Lett. **11**, 1551 (1999).
5. J. E. Hastie, C. W. Jeon, D. Burns, J.-M. Hopkins, S. Calvez, R. Abram, and M. D. Dawson, Proc. SPIE **5137**, 201 (2003).
6. S.-S. Beyertt, U. Brauch, F. Demaria, N. Dhidah, A. Giesen, T. Kübler, S. Lorch, F. Rinaldi, and P. Unger, IEEE J. Quantum Electron. **43**, 869 (2007).
7. P. J. Schlosser, J. E. Hastie, S. Calvez, A. B. Krysa, and M. D. Dawson, Opt. Express **17**, 21782 (2009).
8. P. J. Schlosser, D. C. Parrotta, V. G. Savitski, A. J. Kemp, and J. E. Hastie, Opt. Express **23**, 8454 (2015).
9. G. N. West, A. C. Sills, and P. O. Leisher, Proc. SPIE **9134**, 913406 (2014).
10. E. J. Saarinen, J. Lyytikäinen, S. Ranta, A. Rantamäki, A. Sirbu, V. Iakovlev, E. Kapon, and O. G. Okhotnikov, Opt. Lett. **40**, 4380 (2015).
11. A. Rantamäki, J. Rautiainen, J. Lyytikäinen, A. Sirbu, A. Mereuta, E. Kapon, and O. G. Okhotnikov, Opt. Express **20**, 9046 (2012).
12. H. Virtanen, T. Uusitalo, M. Karjalainen, S. Ranta, J. Viheriälä, and M. Dumitrescu, IEEE Photon. Technol. Lett. **30**, 51 (2018).
13. K. Shokrollahi, E. Raymond, and M. Murison, J. Surg. **2**, 28 (2004).
14. M. H. Gold, Clin. Dermatol. **25**, 443 (2007).
15. F. H. Mustafa, M. S. Jaafar, A. H. Ismail, and K. N. Mutter, J. Lasers Med. Sci. **5**, 188 (2014).
16. A. Teppitaksak, A. Minassian, G. M. Thomas, and M. J. Damzen, Opt. Express **22**, 16386 (2014).
17. M. J. Damzen, G. M. Thomas, and A. Minassian, Opt. Express **25**, 11622 (2017).
18. S. C. Burd, D. T. C. Allcock, T. Leinonen, J.-P. Penttinen, D. H. Slichter, R. Srinivas, A. C. Wilson, R. Jördens, M. Guina, D. Leibfried, and D. J. Wineland, Optica **3**, 1294 (2016).
19. S. C. Burd, D. Leibfried, A. C. Wilson, and D. J. Wineland, Proc. SPIE **9349**, 93490P (2015).
20. T. R. Mazur, B. Klappauf, and M. G. Raizen, Nat. Phys. **10**, 601 (2014).
21. E. Arimondo, M. Inguscio, and P. Violino, Rev. Mod. Phys. **49**, 31 (1977).
22. B. Monemar, K. K. Shih, and G. D. Pettit, J. Appl. Phys. **47**, 2604 (1976).
23. Z. L. Liau, Appl. Phys. Lett. **77**, 651 (2000).
24. J. Park, H. Kim, and H. S. Moon, Opt. Express **25**, 32064 (2017).
25. Y. Ding, G. Ternent, A. Saeed, C. J. Hamilton, N. Hempler, G. P. A. Malcolm, G. T. Maker, M. Sorel, and D. J. Paul, in *Conference on Lasers and Electro-Optics/Europe and the European Quantum Electronics Conference (CLEO/Europe-EQEC)* (2017), p. 1.
26. D. Pabœuf and J. E. Hastie, Appl. Opt. **55**, 4980 (2016).
27. W. W. Chow and S. W. Koch, *Semiconductor—Laser Fundamentals: Physics of the Gain Materials* (Springer, 1999).
28. S. Adachi, J. Appl. Phys. **58**, R1 (1985).
29. F. Agahi, K. M. Lau, H. K. Choi, A. Baliga, and N. G. Anderson, IEEE Photon. Technol. Lett. **7**, 140 (1995).
30. G. Erbert, F. Bugge, A. Knauer, J. Sebastian, A. Thies, H. Wenzel, M. Weyers, and G. Trankle, IEEE J. Sel. Top. Quantum Electron. **5**, 780 (1999).
31. H. Christopher, E. V. Kovalchuk, H. Wenzel, F. Bugge, M. Weyers, A. Wicht, A. Peters, and G. Tränkle, Appl. Opt. **56**, 5566 (2017).
32. Y. Zhang, Y. Ning, L. Zhang, J. Zhang, J. Zhang, Z. Wang, J. Zhang, Y. Zeng, and L. Wang, Opt. Express **19**, 12569 (2011).

# PUBLICATION II

**AlGaAs/AlGaInP VECSELs With Direct Emission at 740–770 nm**

Kostiantyn Nechay, Hermann Kahle, Jussi-Pekka Penttinen, Patrik Rajala, Antti Tukiainen, Sanna Ranta and Mircea Guina

IEEE Photonics Technology Letters, vol. 31, no. 15, pp. 1245-1248, 2019. Available: 10.1109/LPT.2019.2924289

# AlGaAs/AlGaInP VECSELs With Direct Emission at 740–770 nm

Kostiantyn Nechay, Hermann Kahle, Jussi-Pekka Penttinen, Patrik Rajala, Antti Tukiainen, Sanna Ranta, and Mircea Guina

***Abstract*— An optically-pumped vertical-external-cavity surface-emitting laser (OP-VECSEL) with 3.25-W output power emitting around 750 nm is demonstrated. The gain structure incorporates AlGaAs quantum wells (QWs) and barriers, and AlGaInP claddings. The emission wavelength could be tuned from 740 to 770 nm. The development addresses the need for high brightness lasers at a wavelength range that has proven difficult to reach. The demonstrated structure exhibits polarization-related peculiarities, which cause polarization switching under increased pump power due to mode competition. The presence of birefringence inside the active region is attributed to known long-range ordering within the AlGaInP claddings which causes distorted beam profiles. This influence on laser features has not been reported in VECSELs so far.**

***Index Terms*— AlGaAs, AlGaInP, quantum well lasers, semiconductor growth, semiconductor disk lasers, semiconductor laser, vertical-external-cavity surface-emitting lasers (VECSELs).**

## I. Introduction

OP-VECSELs have successfully combined features of open cavities used in solid-state lasers with wavelength versatility of semiconductor gain heterostructures [1]. An external resonator enables efficient second-harmonic generation, narrow-linewidth operation, and the generation of ultra-short pulses via integration of various optical components inside the resonator. Owing to semiconductor bandgap engineering, the VECSEL platform is suitable for covering a vast wavelength range with Watt-level output power and good beam quality [2], [3]. However, several spectral gaps still remain uncovered so far, largely due to the lack of suitable material systems that would enable realization of high-quality gain mirrors. An example is the spectral region between 700–800 nm, which has recently attracted more attention. There is a great interest for high-brightness tunable and narrow-linewidth lasers at this wavelength range for applications in atomic and molecular physics [4] and nuclear medicine [5]. Moreover, due to low absorption of both hemoglobin and water at these wavelengths [6], there is a large penetration depth of the light into human tissue, which is relevant for a number of medical applications, including dermatology and photodynamic therapy.

To create high-power emission for the 700–800 nm region, intra-cavity frequency-doubling of VECSELs, based on wafer-fused gain mirrors, has been previously applied. The leading results of this approach include the demonstration of 1 W at 785 nm [7], and 1.5 W at 750 nm with 44 nm tuning range [8]. The first approach for fundamental emission was demonstrated by incorporating InP quantum dots as a lasing medium [9]. In this demonstration the output power was limited to several tens of milliwatts at the wavelengths spanning from 716 to 755 nm. Just recently, the AlGaAs-based VECSEL with an output power of $> 4$ W and a tunable range of over 40 nm around 770 nm was demonstrated [10]. Despite the high output powers achieved at 770 nm, shifting the emission towards shorter wavelengths might be challenging with the AlGaAs-cladding gain mirror design, since the carrier confinement diminishes correspondingly with the wavelength. To address this problem, we propose a slight alteration in the gain mirror design: namely, replacing these AlGaAs-claddings with higher bandgap AlGaInP barrier layers.

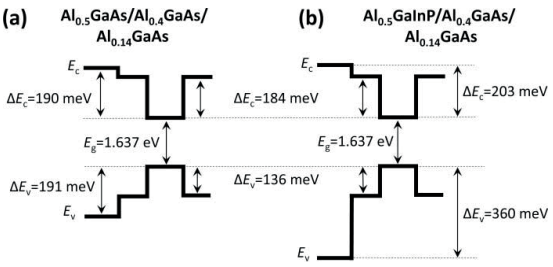


Fig. 1. Calculated bandgap profile of the quantum-well gain structure reported in the reference structure [10] (a) and in this letter (b).

Here we present the performance of a VECSEL emitting in the 740–770 nm wavelength range employing $[(Al_{0.48}Ga_{0.52})_{0.5}In_{0.5}]P$ cladding layers (hereinafter named as AlGaInP). Compared to the AlGaAs-only based design in Fig. 1(a) [10], the AlGaInP claddings [see Fig. 1(b)] improve the confinement of charge carriers, especially holes, which theoretically enhances the device performance at elevated temperatures. On the other hand, the use of AlGaInP-based active region has been traditionally associated with polarization and mode instabilities of the emitted light, linked to long range ordering of the AlGaInP cladding [11]. GaInP/AlGaInP compounds can form super lattices of alternating ordered Al/Ga-rich and In-rich planes along the [111]-direction [12]. The ordering effect has implications on valence band splitting, bandgap reduction and breaking crystal cubic symmetry; the latter may lead to ordering-induced birefringence [13]. Ordered birefringent AlGaInP layers, with the optical axis tilted away from growth direction,

Manuscript received April 3, 2019; accepted June 19, 2019. Date of publication June 21, 2019; date of current version July 17, 2019. *(Corresponding author: Kostiantyn Nechay.)*

The authors are with the Optoelectronics Research Centre, Physics Unit, Tampere University, 33720 Tampere, Finland (e-mail: kostiantyn.nechay@tut.fi).

Color versions of one or more of the figures in this letter are available online at http://ieeexplore.ieee.org.

Digital Object Identifier 10.1109/LPT.2019.2924289

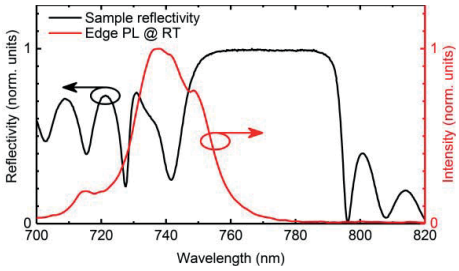


Fig. 2. Normalized edge PL and reflectivity curves of the VECSEL.

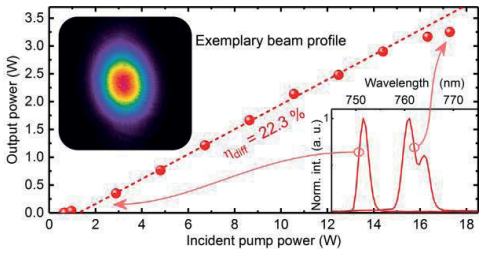


Fig. 3. Output power of the free-running VECSEL as a function of incident pump power. The inset shows an exemplary beam profile from the linear cavity.

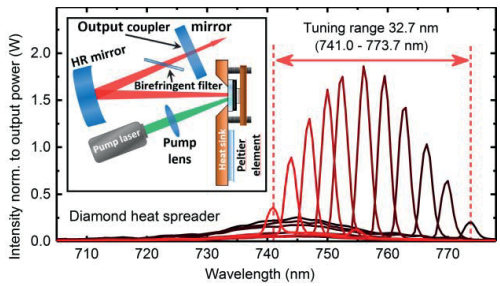


Fig. 4. Measured optical spectra obtained by means of intra cavity birefringent filter rotation at 14.4 W of incident pump power.

are responsible for coupling of TE and TM modes [14]. These "super modes" in their turn can govern the polarization of the laser. This effect is also identified for the VECSEL structure reported in this letter, both in terms of polarization variation across the gain chip and in terms of polarization switching as a function of pump power.

## II. Gain Mirror Fabrication

The structure was grown by solid-source molecular beam epitaxy (MBE) on an undoped 2″ (100) ± 0.5° GaAs substrate. It comprised an active region and a distributed Bragg reflector (DBR) consisting of 33.5 pairs of quarter-wave thick AlAs and $Al_{0.28}GaAs$ layers. The active region consisted of twelve QWs that were organized in four groups, with three QWs per group, and placed at the antinodes of the simulated optical field. The QW-packages contained 7 nm thick $Al_{0.14}GaAs$ QWs separated by 8 nm thick $Al_{0.4}GaAs$ barriers, and the QW-packages were separated by 47 nm thick AlGaInP claddings. The growth temperatures were measured with an IRCON pyrometer and were 580°C for the GaAs buffer, 565 – 570°C for the AlAs/$Al_{0.28}GaAs$ DBR and the AlGaInP cladding layers, and 580 – 590°C for the $Al_{0.14}GaAs$ QWs and the $Al_{0.4}GaAs$ barriers. The temperature was raised before each AlGaInP layer during growth interruptions. The microcavity between the DBR and the air-semiconductor interface was designed to be resonant at 750 nm. As a standard quality check, a cross section scanning electron microscopy investigation as well as large area photoluminescence (PL) were performed to identify major growth issues. Neither major growth defects nor dark lines and only a few dark spots ($\sim 10\ mm^{-2}$) were detected on the sample. However, the layer thickness measurement revealed a slightly blue shifted resonance.

Room temperature reflectivity of the grown structure was measured using an Accent RPM 2000 PL-mapper and is shown in Fig. 2. The microcavity resonance of the structure was determined to be at 747 nm (measured at 75°C with temperature dependent reflectivity measurement), while the room temperature emission peak of the edge PL was at 738 nm (see Fig. 2).

## III. VECSEL Characterization

The gain mirror was cleaved into chips with a size of 2.7 mm × 2.7 mm. The chips were subsequently capillary bonded to a flat uncoated 3 mm × 3 mm single crystalline diamond heat spreader with a thickness of approximately 300 $\mu$m. Furthermore, the samples were mounted to a thermo-electrically cooled copper block, with temperature stabilized at 14°C throughout all measurements. Basic output characteristics of the VECSEL were investigated in a linear cavity. A Coherent Verdi V-18 emitting at 532 nm was used to pump the structure. The output pump beam was focused by a spherical lens (f = 200 mm) down to a pump spot with an estimated diameter of $\sim$ 62 $\mu$m. This pumping spot diameter resulted in highest output power in this setup and is the same as in [10]. Therefore, the cavity was set to a length of $\sim$ 99.8 mm, with a 3%-outcoupler with a radius of curvature of 100 mm. This setting resulted in a simulated mode diameter of $\sim$ 60 $\mu$m.

Output power characteristics and spectra are presented in Fig. 3. The laser exhibited a linear power transfer behavior with a maximum output power of 3.25 W at an incident pump power of 17.3 W with differential efficiency of $\eta_{diff.} = 22.3\%$. A further increase of pump power led to an output power decrease due to thermal roll-over.

The tuning measurement, illustrated in Fig. 4, was performed in a V-cavity (see Fig. 4 inset), identical to the one described in [10], with an inserted 0.5 mm thick birefringent filter. The measured tuning range of $\sim$ 33 nm under incident pump power of 14.4 W shows a performance maximum at 757 nm.

At the highest pump power, we observed changes of intensity inside the beam profile, when measured both in I- and V-cavities, which we assumed to be polarization instabilities. To clarify this, the polarization of the laser output was investigated with a Glan-Taylor calcite polarizer with an extinction ratio of $10^5$ : 1. The polarizer was aligned to have a horizontal transmission (P-polarization) at 0°. All polarization related measurements were done in the linear cavity in order to minimize cavity influence on the laser polarization.

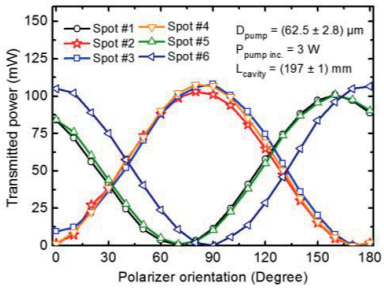


Fig. 5. Output power as a function of polarizer rotation angle at different spots across the VECSEL chip.

Moreover, as a precaution, a 350 $\mu$m thick and 3 mm sized flat silicon carbide (SiC) was applied instead of diamond as an intra-cavity heat spreader in the measurement. Since diamond heat spreaders possess a slight amount of wedging influencing the polarization of the laser, it was considered more straightforward to avoid using diamond heat spreaders at all. On the other hand, the SiC heat spreader has considerably worse thermal properties hence limiting the output power. However, the focus of the study at this point was purely on understanding the polarization variation linked to the gain mirror.

We observed that the polarization of the laser varied across the gain chip. This behavior is illustrated in Fig. 5, by the transmitted output power as a function of the polarizer orientation angle in six different locations on the chip. The nominal incident pump power was set to 3 W and was kept constant throughout the measurements. As it can be seen from Fig. 5, the polarization of the laser is likely to take one of either two polarization orientations, which are orthogonal to each other. The investigated VECSEL chip was oriented inside the copper mount always in a way that the (011) crystal plane was parallel to the plane of the optical table. Thus, we can assume that the lowest order modes are highly linearly polarized along the crystal axes. However, the output polarization extinction ratio tends to decrease dramatically with an increase of pump power. At certain pump powers we have observed a polarization extinction ratio equal to 1 dB.

Figure 6(a) shows typical beam profiles of the free-running VECSEL recorded at different spots across the chip and under a constant pump power of 0.9 W. Although variations in the mode shape were visible, the mode tended to be an elliptical $TEM_{00}$, at least in most cases. While scanning over the gain chip, these variations were observed to be inhomogeneously distributed. This fact can be attributed to ordering-induced birefringence, a phenomena studied in edge-emitting lasers [11]. Figure 6(b) shows a beam profile evolution, in regards to a pump power increase when the polarizer was set to transmission minimum for the fundamental polarization mode present at low pump powers. The measurement was performed in a single spot. We were able to observe at least one other laser mode of different polarization overlapping with the fundamental one. This additional mode became stronger with increasing pump power and later competed with the fundamental one.

Thus, it is assumed that at high pump powers the output may consist of simultaneous laser modes of different polarizations. In order to confirm this, the next experiment aimed to measure the laser output transmitted through the polarizer at

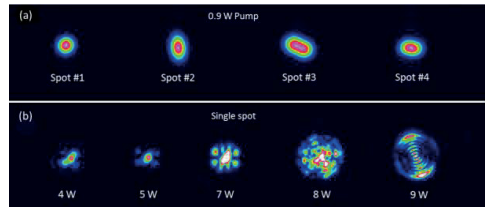


Fig. 6. (a) Output beam profiles recorded at different spots across the chip at 0.9 W pump power. (b) Polarized beam profiles of the output, under different pump powers, when polarizer transmission was set to minimum. Measurement has been performed at the same single spot.

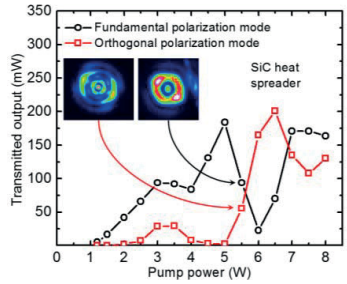


Fig. 7. Transmitted output power through the polarizer as a function of pump power, when polarizer was set to transmission maximum (Fundamental polarization mode) and 90° rotated (Orthogonal polarization mode).

two orientations. Thus, the polarizer was set, in turns, to two predetermined, orthogonal to each other, transmissions. One of the orientations of the polarizer was chosen to transmit fundamental polarization mode of the chosen spot. The other orientation of the polarizer, orthogonal to the polarization mode, did not transmit any detectable light at low pump powers. However, with increasing pump power we were able to measure a substantial amount of transmitted light from this orientation as well. Therefore, it can be concluded that the orientation of the polarization changed along with the pump power increase. Power characteristics have been recorded separately for two orthogonal orientations of the polarizer. The exchange of power between the two orthogonal polarization modes with respect to the incident pump power can be seen in Fig. 7. These measurements have been taken at the same spot in two subsequent runs. The recorded beam profiles (see insets Fig. 7) are typical for higher order mode operational regime. Intensities of the beam profiles were normalized.

The multimode output beam being comprised of simultaneous modes of different polarizations, as well as polarization switching under high pump powers, suggests the presence of polarization dependent and competing gain. To explain the origin of such competing gain, we assume two types of QW emission which contribute to lasing. These emission types are directed perpendicularly to the planes of the QWs and polarized along the corresponding crystal axes. The origin of these two types of emission may arise from the valence band splitting and strain-induced breaking of the cubic symmetry in the plane of the QWs. We assume the strain in the AlGaInP claddings to be the origin of this behavior. In order to verify the presence of strain, the curvature of strain-induced bending of the crystalline planes was measured with an X-ray diffractometer on a quarter wafer gain mirror sample.

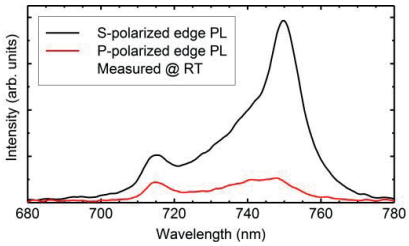


Fig. 8. Polarized edge PL taken perpendicularly from the facets. The left peaks at ∼ 715 nm corresponds to the emission from the $Al_{0.28}GaAs$ DBR layers.

The radius of curvature was smaller for the present VECSEL gain mirror structure (around 5.7 m in [011]-direction and 5.9 m in [01-1]-direction) than for a standard high-quality 1120 nm GaInAs/GaAs VECSEL gain mirror structure (around 7.3 m in both [011]- and [01-1]-direction) [15], which confirms the presence of strain inside the structure. To confirm the presence of strain-induced emission anisotropy, polarization dependent edge PL was measured (Fig. 8) perpendicularly to the {011} planes and it was filtered through the polarizer (S-polarization was defined to be parallel to [011]-direction). The edge PL was measured from cleaved facets, when the excitation was done by focusing pump light into a line (with a cylindrical lens), which covered the whole chip edge length (2.7 mm). As it can be seen from Fig. 8, the polarized PL emission is spectrally splitted and its intensity is depending on polarization. Thus, we have two emission types different in polarization and spectrum.

In order to ensure a polarization mode, it must experience a lower amount of losses compared to the competing mode. To fulfill this, the polarization mode should spectrally align with laser gain while also spectrally aligning with the polarization cavity resonance [16]. In this case the polarization cavity resonance may be understood as polarization dependent micro-cavity resonance which can exist under the condition of birefringence inside the structure.

## IV. Summary & Conclusion

In summary, a VECSEL structure incorporating AlGaAs QWs and barriers, and AlGaInP claddings with emission in the 750 nm range was reported. We demonstrated direct emission with more than 3 W of output power and wavelength tunability of 30 nm. The incorporation of AlGaInP claddings was meant to improve the confinement of charge carriers. On the other hand, it induced birefringence and resulted in polarization mode competition and multimode operation, which compromises the beam profile. None of the above mentioned issues were detected in the all-AlGaAs structure at a similar wavelength range reported in [10]. As well, we attributed the polarization features to internal strain of the AlGaInP cladding layers, which does not originate in the QWs, but strongly influences QWs. The polarization switch, partitioning and exchanging the power between orthogonal modes under the increase of pump power, will occur due to red-shifting gain and as a result of changing the relative strength of the net gain for the existing polarization modes due to polarization dependent microcavity resonance. Partially and inhomogeneously distributed ordering in the same layers seems to be responsible for inhomogeneous birefringence, which influences the transmitted light and results in peculiar mode behavior.

Further work will focus on testing different growth conditions. The use of off-cut oriented substrates as well as higher growth temperatures are known to reduce potential ordering effects in GaInP [17], which may have the same impact on the growth of AlGaInP. Moreover, optimization of detuning parameter may improve power and tuning characteristics.

## Acknowledgment

The authors would like to thank Turkka Salminen from Tampere University, Tampere, Finland, for his technical help.

## References

[1] M. Kuznetsov, F. Hakimi, R. Sprague, and A. Mooradian, "High-power (>0.5-W CW) diode-pumped vertical-external-cavity surface-emitting semiconductor lasers with circular $TEM_{00}$ beams," *IEEE Photon. Technol. Lett.*, vol. 9, no. 8, pp. 1063–1065, Aug. 1997.

[2] M. Guina, A. Rantamäki, and A. Härkönen, "Optically pumped VECSELs: Review of technology and progress," *J. Phys. D, Appl. Phys.*, vol. 50, no. 38, Aug. 2017, Art. no. 383001.

[3] B. W. Tilma *et al.*, "Recent advances in ultrafast semiconductor disk lasers," *Light Sci. Appl.*, vol. 4, no. 7, p. e310, Jul. 2015.

[4] S. Burd, D. Leibfried, A. C. Wilson, and D. J. Wineland, "Optically pumped semiconductor lasers for atomic and molecular physics," *Proc. SPIE*, vol. 9349, Mar. 2015, Art. no. 93490P.

[5] T. R. Mazur, B. Klappauf, and M. G. Raizen, "Demonstration of magnetically activated and guided isotope separation," *Nature Phys.*, vol. 10, pp. 601–605, Jun. 2014.

[6] S. L. Jacques, "Optical properties of biological tissues: A review," *Phys. Med. Biol.*, vol. 58, no. 11, pp. R37–R61, May 2013.

[7] A. Rantamäki *et al.*, "1 W at 785 nm from a frequency-doubled wafer-fused semiconductor disk laser," *Opt. Express*, vol. 20, no. 8, pp. 9046–9051, Apr. 2012.

[8] E. J. Saarinen *et al.*, "750 nm 1.5 W frequency-doubled semiconductor disk laser with a 44 nm tuning range," *Opt. Lett.*, vol. 40, no. 19, pp. 4380–4383, Sep. 2015.

[9] P. J. Schlosser, J. E. Hastie, S. Calvez, A. B. Krysa, and M. D. Dawson, "InP/AlGaInP quantum dot semiconductor disk lasers for CW $TEM_{00}$ emission at 716–755 nm," *Opt. Express*, vol. 17, no. 24, pp. 21782–21787, Nov. 2009.

[10] H. Kahle, K. Nechay, J.-P. Penttinen, A. Tukiainen, S. Ranta, and M. Guina, "AlGaAs-based vertical-external-cavity surface-emitting laser exceeding 4 W of direct emission power in the 740–790 nm spectral range," *Opt. Lett.*, vol. 43, no. 7, pp. 1578–1581, Apr. 2018.

[11] A. Moritz, R. Wirth, C. Geng, F. Scholz, and A. Hangleiter, "Effects of birefringence in ordered GaInP/AlGaInP lasers," in *Proc. Symp. EE-Optoelectron. Mater.-Ordering, Composition Modulation, Self-Assembled*, Feb. 1995, vol. 417, no. 97, pp. 97–102.

[12] A. Gomyo, T. Suzuki, and S. Iijima, "Observation of Strong Ordering in $Ga_xIn_{1-x}P$ alloy semiconductors," *Phys. Rev. Lett.*, vol. 60, no. 25, pp. 2645–2648, Jun. 1988.

[13] R. Wirth, A. Moritz, C. Geng, F. Scholz, and A. Hangleiter, "Determination of ordering induced birefringence in (Al)GaInP," *J. Electron. Mater.*, vol. 27, no. 3, pp. 122–126, Mar. 1998.

[14] A. Moritz, R. Wirth, C. Geng, F. Scholz, and A. Hangleiter, "Birefringence and tilted modes in ordered GaInP/AlGaInP waveguides and lasers," *Appl. Phys. Lett.*, vol. 68, pp. 1217–1219, Jan. 1996.

[15] S. Ranta, T. Hakkarainen, M. Tavast, J. Lindfors, T. Leinonen, and M. Guina, "Strain compensated 1120 nm GaInAs/GaAs vertical external-cavity surface-emitting laser grown by molecular beam epitaxy," *J. Cryst. Growth*, vol. 335, no. 1, pp. 4–9, Nov. 2011.

[16] K. D. Choquette, R. P. Schneider, K. L. Lear, and R. E. Leibenguth, "Gain-dependent polarization properties of vertical-cavity lasers," *IEEE J. Sel. Topics Quantum Electron.*, vol. 1, no. 2, pp. 661–666, Jun. 1995.

[17] C. Meenakarn, A. Staton-Bevan, S. Najda, G. Duggan, and A. Kean, "The effect of growth temperature and substrate misorientation on degree of order and antiphase domain size in $Ga_{0.52}In_{0.48}P$ epilayers grown on GaAs (001) substrates by Gs-Mbe," in *Proc. MRS*, vol. 523, 1998, p. 235. doi: 10.1557/PROC-523-235.

# PUBLICATION III

**Flip-Chip Wafer-Fused OP-VECSELs Emitting 3.65 W at the 1.55-μm Waveband**

Alexandru Mereuta, Kostiantyn Nechay, Andrei Caliman, Grigore Suruceanu, Alok Rudra, Pascal Gallo, Mircea Guina, and Eli Kapon

IEEE Journal of Selected Topics in Quantum Electronics, vol. 25, no. 6, 2019. Available: 10.1109/JSTQE.2019.2922819

# Flip-chip Wafer-fused OP-VECSELs emitting 3.65 W at the 1.55-μm waveband

| | |
|---|---|
| Journal: | *Journal of Selected Topics in Quantum Electronics* |
| Manuscript ID | Draft |
| Manuscript Type: | Contributed |
| Date Submitted by the Author: | n/a |
| Complete List of Authors: | Mereuta, Alexandru; Ecole Polytechnique Federale de Lausanne, Physics<br>Nechay, Kostiantyn; Tampereen yliopisto, Optoelectronic Research Center<br>Caliman, Andrei; LakeDiamond SA<br>Suruceanu, Grigore<br>Rudra, Alok; Ecole polytechnique federale de Lausanne Faculte des sciences de base<br>Gallo, Pascal; LakeDiamond SA<br>Guina, Mircea; Tampereen yliopisto<br>Kapon, Eli; Ecole Politechnique Federale de Lausanne, Station 3, 1015 Lausanne, Switzerland |
| Keyword: | Semiconductor lasers, Optical pumping |
| | |

# Flip-chip Wafer-fused OP-VECSELs emitting 3.65 W at the 1.55-μm waveband

Alexandru Mereuta, Kostiantyn Nechay, Andrei Caliman, Grigore Suruceanu, Alok Rudra, Pascal Gallo, Mircea Guina, *Fellow, IEEE* and Eli Kapon, *Fellow, IEEE*

***Abstract*—Optically-pumped vertical external cavity surface emitting lasers (VECSELs) based on flip-chip gain mirrors emitting at the 1.55-μm wavelength range are reported. The gain mirrors employ wafer-fused InAlGaAs/InP quantum well heterostructures and GaAs/AlAs distributed Bragg reflectors fixed on a diamond heat-sink substrate in a flip-chip geometry, incorporated in a V-cavity configuration. A maximum output power of 3.65 W was achieved for a heatsink temperature of 11°C and employing a 2.2% output coupler. The laser exhibited circular beam profiles for the full emission power range. This demonstration represents more than 10-fold increase of the output power compared to state-of-the-art flip-chip VECSELs previously reported at the 1.55 μm wavelength range. It opens new perspectives for developing practical VECSEL-based laser systems operating at a wavelength range widely used in many applications.**

***Index Terms*—Lasers, diode pumped, Optical pumping, Semiconductor lasers, Vertical emitting lasers.**

## I. Introduction

Since the first demonstration of vertical external cavity surface emitting lasers (VECSELs) by M. Kuznetsov and A. Mooradian in 1997 [1], continuous development of this laser technology has secured their position as the most flexible laser platform. In particular, the increasing interest in VECSELs technology is powered by the unique combination of their properties, including wavelength versatility, high-power operation, possibility to achieve single frequency emission with a broad tuning range, or efficient frequency doubling. Despite the impressive spectral coverage and output powers demonstrated to date [2], their level of performance is very different within different spectral bands, being largely determined by the intrinsic properties of the semiconductor materials used for the gain mirrors and the maturity of the fabrication technology. In this respect, the 1.3–1.5-μm wavelength region is less advanced compared to the 1-μm wavelength region, mainly due to lack of adequate InP-based distributed Bragg reflectors (DBRs) that would ensure lattice matching to quantum-well (QW) gain structures for these wavelengths. The highest output powers have been achieved around 1-μm wavelength, where the InGaAs QWs provide high gain, and can be grown on high-quality GaAs/AlAs DBRs. Emission at longer wavelength using GaAs-based materials has been demonstrated using dilute-nitride InGaAsN/GaAs QW structures, yet achieving high power operation with this material system was limited to the 1.3-μm range [3]. This is because incorporation of nitrogen is associated with formation of point defects, especially at the higher N content required for reaching longer emission wavelengths; in this respect we note that the maximum output power for InGaAsN/GaAs-based VECSELs at 1.55-μm is in the range of 100-mW only [4]. On the other hand, InP-based structures have shown similar limitation at 1.55 μm, with relatively low maximum output power of 170 mW [5]. In particular, for this material system the output power is limited by the absence of high-quality DBRs that could be monolithically integrated with the InP-based QWs.

To mitigate these limitations and demonstrate high-power VECSELs at wavelengths beyond 1.2 μm, wafer fusion has emerged as the technology of choice. This technique allows the combination of different classes of materials while preserving their intrinsic photonic features [6]. In particular for VECSELs, wafer fusion has been used to combine high-reflectivity GaAs/AlGaAs DBRs with InP/AlInGaAs QW gain structures. This approach made possible reaching output power levels as high as 5W at 1.48 [7] and 4.6 W at 1.57-μm [8] wavelengths. An important detail related to these long-wavelength results is the fact that thermal management, an essential aspect of VECSEL operation, was implemented using intra-cavity heat spreaders [9], where a diamond film is bonded to the surface of the gain mirror facing the laser cavity. Although this approach is easy to implement and enables efficient cooling, it brings certain limitations on laser characteristics owing to etalon effects and birefringence associated with the diamond heat-spreader.

Manuscript received February 1, 2019. This work was supported in part by the ANR-FNS IDYLIC Project.

Alexandru Mereuta, Alok Rudra and Eli Kapon are with Laboratory of Physics of Nanostructures, Ecole Polytechnique de Lausanne, Lausanne, CH-1015, Switzerland. (Corresponding author - A. Mereuta: +41-21-6933154; fax: +41-21-6935480; e-mail: azmereuta@gmail.com).

Kostiantyn Nechay and Mircea Guina are with Optoelectronics Research Center, Tampere University, 33720 Tampere, Finland. (e-mail: mircea.guina@tuni.fi).

Andrei Caliman, Grigore Suruceanu and Pascal Gallo are with LakeDiamond SA, CH-1400, Yverdon-les-Bains, Switzerland (e-mail: andrei.caliman@lakediamond.ch).

The alternative flip-chip thermal management approach, where the heat from the active region is extracted through the bottom of the gain element [10], alleviates the issues present in using intra-cavity heat-spreaders, and also brings further advantages in terms of volume manufacturing as it enables parallel processing. On the other hand, the flip-chip technology is clearly more intensive in process developments, and therefore the bulk of research demonstrations so far has been based on intra-cavity heat-spreaders. In fact, the use of flip-chip gain mirrors has been largely concentrated at 1-µm wavelength range for monolithic GaAs-based gain mirrors. The leading results for flip-chip gain mirrors in terms of high-power operation as a function of wavelength are summarized in Figure 1. We should note that the number of demonstrations shown at each wavelength does not reflect the effort made at specific wavelength; in fact, the vast majority of results were reported for 1-µm wavelength. The figure also indicates the fabrication technology employed; whereas results for 1-µm wavelength are dominated by monolithic gain/DBR structures, wafer-fused gain mirrors have been naturally employed at longer wavelengths. In particular, we note that the highest-power flip-chip results at the 1.3-µm range were obtained with wafer-fused structures [16-17]. On the other hand, the only flip-chip VECSELs emitting at 1.55–1.62-µm range were demonstrated by a combination of InP-based active regions and hybrid metal-metamorphic GaAs/AlAs DBRs, with modest output powers below 200 mW [18,19].

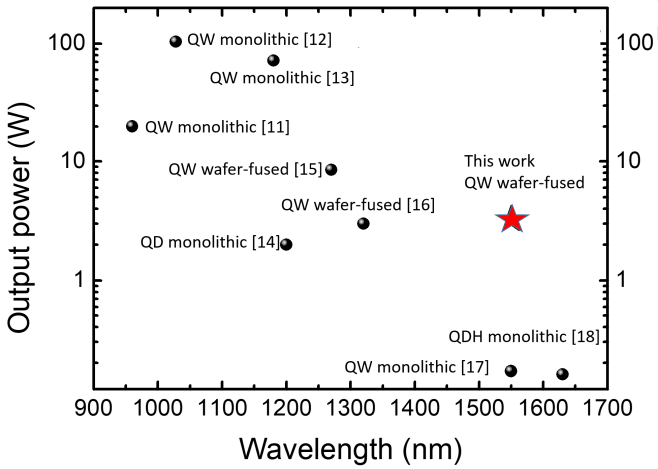


Fig. 1. Summary of output power levels achieved with OP-VECSELs using flip-chip heat-spreading technology. References are inserted by each reported result.

Here we report the first 1.55-µm wafer-fused flip-chip, optically pumped VECSELs with a maximum output power of 3.65 W at 11°C. Such power levels open new perspectives for developing emerging applications, such as wind LIDAR systems [18]. Frequency doubling of 1.55-µm VECSELs would allow reaching 750 nm wavelength, which is not well covered by alternative semiconductor-based high-brightness light sources. This wavelength range is particularly attractive for medical applications, such as photodynamic therapy, owing to the deeper penetration in human tissues [20]. Due to their inherent potential to operate as class-A lasers, the 1.55-µm VECSELs are also attractive sources for dual-frequency generation for high-purity terahertz radiation [21] and for high dynamic range and broadband RF/optical links [22].

## II. Gain Mirror Design and Fabrication

A schematic of the gain mirror design is presented in Fig. 2. The VECSEL structure comprises an InP-based gain region and a GaAs-based DBR, which were separately grown by metalorganic vapor phase epitaxy (MOVPE). The gain section consists of 10 InAlGaAs/InP QWs arranged into four groups, with three or two QWs per group, placed at the antinodes of the electric field of the 4/2λ-thick InAlGaAs micro-cavity. The 7-nm-thick InAlGaAs compressively strained (~1.4%) QWs are sandwiched between tensile strained 7.5-nm thick barriers for overall strain compensation. The measured room temperature photoluminescence peak of the InAlGaAs QWs is centered near 1518-nm wavelength. The multiple-QW region is surrounded by an InP cap and spacer layers for better heat dissipation. The top-most InP layer of the gain section provides additional carrier confinement, preventing carrier diffusion and subsequent non-radiative recombination at the surface.

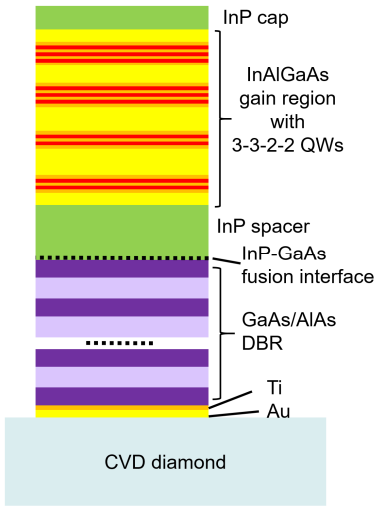


Fig. 2. Schematic cross section of the gain mirror structure.

The total sub-cavity length was designed for emission at 1540-nm wavelength. The InP-based active structure was wafer-fused to a 21.5 pair AlAs/GaAs DBR with stop band centered at ~1540-nm, as described in [6]. After selective GaAs substrate removal, 5- and 150-nm of Ti and Au layers, respectively, were deposited on the DBR-side of the fused structure to form a hybrid metal (Au) – AlAs/GaAs DBR. Subsequently, the wafer was cleaved into ~3x3-mm chips, which were then bonded to a metalized 6x6x0.3-mm diamond heat spreader. Finally, the VECSEL chip-on-diamond was attached to a copper heatsink by means of Ag-filled thermos conductive paste. The temperature of the gain mirror was controlled by mounting the assembly on a temperature-

stabilized holder. No antireflection coating was deposited on the chip surface.

## III. VECSEL TEST SET-UP AND LASING CHARACTERISTICS

The VECSEL devices were tested in a V-cavity configuration as shown in Fig.3. The optical pumping was performed with a 980-mm fiber-coupled diode laser, with its beam focused to a spot of approximately 470-μm diameter.

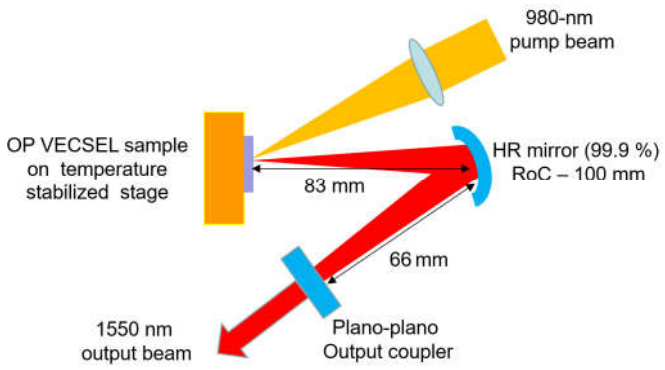


Fig. 3. Schematic of the OP-VECSEL cavity. HR – high reflective; RoC – radius of curvature.

Two planar couplers, with transmission of 2.2 and 2.5%, respectively, were used.

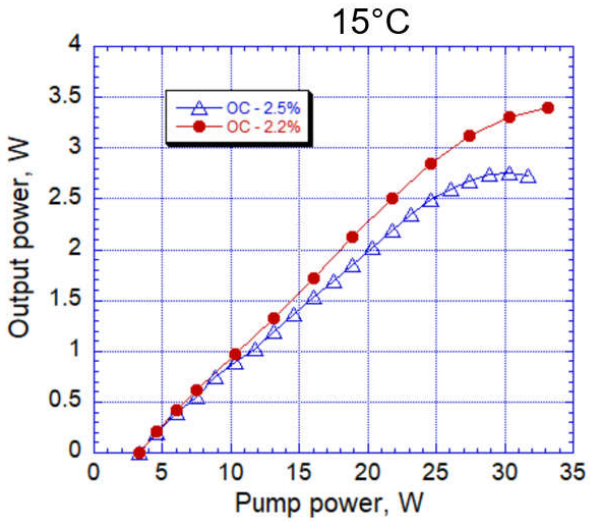


Fig. 4. Output power versus pump power for the flip-chip OP-VECSELs with 2.5 and 2.2% OC, respectively, measured at 15°C heatsink temperature.

The VECSEL output power as a function of the pump power is shown in Fig. 4 for the two different output couplers (2.2 and 2.5%) and a heat sink temperature of 15°C. The data were measured up to values when the output power starts to decrease due to sample heating. The threshold powers are approximately the same (~3W) for the two configurations, whereas the maximum output power and the thermal roll over is higher for the 2.2% OC as compared with the 2.5% OC (3.4 and 2.75 W, respectively). The slope efficiencies are 13.4 and 11.7%, correspondingly. This trend was observed for all measured chips, indicating that the measuring configuration with 2.2% OC is more appropriate for our gain mirror.

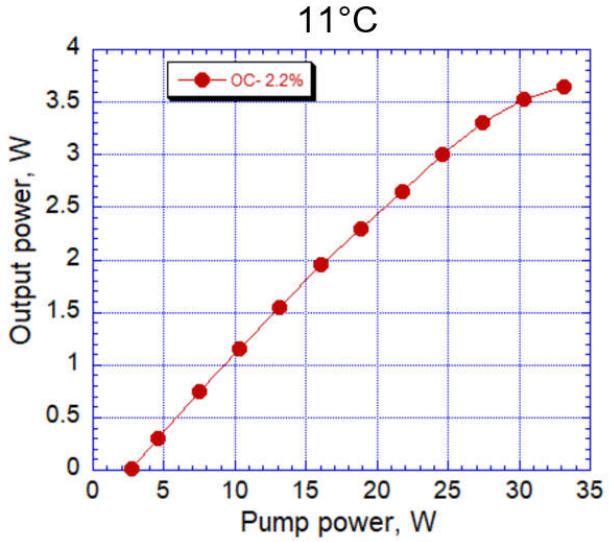


Fig. 5. Output power versus pump power for the flip-chip OP-VECSELs with 2.2% OC measured at 11°C heatsink temperature.

Thus, by using the 2.2% OC and reducing the heatsink temperature to 11°C, the maximum output power increased up to 3.65 W at 33.2 W excitation power of the 980-nm pumping source, with a slope efficiency of 13.5% (see Fig. 5). The beam quality factor $M^2$ remained below 1.25 at all levels of pump power.

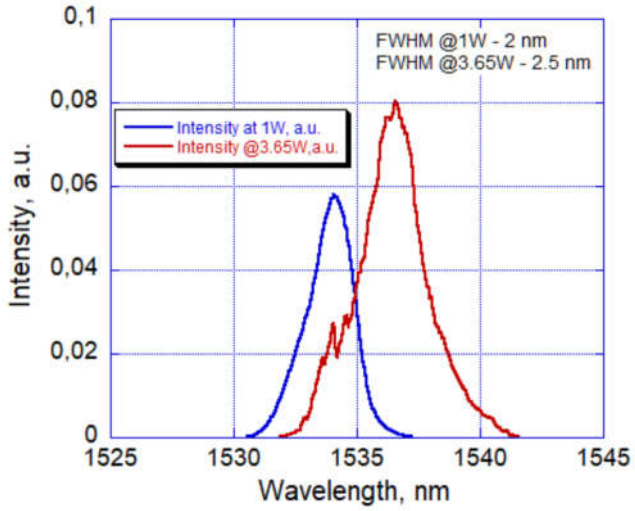


Fig. 6. Lasing spectra of the OP-VECSEL, measured, respectively at 1 and 3.65 W of output powers at 11°C heatsink temperature.

The VECSEL lasing spectra and beam profiles measured at 11°C heat sink temperature for 1 W and 3.65 W output power levels are shown in Fig. 6 and Fig. 7, respectively. The lasing wavelengths correspond well to the emission wavelength of the designed structure (~1540-nm). As one can observe from the lasing spectra and beam profiles, the OP-VECSEL operates in the fundamental $TEM_{00}$ mode with spectral FWHM of 2 and

2.5-nm at, respectively, 1 and 3.65 W of output power. We note that the typical spectral modulations observed in the case of intra-cavity etalon effects are absent for our device, as expected. A thermal impedance value of ~4 K/W was estimated from the shift of lasing spectra with dissipated power and heat sink temperature. The dissipated power was calculated as the difference between the absorbed 980-nm pump light and VECSEL emitted power, ignoring intra-cavity scattering and spontaneous emission losses.

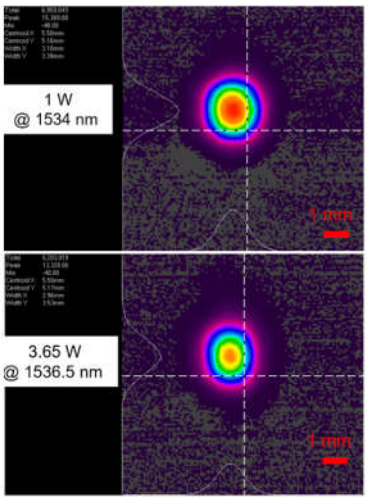


Fig. 7. Lasing beam profiles of the OP-VECSEL, measured, respectively at 1 and 3.65 W of output powers at 11°C heatsink temperature.

## IV. Conclusion

We reported the structure, fabrication and operation characteristics of optically pumped VECSELs emitting at ~1.535-µm wavelength and employing gain mirrors with flip-chip heat dissipation architecture. These devices are based on InAlGaAs/InP/GaAs/AlAs wafer-fused gain mirrors using 6x6x0.3-mm diamond films and were tested in a V-cavity configuration. The diameters of the 980-nm pump-spot and the 1.54-µm laser mode size on the gain chip were ~470-µm and ~360-µm, respectively. The maximum output power of 3.65 W was measured at 11°C heatsink temperature by employing a 2.2% OC. Single transverse mode lasing spectra and measured beam profiles show that the VECSEL operates in fundamental $TEM_{00}$ mode in the full emission power range. These results demonstrate, for the first time to our knowledge, gain mirrors in the 1550-nm wavelength band in a flip-chip thermal management scheme that approach the performance of previous results based on intra-cavity heat-spreader configurations [7,8]. Higher output power is expected by further optimization of the gain mirror structure and its fabrication process, and by employing thicker CVD diamond crystals for better thermal management.



## Acknowledgment

The authors acknowledge the support and CVD diamond crystal growth of Nicolas Malpiece and Mehdi Naamoun from LakeDiamond SA, Yverdon-les-Bains, Switzerland.

## References

[1] M. Kuznetsov, F. Hakimi, R. Sprague, and A. Mooradian, "High-power (0.5-W CW) diode-pumped vertical-external-cavity surface-emitting semiconductor lasers with circular TEM00 beams," IEEE Photon. Technol. Lett. **9**(8), 1063–1065 (1997).

[2] M. Guina, A. Rantamäki, and A. Härkönen, "Optically pumped VECSELs: review of technology and progress," J. Phys. D: Appl. Phys. **50**, 383001 (2017).

[3] J-M. Hopkins, S. Smith, C-W. Jeon, H. Sun, D. Burns, S. Calvez, M. Dawson, T. Jouhti and M. Pessa, "0.6 W CW GaInNAs vertical external-cavity surface emitting laser operating at 1.32 µm," Electron. Lett. **40**(1), (2004).

[4] V.-M. Korpijarvi, E. L. Kantola, T. Leinonen, R. Isoaho, and M. Guina, "Monolithic GaInNAsSb/GaAs VECSEL Operating at 1550 nm," IEEE J. Sel. Top. Quantum Electron. **21**(6), 1700705 (2015).

[5] H. Lindberg, A. Larsson and M. Strassner, "Single-frequency operation of a high-power, long-wavelength semiconductor disk laser," Opt. Lett. **30**, 2260-2262 (2005).

[6] A. Sirbu, V. Iakovelv, A. Mereuta, A. Caliman, G. Suruceanu, and E. Kapon. "Wafer-fused heterostructures: application to vertical cavity surface-emitting lasers emitting in the 1310 nm band," Semicond. Sci. Technol., **26** (1), 014016, (2011).

[7] J. Lyytikainen, J. Rautiainen, A.Sirbu, V.Iakovlev, A.Laakso, S. Ranta, M.Tavast, E.Kapon, O.G.Okhotnikov, "High-Power 1.48 µm Wafer-Fused Optically Pumped Semiconductor Disk Laser," Photonics Technology Letters **23** (13), 917-919 (2011).

[8] A. Rantamäki, J. Rautiainen, J. Lyytikäinen, A. Sirbu, A. Mereuta, E. Kapon, and O. G. Okhotnikov, "1 W at 785 nm from a frequency-doubled wafer-fused semiconductor disk laser," Opt. Express **20**, 9046-9051 (2012).

[9] F. van Loon, A. J. Kemp, A. J. Maclean, S. Calvez, J.-M. Hopkins, J. E. Hastie, M. D. Dawson and D. Burns, "Intracavity diamond heatspreaders in lasers: the effects of birefringence," Opt. Express **14**(20), 9250-9260 (2006).

[10] J. E. Hastie, J. M. Hopkins, S. Calvez, C. W. Jeon, D. Burns, R. Abram, E. Riis, A. I. Ferguson, and M. D. Dawson, "0.5-W single transverse-mode operation of an 850-nm diode-pumped surface-emitting semiconductor laser," IEEE Photon. Tech. Lett. **15,** 894-896 (2003).

[11] B. Rudin, A. Rutz, M. Hoffmann, D. J. H. C. Maas, A.-R. Bellancourt, E. Gini, T. Südmeyer, and U. Keller, "Highly efficient optically pumped vertical-emitting semiconductor laser with more than 20 W average output power in a fundamental transverse mode," Opt. Lett. **33**, 2719-2721 (2008).

[12] B. Heinen, T.-L. Wang, M. Sparenberg, A. Weber, B. Kunert, J. Hader, S.W. Koch, J.V. Moloney, M. Koch, W. Stolz, "106 W continuous-wave output power from vertical-external-cavity surface-emitting laser,"Electron. Lett. **48** (9), 516-517 (2012).

[13] E. Kantola, J.-P. Penttinen, S. Ranta, M. Guina, "72-W vertical-external-cavity surface-emitting laser with 1180-nm emission for laser guide star adaptive optics," Electron. Lett. **54**(19), 1135-1137, (2018).

[14] A. Rantamaki, J. Rautiainen, L. Toikkanen, I. Krestnikov, M. Butkus, E. U. Rafailov, O. Okhotnikov, "Flip chip quantum-dot semiconductor disk laser at 1200 nm," IEEE Photon. Technol. Lett. **24**(15), 1292-1294 (2012).

[15] S.T. Keller, A. Sirbu, V. Iakovlev, A. Caliman, A. Mereuta, and E. Kapon, "8.5 W VECSEL output at 1270 nm with conversion efficiency of 59 %," Opt. Express **23**, 17437-17442 (2015).

[16] A. Rantamäki, E. Saarinen, J. Lyytikäinen, J. Heikkinen, J. Kontio, K. Lahtonen, M. Valden, and O. Okhotnikov, "Thermal management in long-wavelength flip-chip semiconductor disk lasers," IEEE J. Sel. Top. Quantum Electron. **21**, 336–342 (2015).

[17] J.-P. Tourrenc, S. Bouchoule, A. Khadour, J.-C. Harmand, A. Miard, J. Decobert, N. Lagay, X. Lafosse, I. Sagnes, L. Leroy, J.-L. Oudar, "Thermal optimization of 1.55 µm OP-VECSEL with hybrid metal-

metamorphic mirror for single-mode high power operation," Opt. Quant. Electron. 40 155-165 (2008).
[18] S. Pes, C. Paranthoën, C. Levallois, N. Chevalier, C. Hamel, K. Audo, G. Loas, S. Bouhier, C. Gomez, J.-C. Harmand, S. Bouchoule, H. Folliot, and M. Alouini, "Class-A operation of an optically-pumped 1.6 µm-emitting quantum dash-based vertical-external-cavity surface-emitting laser on InP," Opt. Express **25**, 11760-11766 (2017).
[19] R. S. Hansen and C. Pedersen, "All semiconductor laser Doppler anemometer at 1.55 µm," Opt. Express **16**(22), 18288-18295 (2008).
[20] S. L. Jacques, "Optical properties of biological tissues: a review," Phys. Med. Biol. **58**, R37 (2013).
[21] S. De, G. Baili, M. Alouini, J.-C. Harmand, S. Bouchoule, and F. Bretenaker, "Class-A dual-frequency VECSEL at telecom wavelength," Opt. Lett. **39** (19), 5586–5589 (2014).
[22] G. Baili, L. Morvan, G. Pillet, S. Bouchoule, Z. Zhao, J.-L. Oudar, L. Ménager, S.Formont, F. Van Dijck, M. Faugeron, M. Alouini, F. Bretenaker, and D. Dolfi, "Ultra-low noise and high power VECSEL for high dynamic range and broadband RF/optical links," Journ. of Lightwave Techn, **32**, 3489-3494 (2014).

**Dr. Alexandru Mereuta** received an M.Sc. in solid state electronics from the Moldova State University (Chisinau, Moldova) in 1983 and a Ph.D. degree in electronic engineering from the Institute of Applied Physics, Chisinau, Moldova in1993. Currently he is with the Laboratory of Physics of Nanostructures of Ecole Polytechnique Fédérale de Lausanne, Switzerland, and is involved in the development of new materials and photonic devices. Before, he was employed by BeamExpress SA, Switzerland, to work on the design, epitaxial growth and fabrication of long wavelength VCSELs. Earlier, 1990-2001, Alexandru activated as research engineer/scientist at CNRS (Laboratoire de Photonique et de Nanostructures), France, France Telecom (Laboratoire de Bagneux) and Optoelectronics Laboratory of Technical University of Moldova, respectively, where he was involved in the design, epitaxial growth, study and development of GaAs and InP-based QW laser diodes and VCSELs. He is co-author of about 150 peer-reviewed publications and 2 patents.

**Mr. Kostiantyn Nechay** received B.Sc degree in electrical engineering from Zaporizhzhya National Technical University, Zaporizhzhya, Ukraine, in 2014 and the M.Sc. in technical physics from Lappeenranta University of Technology, Lappeenranta, Finland in 2016. He is currently pursuing the D.Sc. degree in optoelectronics at the Optoelectronics Research Centre, Tampere University, Tampere, Finland.
From 2015 to 2016 he was a Research assistant with the Optoelectronics Research Centre, Tampere University of Technology, Tampere, Finland. His research interest includes the development of semiconductor disk lasers, exploring new wavelength ranges for the number of applications in quantum technology, biophotonics and medicine.

**Mr. Andrei Caliman** received a Master's degree in Solid State Physics from Moldova State University in 1983. He has more than 30 years of work experience in R&D as well as manufacturing of semiconductor devices: edge emitting semiconductors lasers, VCSELs and VECSEL for different applications like gas sensing and optical data communications.
Since 2002 he was involved in developing and fabrication of long wavelength wafer fused VCSELs and VECSELS at LPN Laboratory EPFL, Switzerland, BeamExpress SA, Switzerland, and LakeDiamond SA, Switzerland. He is a coauthor of 2 patents and more than 100 scientific papers and conference communications. Currently, Mr. Caliman is working on development and fabrication of diamond-based high-power IR disc lasers at LakeDiamond SA.

**Mr. Grigore Suruceanu** received a Master's degree in Physics with specialization in Optoelectronics & Microelectronics from Moldova State University. He has more than 29 years of work experience in R&D as well as manufacturing of the edge emitting semiconductors lasers/VCSELs and different optoelectronics systems for optical data communications as well as laser scanning projection systems.
He worked for companies BeamExpress SA, Synova SA, Lemoptix SA and Intel. He is a co-author of 4 patents, 3 patent's applications and more than 70 scientific communications published in specialized scientific journals and presented at different conferences.
Currently Mr. Suruceanu is working on development of diamond-based high-power IR lasers at LakeDiamond SA.

**Dr. Alok Rudra received** an MSc. in Materials Science from the University of Aix-Marseille (France) in 1983 and a PhD in Physics from the the University of Nice in 1987. Since 1987, he has been working as a Research Associate, then as a Senior Scientist at the Faculty of Basic Science of EPFL (Ecole Polytechnique Fédérale de Lausanne, Switzerland). His main scientific contributions are in materials sciences through the epitaxial growth of high purity III-V semiconductors alloys, integrated in quantum wells, quantum wires, quantum dots and nanowires, with applications to optical communication devices (lasers, modulators and photodetectors). He is currently in charge of the Metalorganic Vapour Phase Epitaxy (MOVPE) lab in the Laboratory of Physics of Nanostructures of the Institute of Physics. He is co-author of about 200 peer-reviewed publications and 5 patents. A guest editor of Journal of Crystal Growth in 2015, Dr. Rudra is a member of the International Advisory Committee of ICMOVPE (International Conference on Metalorganic Vapour Phase Epitaxy).

Dr. **Pascal Gallo** has extensive experience of design, simulation, growth and fabrication of photonic devices. He

authored more than 50 peer-reviewed articles covering fundamental aspects of light-matter interaction, design of novel photonic and electrical devices and growth of nanostructures. He was involved in the study and development of innovative photonic devices for new market perspectives. Pascal is co-founder and the CEO of LakeDiamond SA, a Swiss based Company involved in the growth of the high quality CVD diamonds and in diamond photonics.

**Prof. Mircea GUINA** obtained the PhD degree in physics in 2002 at the Tampere University of Technology, Tampere, Finland. He is a professor of optoelectronics since 2008 and currently leads the Optoelectronics Research Centre team, a research group part of the Faculty of Natural Sciences and Engineering at the Tampere University. He conducts research on several major topics including molecular beam epitaxy of novel optoelectronic compounds, development of semiconductor lasers and high-efficiency solar cells, photonic integration, and use of lasers in medicine, LIDAR, and sensing. He has published more than 180 journal papers, several book chapters, has given more than 35 invited talks at major international conferences, and holds four international patents. Prof. Guina has an outstanding track record in initiating and leading large-scale research projects extending from basic science to technology transfer. He is a current recipient of an ERC Advanced Grant for development of high efficiency solar cell technology (AMETIST). He is also co-founder and Chairman of three start-ups related to laser technologies (Vexlum Oy, Reflekron Oy, and Picophotonics Oy). Prof. Guina is a Topical Editor for the Optics Letters journal and the Journal of European Optical Society. Recently, he was awarded the *OSA Fellow* and *SPIE Fellow* distinctions for his work on various optoelectronics and laser technologies.

**Prof. Eli Kapon,** director of Laboratory of Physics of Nanostructures (LPN), works mainly on semiconductors nanostructures, including fabrication, physics and applications in optoelectronic devices. Published >400 journal articles and 14 patents on semiconductor photonics. Founder of BeamExpress SA, a manufacturer of long wavelength VCSELs.

# PUBLICATION IV

**InAs/InP Quantum Dot VECSEL emitting 1.5 μm**

Kostiantyn Nechay, Alexandru Mereuta, Cyril Paranthoen, Gaelle Brévalle, Christophe Levallois, Mehdi Alouini, Nicolas Chevalier, Mathieu Perrin, Grigore Suruceanu, Andrei Caliman, Mircea Guina and Eli Kapon

Applied Physics Letters, vol. 117, no. 17, pp. 171105, 2019. Available: 10.1063/1.5125632

Applied Physics Letters ARTICLE scitation.org/journal/apl

# InAs/InP quantum dot VECSEL emitting at 1.5 $\mu$m

Cite as: Appl. Phys. Lett. **115**, 171105 (2019); doi: 10.1063/1.5125632
Submitted: 24 August 2019 · Accepted: 3 October 2019 ·
Published Online: 22 October 2019



K. Nechay,[1,a] A. Mereuta,[2] C. Paranthoen,[3] G. Brévalle,[3] C. Levallois,[3] M. Alouini,[3] N. Chevalier,[3] M. Perrin,[3] G. Suruceanu,[4] A. Caliman,[4] M. Guina,[1] and E. Kapon[2]

## AFFILIATIONS

[1]Optoelectronics Research Centre, Physics Unit, Tampere University, Tampere 33720, Finland
[2]École Polytechnique Fédérale de Lausanne, Laboratory of Physics of Nanostructures, Institute of Physics, 1015 Lausanne, Switzerland
[3]Univ Rennes, CNRS, Institut FOTON - UMR 6082, F-35000 Rennes, France
[4]LakeDiamond SA, Rue Galilée 7, 1400 Yverdon-les-Bains, Switzerland

[a]**Author to whom correspondence should be addressed:** kostiantyn.nechay@tuni.fi

## ABSTRACT

A high-power InAs quantum dot (QD) vertical-external-cavity surface-emitting laser emitting at 1.5 $\mu$m is reported. The active region employs 20 layers of high-density Stranski–Krastanow InAs quantum dots on an InP substrate. The QD density and emission wavelength were independently adjusted by employing a double-cap growth sequence. Optimization of the spacer layer thickness and strain compensation rendered possible nucleation of a relatively high number of QD layers per antinode of the electromagnetic standing wave, which in turn enabled a high output power continuous wave operation of about 2.2 W. The operation wavelength could be tuned over 60 nm, taking advantage of the broadband gain characteristic of QD media.



Vertical-external-cavity surface-emitting lasers (VECSELs)[1] have firmly secured their position as a flexible and multipurpose laser platform for photonic applications ranging from fundamental science to medical technology. The VECSEL concept has excellently coupled the advantages of external cavities, typically used in solid-state lasers, together with the wavelength versatility of semiconductor gain media.[2] Thus, this platform has allowed the demonstration of lasers with watt-level output powers and excellent beam quality across vast wavelength ranges.[3] Moreover, the use of external cavities enables efficient intracavity second-harmonic generation, narrow-linewidth operation, and generation of short pulses via the incorporation of intracavity elements, such as nonlinear crystals, etalons, and semiconductor saturable absorbers.[4]

The majority of conventional VECSELs exploit quantum well (QW)-based gain media. Also, less developed quantum dots (QDs) as VECSEL gain media have captured interest owing to their unique features, such as reduced threshold, low temperature sensitivity, broader gain bandwidth, ultrafast gain dynamics, and possibility to reach wavelengths where the QW system cannot easily fulfill lattice-matching requirements.[5] QDs fabricated by means of the Stranski–Krastanow (SK) growth mode exhibit density and size distribution, which in turn results in a large gain bandwidth. On the other hand, the effective gain of QDs is lower in comparison to that of QWs owing to the smaller active volumes overlapping with the optical field. To date, prominent QD VECSEL results have been obtained based on the InAs/GaAs QD system emitting in the 1–1.3 $\mu$m range. The leading performances include the demonstration of high output power in the range of 8 W,[6] demonstration of the reduced temperature dependence of threshold and emission spectra,[7] and broad wavelength tuning in the range of 60–70 nm.[8] In terms of the emission wavelength, particular emphasis has been put on the demonstration of operation at 1.2–1.3 $\mu$m, where InGaAs/GaAs-based QWs suffer from lattice mismatching to GaAs/AlAs distributed Bragg reflectors (DBRs).[9,10] On the other hand, the exploitation of QDs grown on InP substrates, already used in efficient edge emitting lasers,[11,12] has remained elusive for the VECSEL research community. In this letter, we introduce an InP-based QD gain mirror and demonstrate a 1.5 $\mu$m emitting VECSEL operating in the CW mode at room temperature. From the material development point of view, the key actions have targeted the modal gain increase, enabling output power as high as 2.2 W, and broad wavelength tuning.

The InAs QD structure was grown by gas source molecular beam epitaxy (MBE) on 2-in. InP(311)B substrates. SK InAs QDs were formed at 480 °C after the deposition of few monolayers (ML) of InAs onto InP-lattice matched $Ga_{0.2}In_{0.8}As_{0.435}P_{0.565}$ alloy with a typical bandgap of 1.18 $\mu$m (addressed as Q1.18 hereinafter). This alloy is

used as the absorbing layer for optical injection in VECSEL operation. When dealing with QDs as the active region of a VECSEL, the most difficult part is to get high enough gain at the operating wavelength. This fact implies a challenge of achieving high QD density per QD layer and stacking of a large number of QD layers.

Figure 1(a) reveals the QD density measured on a single uncapped QD layer as a function of the nominal thickness of InAs in MLs. By increasing the thickness of InAs from 1 to 2.5 ML, the QD density was increased from $5 \times 10^{10}$ cm$^{-2}$ [Fig. 1(b)] up to a value of $11 \times 10^{10}$ cm$^{-2}$ [Fig. 1(c)]. Such high-density QDs (HD-QDs) are placed in close proximity, with a typical layer-to-layer separation of 30–40 nm. The integrated photoluminescence variation as a function of the InAs thickness is presented in Fig. 1(d). No significant intensity variation is observed with InAs thickness up to 2.5 MLs. A further increase in InAs nominal thickness above 2.5 ML leads to QD coalescence and the formation of large and plastically relaxed QDs, leading to the decrease in PL efficiency. This fact evidences the formation of nonradiative recombination centers, which can prohibit VECSEL operation. Furthermore, Fig. 1(e) shows the evolution of the QD wavelength emission at room temperature, derived from PL spectra. Simultaneously with the QD density increase, the QD height increases as evidenced by the continuous redshift of the QD from 1530 to 1580 nm. In the case of InAs/InP QDs, independent control between QD density and wavelength emission can be achieved by applying a double-cap (DC) growth sequence.[13]

Figure 2(a) reveals the PL spectrum of a single layer of the high-density (HD)-QD as-grown sample, while Fig. 2(b) presents the PL of the sample grown according to the DC procedure. To decrease the HD-QD emission wavelength, the DC growth process was applied at the same QD growth temperature. At first, a 2.8 nm thick cap layer of Q1.18 was deposited on the QDs followed by a 20 s growth interruption under the mixture of $AsH_3$ + $PH_3$ overpressure flux.[14] Thus, HD-QDs with a central wavelength at 1517 nm with a full width at

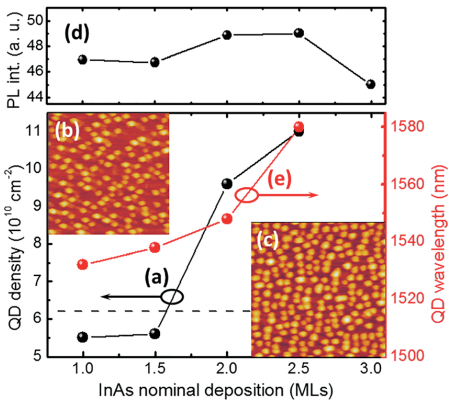


**FIG. 1.** QD density (a) and emission wavelength (e) variation as a function of InAs thickness (in MLs). Insets (b) and (c) show the AFM scans ($0.5 \times 0.5$ $\mu$m$^2$) of the uncovered QDs for InAs thicknesses of 1 and 2.5 MLs, respectively. The dotted line represents the target wavelength at 1515 nm. (d) Integrated photoluminescence intensity of a single QD layer as a function of InAs MLs.

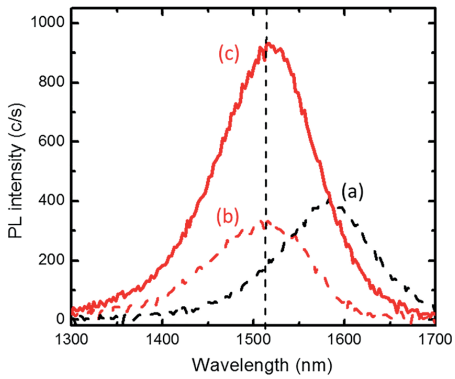


**FIG. 2.** PL spectra of a single layer of the as grown HD-QD (a) and DC HD-QD (b) measured at 300 K and with the same input power density (500 W/cm$^2$). The PL spectrum of 5 DC HD-QD layers with 15 nm spacer layers (c) before the fusion of DBR. The dashed line as an eye guide appears at 1510 nm.

half maxima (FWHM) of 115 nm have been fabricated. The stacking of QD layers, separated by spacer layers (SLs), was performed in order to further increase the gain volume. Since QD formation is governed by strain effects, the thickness of the SL between two QD layers is known to play an important role in the upper QD layer. Thicker SLs have been shown to decrease the upper QD layer density because of size filtering effects. Thinner SLs enable keeping QD density per layer constant due to the strain mediated vertical alignment of QDs; however, strain accumulation still limits the number of defect-free stacked layers.[15,16] Consequently, when considering QDs as active layers in photonic devices, the optimal thickness of SLs typically lies around 25–40 nm in order to avoid any defects, which also enables us to stack up to 10 layers when necessary. When dealing with VECSELs, such a thick SL limits the number of QD layers per electric field antinode to approximately three layers. In order to realize QD stacking with a reduced SL thickness, we have used a strain compensation technique,[17] and thus, after the growth of the first DC HD-QD, slightly tensile stressed 15-nm thick Q1.18 SL has been grown in order to mitigate the strain effect for the next QD layer. This cycle has been carried out five times. Figure 2(c) shows the PL spectrum of the QD layer stack sample. The wavelength emission and linewidth of the QD stack are identical to those of the single DC HD-QD sample. Furthermore, the PL intensity of the stack has been increased threefold, evidencing the good optical quality of these QD layers.

Following these QD growth optimizations, we have developed a VECSEL gain structure illustrated in Fig. 3(b). The structure is composed of the InP-based QD active region and a GaAs-based distributed Bragg reflector, which was grown by metalorganic vapor-phase epitaxy (MOVPE). The gain section consists of 20 QD layers arranged into four groups of five DC HD-QDs with 15 nm thick SLs. Each group was placed at the antinode of the microcavity electric field formed between DBR and a top-surface of the gain region. Subsequently, the InP-based QD gain structure was wafer-fused to a DBR composed of 29.5 AlAs/GaAs pairs, following the fusion process described by Sirbu *et al.*[18]

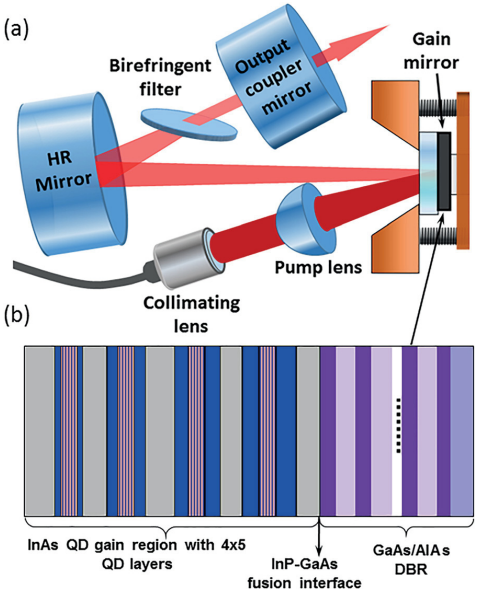


**FIG. 3.** Schematics of the V-shaped cavity with the inserted birefringent filter for tuning measurements (a) and gain mirror structure (b).

After the wafer fusion and selective etching of the InP substrate, the resulting wafer was cleaved into rectangular chips ($2.7 \times 2.7\,mm^2$), which were subsequently capillary bonded to an uncoated intracavity diamond heat spreader, with a dimension of $3 \times 3 \times 0.35\,mm^3$. The chip-diamond assembly was mounted onto a thermoelectrically cooled copper plate, which was kept at 15 °C throughout the measurements. The structure was tested in a V-shape resonator, which is shown in Fig. 3(a) and is composed of a highly reflective mirror ($R > 99.8\%$) with a curvature radius of 200 mm and a flat output coupler with reflectivity of 99%. The distance between gain mirror and curved mirror was 150 mm, while the distance between curved mirror and the output coupler was 276 mm; such resonator geometry provided a calculated mode diameter of 190 $\mu$m on the gain mirror. The VECSEL was pumped by using a 980 nm fiber coupled diode laser, which collimated output was focused down to a pump spot with a diameter of $\sim$220 $\mu$m. A birefringent filter with a thickness of 0.5 mm was used for tuning measurements and was placed at a Brewster angle inside the cavity.

Figure 4 shows the output power and threshold spectra (lower inset) of two exemplary VECSEL chips with different detuning (offset between the microcavity resonance wavelength and the PL peak). The top inset shows the spectra of one of the chips at different incident pump powers. The maximum output power was measured to be 2.2 W at 24 W of incident pump power, resulting in 11.7% of slope efficiency (the nominal incident power was used for the fit).

Unlike QWs, the PL peak of QDs undergoes a thermal redshift at a much slower rate, resulting in a considerably smaller detuning factor. The measured threshold spectra, recorded at 1.4 W of incident pump

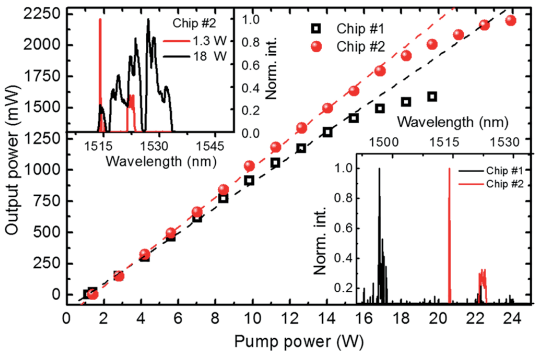


**FIG. 4.** Output power and threshold spectra of the free-running VECSELs, measured at 15 °C. Chips were taken from across the wafer, exhibiting different microcavity resonances.

power, allow approximate estimation of microcavity resonances of the chips. Thus, the optimal detuning factor was experimentally determined by testing chips across the wafer since the variation of microcavity resonance corresponds to active region thickness fluctuation across the wafer. Although the slope curves of the two demonstrated chips are virtually identical at low pump powers (due to broad QD gain), closer to thermal roll-over the chip #1 with a larger detuning becoming less efficient, yielding lower output powers. The optimal detuning value gains significance in the context of the resonant microcavity, where the round trip gain directly depends on the overlap factor between the electric field antinodes and the QD packages within the microcavity.[19]

The wavelength tuning ability is shown in Fig. 5; the tuning was achieved with the intracavity birefringent filter. Operation in a wavelength window of about 60 nm was obtained from the single chip. The tuning curve was recorded under an incident pump power of 6 W. The inset of Fig. 5 shows the exemplary beam profile measured at 22 W

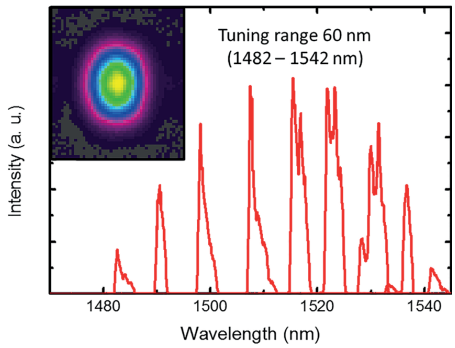


**FIG. 5.** Wavelength tuning recorded as a function of birefringent filter rotation. The figure is composed of nine different spectra. Tuning was obtained with chip #2 under the incident power of 6 W.

of incident pump power, revealing a slightly elliptical beam profile due to the V-shape resonator geometry.

In conclusion, the implementation of the DC growth sequence coupled with the optimization of SL thickness by means of strain compensation allowed us to demonstrate an InP-based QD gain mirror comprising dense QD layers. Such a gain structure enabled the demonstration of the first QD-based VECSEL emitting at 1.5 $\mu$m with an output power of 2.2 W. The emission wavelength could be tuned over 60 nm using an intracavity birefringent filter. In terms of output power, the results obtained with this type of gain mirror are on par with earlier demonstrations for quantum well-based VECSELs in the same wavelength range,[20] yet opening the way for superior performance in terms of broadband tuning, temperature stability, and lower threshold.

Second-harmonic generation of the VECSEL with emission at 1.5 $\mu$m constitutes a viable alternative to 750 nm direct emitting VECSEL,[21,22] by offering a much longer lifetime and wider wavelength tunability. In turn, lasers in the 750 nm range are needed for isotope separation,[23] spectroscopy,[24] and medicine due to the large penetration depth into tissues at the wavelengths around 750 nm.[25]

This work was partly supported by Agence Nationale de la Recherche (ANR) and Suisse National Science Foundation (ANR-SNSF IDYLIC Project, Grant No. ANR-15-CE24-0034-01).

## REFERENCES

[1]M. Kuznetsov, F. Hakimi, R. Sprague, and A. Mooradian, IEEE Photonics Technol. Lett. **9**, 1063 (1997).
[2]M. Stephane Calvez, J. E. Hastie, M. Guina, O. G. Okhotnikov, and M. D. Dawson, Laser Photonics Rev. **3**, 407 (2009).
[3]M. Guina, A. Rantamäki, and A. Härkönen, J. Phys. D: Appl. Phys. **50**, 383001 (2017).
[4]B. W. Tilma, M. Mangold, C. A. Zaugg, S. M. Link, D. Waldburger, A. Klenner, A. S. Mayer, E. Gini, M. Golling, and U. Keller, Light Sci. Appl. **4**, e310 (2015).
[5]M. Butkus, J. Rautiainen, O. G. Okhotnikov, S. S. Mikhrin, I. L. Krestnikov, and E. U. Rafailov, in Proceedings of the 22nd IEEE International Semiconductor Laser Conference (ISLC), Kyoto, Japan, September, 2010, pp. 71–72.
[6]D. Al Nakdali, M. Khaled Shakfa, M. Gaafar, M. Butkus, K. A. Fedorova, M. Zulonas, M. Wichmann, F. Zhang, B. Heinen, A. Rahimi-Iman, W. Stolz, E. U. Rafailov, and M. Koch, IEEE Photonics Technol. Lett. **26**, 1561 (2014).
[7]T. D. Germann, A. Strittmatter, J. Pohl, U. W. Pohl, D. Bimberg, J. Rautiainen, M. Guina, and O. G. Okhotnikov, Appl. Phys. Lett. **93**, 051104 (2008).
[8]M. Butkus, J. Rautiainen, O. G. Okhotnikov, C. J. Hamilton, G. P. A. Malcolm, S. S. Mikhrin, I. L. Krestnikov, D. A. Livshits, and E. Rafailov, IEEE J. Sel. Top. Quantum Electron. **17**, 1763 (2011).
[9]T. Schwarzbäck, R. Bek, F. Hargart, C. A. Kessler, H. Kahle, E. Koroknay, M. Jetter, and P. Michler, Appl. Phys. Lett. **102**, 092101 (2013).
[10]P. J. Schlosser, J. E. Hastie, S. Calvez, A. B. Krysa, and M. D. Dawson, Opt. Express **17**, 21782 (2009).
[11]P. Caroff, C. Paranthoen, C. Platz, O. Dehaese, H. Folliot, N. Bertru, C. Labbé, R. Piron, E. Homeyer, A. Le Corre, and S. Loualiche, Appl. Phys. Lett. **87**, 243107 (2005).
[12]A. Becker, V. Sichkovskyi, M. Bjelica, A. Rippien, F. Schnabel, M. Kaiser, O. Eyal, B. Witzigmann, G. Eisenstein, and J. P. Reithmaier, Appl. Phys. Lett. **110**, 181103 (2017).
[13]C. Paranthoen, N. Bertru, O. Dehaese, A. Le Corre, S. Loualiche, and B. Lambert, Appl. Phys. Lett. **78**, 1751 (2001).
[14]P. Caroff, N. Bertru, C. Platz, O. Dehaese, A. Le Corre, and S. Loualiche, J. Cryst. Growth **273**, 357 (2005).
[15]Q. Xie, A. Madhukar, P. Chen, and N. P. Kobayashi, Phys. Rev. Lett. **75**, 2542 (1995).
[16]L. Li, G. Patriarche, N. Chauvin, P. Ridha, M. Rossetti, J. Andrzejewski, G. Sek, J. Misiewicz, and A. Fiore, IEEE J. Sel. Top. Quantum Electron. **14**, 1204 (2008).
[17]K. Akahane, N. Yamamoto, and T. Kawanishi, IEEE Photonics Technol. Lett. **22**, 103 (2010).
[18]A. Sirbu, V. Iakovelv, A. Mereuta, A. Caliman, G. Suruceanu, and E. Kapon, Semicond. Sci. Technol. **26**, 014016 (2011).
[19]F. Zhang, C. Möller, M. Koch, W. S. Koch, A. Rahimi-Iman, and W. Stolz, Appl. Phys. B **123**, 291 (2017).
[20]A. Rantamäki, J. Rautiainen, J. Lyytikäinen, A. Sirbu, A. Mereuta, E. Kapon, and O. G. Okhotnikov, Opt. Express **20**, 9046 (2012).
[21]H. Kahle, K. Nechay, J.-P. Penttinen, A. Tukiainen, S. Ranta, and M. Guina, Opt. Lett. **43**, 1578 (2018).
[22]K. Nechay, H. Kahle, J.-P. Penttinen, P. Rajala, A. Tukiainen, S. Ranta, and M. Guina, IEEE Photonics Technol. Lett. **31**, 1245 (2019).
[23]T. Mazur, B. Klappauf, and M. Raizen, Nat. Phys. **10**, 601 (2014).
[24]L. Gianfrani, R. W. Fox, and L. Hollberg, J. Opt. Soc. Am. B **16**, 2247 (1999).
[25]S. L. Jacques, Phys. Med. Biol. **58**, 5007 (2013).

# PUBLICATION V

**High-power 760 nm VECSEL based on quantum dot gain mirror**

Hermann Kahle, Kostiantyn Nechay, Jussi-Pekka Penttinen, Antti Tukiainen, Sanna Ranta and Mircea Guina

IEEE Journal of Quantum Electronics (Submitted)